

EDITORIAL BOARD

Editor-in-Chief

I.V. Krivtsun E.O. Paton Electric Welding Institute, Kyiv, Ukraine

Deputy Editor-in-Chief

S.V. Akhonin E.O. Paton Electric Welding Institute, Kyiv, Ukraine

Deputy Editor-in-Chief

L.M. Lobanov E.O. Paton Electric Welding Institute, Kyiv, Ukraine

Editorial Board Members

O.M. Berdnikova	E.O. Paton Electric Welding Institute, Kyiv, Ukraine
Chang Yunlong	School of Materials Science and Engineering, Shenyang University of Technology, Shenyang, China
V.V. Dmitrik	NTUU «Kharkiv Polytechnic Institute», Kharkiv, Ukraine
Dong Chunlin	Guangzhou Jiao Tong University, Guangzhou, China
M. Gasik	Aalto University Foundation, Finland
A. Gumenyuk	Bundesanstalt für Materialforschung und –prüfung (BAM), Berlin, Germany
V.V. Knysh	E.O. Paton Electric Welding Institute, Kyiv, Ukraine
V.M. Korzhyk	E.O. Paton Electric Welding Institute, Kyiv, Ukraine
V.V. Kvasnytskyi	NTUU «Igor Sikorsky Kyiv Polytechnic Institute», Kyiv, Ukraine
Yu.M. Lankin	E.O. Paton Electric Welding Institute, Kyiv, Ukraine
O.V. Makhnenko	E.O. Paton Electric Welding Institute, Kyiv, Ukraine
S.Yu. Maksymov	E.O. Paton Electric Welding Institute, Kyiv, Ukraine
Yupiter HP Manurung	Smart Manufacturing Research Institute, Universiti Teknologi MARA, Shah Alam, Malaysia
M.O. Pashchin	E.O. Paton Electric Welding Institute, Kyiv, Ukraine
V.D. Poznyakov	E.O. Paton Electric Welding Institute, Kyiv, Ukraine
U. Reisgen	Welding and Joining Institute, Aachen, Germany
I.O. Ryabtsev	E.O. Paton Electric Welding Institute, Kyiv, Ukraine
V.M. Uchanin	Karpenko Physico-Mechanical Institute, Lviv, Ukraine
Yang Yongqiang	South China University of Technology, Guangzhou, China
Executive Director	O.T. Zelnichenko, International Association «Welding», Kyiv, Ukraine

Address of Editorial Board

E.O. Paton Electric Welding Institute, 11 Kazymyr Malevych Str., 03150, Kyiv, Ukraine
Tel./Fax: (38044) 205 23 90, E-mail: journal@paton.kiev.ua, patonpublishinghouse@gmail.com
<https://patonpublishinghouse.com/eng/journals/tpwj>

State Registration Certificate 24933-14873 ПП from 13.08.2021

ISSN 0957-798X, DOI: <http://dx.doi.org/10.37434/tpwj>

Subscriptions, 12 issues per year:

\$384 — annual subscription for the printed (hard copy) version, air postage and packaging included;

\$312 — annual subscription for the electronic version (sending issues in pdf format or providing access to IP addresses).

Representative Office of «The Paton Welding Journal» in China:

China-Ukraine Institute of Welding, Guangdong Academy of Sciences

Address: Room 210, No. 363 Changxing Road, Tianhe, Guangzhou, 510650, China.

Zhang Yupeng, Tel: +86-20-61086791, E-mail: patonjournal@gwi.gd.cn

The content of the Journal includes articles received from authors from around the world in the field of welding, cutting, cladding, soldering, brazing, coating, 3D additive technologies, electrometallurgy, material science, NDT and selectively includes translations into English of articles from the following journals, published in Ukrainian:

- Automatic Welding (<https://patonpublishinghouse.com/eng/journals/as>);
- Electrometallurgy Today (<https://patonpublishinghouse.com/eng/journals/sem>);
- Technical Diagnostics & Nondestructive Testing (<https://patonpublishinghouse.com/eng/journals/tdn>).

CONTENTS

ORIGINAL ARTICLES

V.M. Korzhyk, A.A. Grynyuk, V.Yu. Khaskin, O.M. Voitenko, O.M. Burlachenko, O.O. Khuan PLASMA-ARC TECHNOLOGIES OF ADDITIVE SURFACING (3D PRINTING) OF SPATIAL METAL PRODUCTS: APPLICATION EXPERIENCE AND NEW OPPORTUNITIES*	3
V.V. Kvasnytskyi, I.M. Lahodzinskyi INFLUENCE OF GMAW AND PAW METHODS OF ADDITIVE ARC SURFACING AND SHIELDING GAS COMPOSITION ON SURFACE GEOMETRY AND METAL STRUCTURE OF PRODUCTS FROM LOW-CARBON 09G2S STEEL*	21
V.O. Shapovalov, Yu.O. Nikitenko, V.V. Yakusha, O.M. Gnizdylo, O.V. Karuskevych 3D TECHNOLOGY OF GROWING LARGE TUNGSTEN CRYSTALS*	30
A.A. Babinets CONTROL OF FORMATION OF METAL PRODUCED BY ARC METHODS OF LAYER-BY-LAYER DEPOSITION OF MATERIAL WITH FLUX-CORED WIRES*	35
O.V. Makhnenko, G.Yu. Saprykina, O.M. Savytska, M.S. Ananchenko RECONDITIONING REPAIR OF STEAM TURBINE BLADES USING ADDITIVE TECHNOLOGY*	41
M.V. Sokolovskyi, A.V. Bernatskyi, N.O. Shamsutdinova, Yu.V. Yurchenko, O.O. Danyleiko ADDITIVE MANUFACTURING OF STRUCTURAL ELEMENTS ON A THIN-WALLED BASE: CHALLENGES AND DIFFICULTIES (REVIEW)**	46
S.A. Nedoseka, A.Ya. Nedoseka, M.A. Yaremenko, M.A. Ovsienko, O.M. Gurianov APPLICATION OF ACOUSTIC EMISSION METHOD TO EVALUATE THE CHANGES IN THE PROPERTIES OF 17G1S STEEL AFTER LONG-TERM SERVICE***	53

*Translated Article(s) from "Automatic Welding", No. 11, 2023.

**Translated Article(s) from "Automatic Welding", No. 10, 2023.

***Translated Article(s) from "Technical Diagnostics & Nondestructive Testing", No. 3, 2023.

DOI: <https://doi.org/10.37434/tpwj2023.11.01>

PLASMA-ARC TECHNOLOGIES OF ADDITIVE SURFACING (3D PRINTING) OF SPATIAL METAL PRODUCTS: APPLICATION EXPERIENCE AND NEW OPPORTUNITIES

V.M. Korzhyk¹, A.A. Grynyuk¹, V.Yu. Khaskin¹, O.M. Voitenko¹,
O.M. Burlachenko¹, O.O. Khuan^{2,3}

¹E.O. Paton Electric Welding Institute of the NASU
11 Kazymyr Malevych Str., 03150, Kyiv, Ukraine

²E.O. Paton Institute of Materials Science and Welding, National Technical University of Ukraine
“Igor Sikorsky Kyiv Polytechnic Institute”

37 Prospect Beresteyskyi (former Peremohy), 03056, Kyiv, Ukraine

³Paton Research Institute of Welding Technologies in Zhejiang Province, People’s Republic of China,
Zhejiang Province, Hangzhou City, Xiaoshan District, St. Shixing Beilu 857, Office 426

ABSTRACT

The growing relevance of 3D printing of finished metal products in recent years is predetermined by the reduction of costs for manufacturing, machining, changing the standard sizes and nomenclature of parts, the possibility of manufacturing solid parts with complex internal geometry. One of the most promising 3D printing processes, which provides a wide range of productivity (0.02–25 kg/h and more) with the possibility of surfacing a wall with a thickness of 2–20 mm, is additive plasma-arc surfacing (APAS) with wires and powder materials. The work examines the state-of-the-art of research on additive manufacturing of metal parts from steels and alloys, determines the state and prospects for the development of APAS. It is shown that APAS allows performing 3D printing using a wide range of filler materials, in particular, compact and composite (powder) wires, powders of light alloys and refractory metals, composite powders and mechanical mixtures of powders of alloys, metal ceramics, carbides, borides, etc. New opportunities for the application of APAS include development of technologies for growing products from materials with gradient functional properties, from dissimilar materials, with accompanying modification of the deposited metal by additional treatment, improving the properties of the deposited metal due to the use of hybrid processes. The state of innovative developments of APAS technologies and equipment carried out at the PWI of the NAS of Ukraine, and their industrial implementation is highlighted.

KEYWORDS: additive manufacturing, 3D printing, plasma-arc surfacing, steel, nickel, aluminium, titanium alloys, structure, mechanical properties, gradient functional properties, equipment

INTRODUCTION, AIM AND TASKS OF WORK

In recent years, there has been a qualitative leap in the approach to the use of 3D printing processes, associated with the transition from the creation of prototype models, according to which metal products were fabricated, to the direct printing of such products from various metals and alloys [1]. Modern AM — Additive Manufacturing is an innovative manufacturing process that offers the manufacture of products with advanced surface geometry of the required size with a surface that requires a minimal mechanical treatment, directly from CAD models, which leads to shortening in manufacturing time, a reduction in the volume of wastes and final cost. For example, the cost of additive surfacing of titanium parts of aircraft engineering is twice as low as the cost of their production from forged billets [2]. Another important area of application of additive manufacturing is military affairs. Thus, due to the extreme flexibility and the possibility

of adaptation to the solution of a wide range of industrial problems, the additive growing of parts is becoming more and more relevant in the modern world.

In modern additive manufacturing, two main approaches are predominantly used to obtain a finished metal product [1, 2]: layer-by-layer selective melting of powder and direct layer-by-layer growing of a part wall from the material in the form of powder or wire. For the processes of selective powder melting, laser (SLM) or electron beam (EBSM) energy is used. Both of these processes provide the formation of parts according to the dimensions specified in the models. After 3D printing by these methods, in most cases, mechanical treatment of a part surface is not used. However, these methods have a number of significant disadvantages, namely: dimensions of parts that can be printed are limited by the dimensions of the installations for printing by these methods (the working field is not more than 800×800×800 mm); complex expensive equipment; the need in using powders of the correct spherical shape of tiny sizes (5–15 μm), which are expensive and explosive

and fire-hazardous; the need in using several times more powder than the volume of a finished part; when growing a part with gradient differences in mechanical properties, when gradually using powders of different chemical composition, their mixing occurs outside the fusion zone, which causes the need in rejecting the powder that remains in the installation after the printing is finished.

Often in production it becomes necessary to form a billet from a certain material with mechanical treatment after growing. In such a case, it is advisable to use additive growing with the help of electric arc melting of the material supplied into the welding pool, namely [3]: argon-arc surfacing with a nonconsumable electrode (TIG) with a filler wire; surfacing using consumable electrode, including submerged-arc surfacing (SAS), shielded-gas consumable electrode (MIG/MAG process and, as a variant, cold metal transfer CMT), as well as additive plasma-arc surfacing (APAS) by powders or filler wires.

Plasma-arc surfacing is the most promising from the point of view of growth productivity, increase in material utilization rate, quality of the deposited metal, and the possibility of reducing the process of mechanical treatment of a billet due to the maximum approximation to the real dimensions of a part [4]. The APAS process can be implemented in the current range of 3–450 A. At the same time, the welding/surfacing process at currents of up to 50 A has received a separate name — microplasma welding/surfacing [5].

A significant contribution to the development of 3D printing of metal materials using constricted arc energy and powder materials and filler wires was made by scientists of the PWI and Paton IMSW [3–5].

Among the additive technologies that use surfacing methods, the processes DED-W/ WAAM/3DMP (Wire Direct Energy Deposition/Wire Arc Additive Manufacturing/3D Metal Print), or WAAM — additive surfacing using metal wire have become most widespread, which include arc processes using a nonconsumable and consumable electrode, as well as processes with a short circuit of the arc gap (of CMT type — Cold Metal Transfer) [3]. CMT is a modified version of welding using consumable electrode in a shielding gas based on the mechanism of the controlled metal transfer mode into the welding pool by using pulsed current and reciprocating wire movement.

Among the arc CMT methods, the process of additive technologies has a number of indisputable advantages. One of the most important is the system of reverse wire feed, synchronized with a high-speed digital control, which determines the arc length, short circuit phase and heat transfer into the welding zone [6]. This process provides minimal spattering of metal, relative stability of weld formation, reduced heat

transfer to the treatment zone. However, the CMT process in terms of using in additive technologies has its disadvantages: relatively low productivity due to the use of small diameters of wires and presence of significant inner defects (pores, inclusions).

The use of APAS provides a number of advantages from both a technological and economic point of view. These include high productivity, wide range regulation of heat transfer to the base and deposited materials and, as a result, control of the penetration depth and width, structure, composition and properties of the material being formed. APAS with the use of direct current of reverse polarity or alternating current provides cleaning of the surface of the previous layer from contaminations due to the effect of cathode atomization, sufficient wetting and spreading of liquid metal at a minimal heating of the surface. At the same time, manufacturing of layered materials with a favorable structure without inner defects is provided. In addition, the compared simplicity and low cost of the equipment for plasma surfacing should provide the interest of manufacturers for using in additive technologies [3, 7].

The abovementioned predetermined the powerful potential of application and development of APAS technologies. Such advantages and wider technological capabilities of APAS over WAAM methods should be noted [3, 8]:

- wide adjustment of the productivity of 3D printing (0.02–25 kg/h) and the degree of detailing volumetric elements (widths from 2.0–2.5 to 10–20 mm) by implementing the process both in the mode of microplasma surfacing with a low-ampere plasma-arc (at currents of 5–35 A), as well as at currents of 50–450 A and higher (depending on the capacity of the power source);
- a wide range of adjustment of the input energy, heating zone and penetration depth of previously deposited layers by means of APAS using a direct or tangential plasma-arc;
- 3D printing at direct current of direct and reverse polarity, alternating current, including the implementation of the process of cathodic cleaning and destruction of oxide films, when surfacing light metals and alloys with refractory oxide films on their surface;
- 3D printing using one to four filler wires, including a conductive filler wire with preheating;
- use of compact and composite (flux-cored) wires, powders of light alloys and refractory metals, composite powders and mechanical mixtures of powders of alloys, metal ceramics, carbides, borides, etc. for 3D printing as a filler material;
- implementation of the 3D printing process using an filler that does not move together with the plasmatron during deposition of a layer (metal grit, foil, thin bands of metal), which is applied alternately af-

Table 1. Comparison of basic technical and economical indicators of different technologies of additive surfacing (3D printing) of volumetric metal products

Number	Technology	Average value of width of single deposited layer, mm	Average sizes of roughnesses of free surface of manufactured products, mm	Deviation of geometric sizes of a product, mm	Productivity of manufacturing of a 3D product, kg/h	Specific losses of electric power, kW/kg	Characteristics of strength (% from the tensile strength of initial filler material)	Characteristics of ductility (% from the parameter of elongation of initial filler material)
1	WAAM (arc additive surfacing using current conducting consumable MIG/MAG wire)	4.0–6.5	0.5–2.0	0.5–1.5	0.3–15.0	6–18	0.80–0.90	0.85
2	WAAM (arc additive argon-arc surfacing using consumable electrode with the feed of neutral filler TIG wire)	6.0–8.0	0.5–1.0	0.5–1.0	1.0–4.8	7–15	0.50–0.80	0.85
3	WAAM (CMT)	2.0–4.0	0.3–0.6	0.2–0.8	0.5–7.0	5–10	0.80–0.90	0.75–0.80
4	Microplasma layer-by-layer powder surfacing	1.6–3.2	0.1–0.5	0.1–0.5	0.01–0.3	4–8	0.9–0.95	0.85–0.90
5	Microplasma layer-by-layer wire surfacing	2.0–3.5	0.2–0.8	0.2–0.8	0.02–0.4	5–10	0.9–0.95	0.85–0.90
6	Plasma layer-by-layer wire surfacing	3.0–4.0	0.5–1.0	0.2–0.8	0.2–10.0	5–12	0.9–0.96	0.85–0.90

ter deposition of each layer (a process similar to the methods of “lamination” or selective melting);

- possibility of launching a plasma-arc without adding wire or powder, which allows preheating of the base or deposited layers before additive surfacing.

A comparison of basic technical and economic indicators of additive surfacing processes using a free arc with the processes using a constricted (plasma) arc also confirms the advantages of additive plasma-arc technologies (Table 1) [3–8].

The aim of the work is to analyze the state-of-the-art of scientific research, technological developments and practical experience of additive manufacturing of metal products from various types of alloys and composite materials; identification of the potential of application and development of additive technologies of plasma-arc surfacing, in which a plasma-arc is used as a heating source; identification of new opportunities and promising directions for their further development and application.

To achieve this aim, the following tasks were solved in the work:

1. Analysis of the state of scientific research and practical experience of APAS of volumetric products from various types of alloys.

2. Identification of new possibilities of plasma-arc technologies in additive manufacturing, including when applying hybrid and combined methods of 3D-printing.

3. Description of the developments of new equipment for the implementation of APAS technologies in additive manufacturing.

1. APPLICATION OF APAS TECHNOLOGIES (3D PRINTING) OF SPATIAL METAL PRODUCTS

1.1 APAS OF VOLUMETRIC PRODUCTS FROM STEELS AND IRON- AND NICKEL-BASED ALLOYS

A number of problems arise during additive manufacturing of 3D objects from steels, iron-, and nickel-based alloys, related to their overheating during the surfacing process. For example, during CMT printing of a wall made of 2Cr13 steel, a small number of pores without cracks in different layers was observed, which indicates a high level of densening [6]. The precipitated microstructure consisted of martensite and ferrite together with the $(Fe, Cr)_{23}C_6$ phase, which is precipitated on α -Fe grain boundaries. However, due to overheating, the content of martensite gradually increased from the 5th to the 25th layers, despite a partial decomposition of metastable martensite into stable ferrite due to the diffusion of carbon atoms. The hardness changed slightly from the 5th to the 15th layers and then increased rapidly from the 20th to the 25th layers; the fracture process transformed from ductile (1st–10th layers) to mixed (15th–20th layers) and, finally, to brittle fracture (25th layer). Thus, in order to adjust the 3D printing process with a stable formation of the product structure, it is

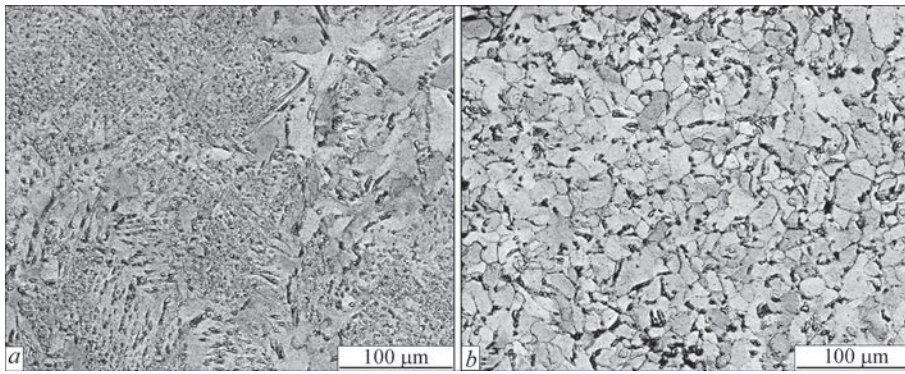


Figure 1. Microstructure of spatial product of the type “thin wall” manufactured by additive microplasma surfacing with the feed of neutral filler wire Sv-08G2S: *a* — upper layer; *b* — middle of the wall (electron microprobe analysis in CamScan-4 analyzer)

necessary to change the technological approach. One of the promising options here is APAS.

Thus, the APAS process is proposed to produce parts with an increased wear resistance from intermetallic alloys, for example, iron aluminide. In [9] it is shown that it is possible to manufacture parts from an iron-nickel-aluminium intermetallic compound using this method. In [10], it is proposed to use plasma-arc 3DPMD technology for the additive manufacturing of wear-resistant functional layers of wear surfaces and the body of the tool from alloys based on nickel Ni 625 and iron-based PS Fe-hard D. Plasma-arc surfacing using wires (up to 120 A) and microplasma surfacing with powder materials (at a current of up to 50 A) for the manufacture of products from carbon and stainless steels is proposed in [11]. The study of the peculiarities of the manufacturing processes of steel spatial primitives of the type “wall”, “glass”, “cone” and “hemisphere” showed that the deviations from the nominal size during their manufacture do not exceed ± 0.5 mm, the porosity lies within 1–2 %, and the mechanical strength is about 90–95 % of the strength of cast metal. The structure of the deposited material is fine-grained and uniform, mixing of layers is extremely low.

The analysis of the microstructures of the specimen of additive microplasma surfacing using the filler wire Sv-08G2S (of 1.2 mm diameter), performed at the PWI

of the NASU, showed the absence of cracks and pores and that the structure is homogeneous and uniform similar to the structure of specimens deposited by the microplasma method using filler powder. The walls are characterized by a density that corresponds to a cast structure, with grains of small sizes, without dendrites. Porosity, inclusions and microcracks are absent. Discontinuity between the contacting layers along the fusion line is absent; the size of the heat-affected-zone of the build-up layer is ~ 2 mm. The microstructure of the deposited material is equiaxial, the grain has approximately the same sizes in all directions (15–20 μm) with clearly visible boundaries and a eutectic component between them (Figure 1). These are grains of ferrite (light grains) and pearlite (dark regions). The multilayer structure of the deposited volumetric specimen is not revealed, mixing of the deposited layers is extremely low, the formation of oxides is not observed.

In the case of the WAAM process using MAG surfacing with Sv-08G2S wire (1.2 mm diameter), the microstructure of the deposited metal is represented with ferrite and pearlite grains (Figure 2). The difference of this structure from the analogues produced by microplasma surfacing using the same wire is the coarser grain size, as well as the presence of primary crystals in the form of dendrites and eutectics. Dendrites appear in the form of tree-like formations with clear axes of individual branches. The interlayers of

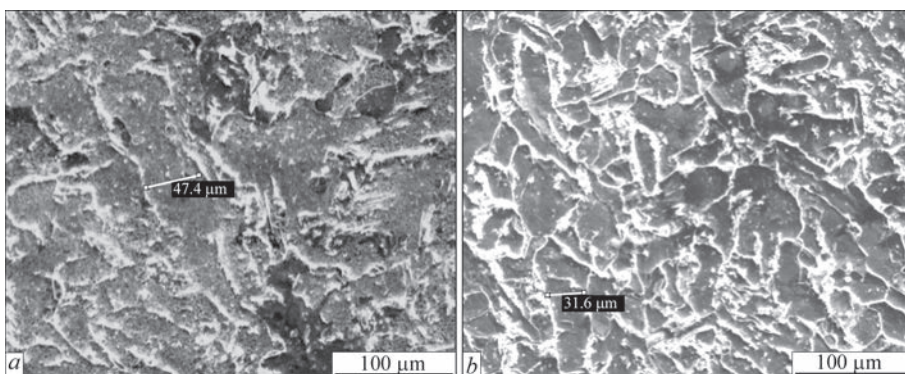


Figure 2. Microstructure of spatial product of the type “thin wall” manufactured by the WAAM (MAG) method using the wire Sv-08G2S: *a* — upper layer; *b* — middle wall of electron microprobe analysis in CamScan-4 analyzer

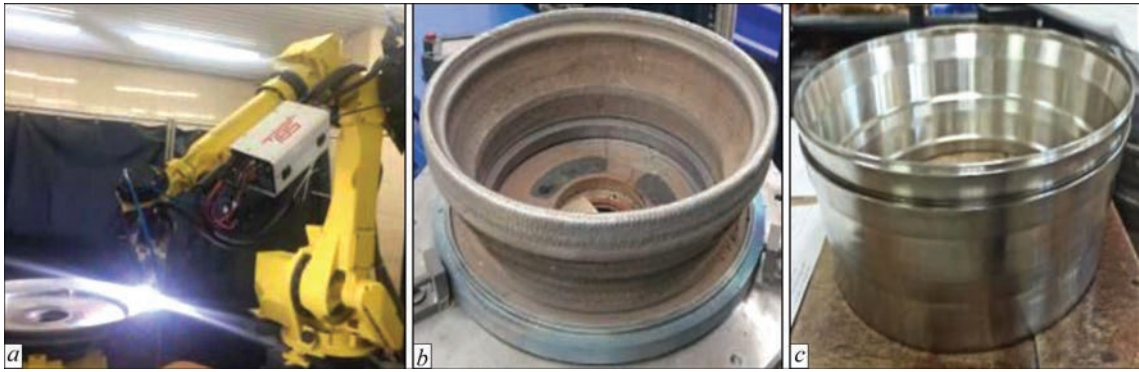


Figure 3. APAS process (3D printing) of a billet of nickel heat-resistant EI 868 (KhN60VT) alloy (a), billet of a part after 3D printing (b), finished part after machining (c) [14]

another phase, which is a part of the eutectic, are revealed between the primary crystals. It can be said, that the eutectic structurally degenerates, it appears in small quantities as a result of nonequilibrium crystallization. Its formation is facilitated by the slowed down cooling compared to microplasma surfacing. The distance between the branches of dendrites of the main ferrite phase during such cooling is quite large, so the eutectic has a coarse structure. There is no formation of oxides, but large sizes of wave-like ridges on the surface can be noted.

The difference between the specimens produced by additive MAG surfacing and the specimens produced by microplasma technology is primarily contained in the tendency of increasing the granularity and sizes of HAZ with an almost unchanged content of silicon and manganese. This can be explained by higher input energies and, accordingly, a higher intensity of heating of the built-up layers during MAG surfacing.

In [12], the principle possibility of using plasma-arc (microplasma) with a pulsed current for 3D printing of steel volumetric metal products with sufficient geometric detailing was also confirmed. At the same time, the grains of the deposited layers change their structure from a relatively small grain size near the substrate to a very coarse structure with a large grain size near the

apex of a product. At the same time, as a material for 3D printing, the possibility of using steel shot with a size of about 1 mm is shown. However, in the case of using such a filler material by the method of microplasma surfacing, the productivity is low (of about 50 g/h) in the case of control of product temperature and cooling after each layer during a certain waiting time [12]. Such an approach allows adjusting the grain size and hardness of printed volumetric steel products.

For the additive manufacturing of components with a complex geometry from carbon and alloy steels, APAS applying wire and powder filler materials is also used in the manufacture of tools with complex contour surfaces for transverse rolling [13].

The successful experience of APAS of critical products of the hot duct of aircraft engines with the use of a filler wire from the nickel heat-resistant EI 868 (KhN60VT) alloy has also been gained (Figure 3) [14].

To provide an optimal combination of a quantity and morphology of strengthening phases of the alloy and a favorable combination of ductility and heat resistance characteristics, the heat treatment was carried out at $T = 1200$ °C. The macrostructure of the specified products, specimens before and after heat treatment is layered, typical for multilayer surfacing with a clear distribution of layers (Figure 4, a, b) [14]. The

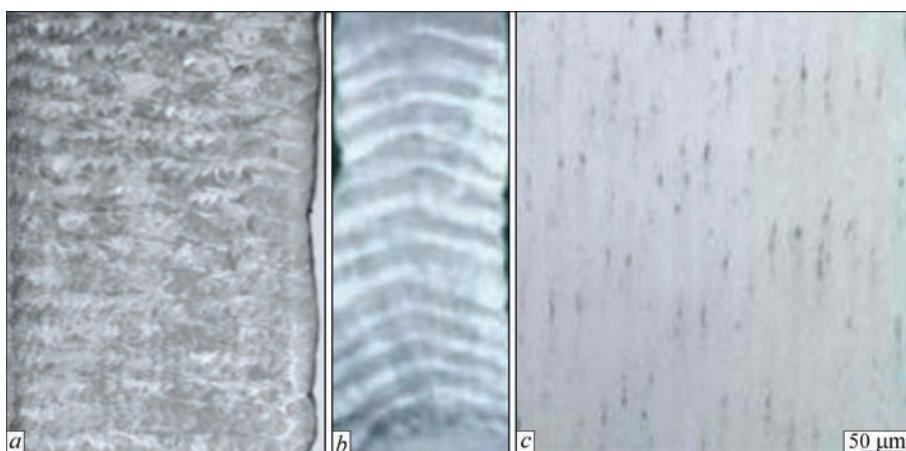


Figure 4. Macro- (a, b) and microstructures (c) of the material of volumetric products of nickel heat-resistant EI 868 (KhN60VT) alloy produced by additive plasma-arc surfacing: a — longitudinal direction; b, c — transverse direction [14]



Figure 5. APAS process of three-dimensional structure of the type “wall” with the use of filler wire from aluminium alloy

microstructure after heat treatment at a magnification of $\times 200$ is shown in Figure 4, *c*. During the analysis of the microstructure of the specimens after heat treatment, the presence of a dendritic structure with elongated grains in the direction of heat removal in the process of layer-by-layer growing (across the layers) was found (Figure 4, *c*). In the microstructure, the fusion lines are invisible and the structure is homogeneous with mutual germination of grains between the layers. The microstructure corresponds to the normal heat-treated state of the EI868 (KhN60VT) alloy, overheating was not detected.

Mechanical tests of the specimens from the indicated heat-resistant nickel EI 868 (KhN60VT) alloy, carried out at $T = 900$ °C, are at the level of values of forgings established by the norms of technical conditions (Table 2).

Thus, the material of volumetric products from the EI868 (KhN60VT) alloy produced by the APAS method meets the requirements of the technical documentation for the manufacture of stator parts of aircraft engines.

1.2. APAS OF VOLUMETRIC PRODUCTS FROM ALUMINIUM ALLOYS

For 3D printing of volumetric products from aluminium alloys, APAS has a number of advantages over other arc methods. In addition to high productivity and ability to regulate heat transfer to the material be-

Table 2. Mechanical properties of specimens from nickel heat-resistant EI 868(KhN60VT) alloy made by APAS [14]

Method of manufacturing specimens for mechanical tests	Mechanical properties		
	σ_p , MPa	$\sigma_{0.2}$, MPa	δ , %
Specimens produced by APAS	Longitudinal direction		
	349	471	48.1
	341	482	59.0
	345	477	53.6
	Transverse direction		
	326	432	64.0
	306	526	66.3
	316	479	65.2
Forging according to TU 27.1001190414-038:2007	> 220	> 450	> 50

ing deposited, this technology helps to overcome the problem of defects arising as a result of oxide refractory films on the surface of aluminium alloys. APAS at direct current of reverse polarity or alternating current provides cleaning of the surface of the previous layer from contaminations due to the effect of cathodic atomization, increased wetting and spreading of liquid metal with minimal heating of the surface, allows providing sufficient detailing of volumetric elements with minimal wall thickness (Figure 5).

In [15, 16], the results of studies of the structure and mechanical properties of 3D specimens produced by additive surfacing of AlMg5 aluminium alloy wire using direct current microplasma technology and the CMT method are given. It was found that these two 3D printing methods are characterized by the same defects as traditional metallurgical processes (Figure 6).

It was found that magnesium is encountered in the form of eutectic veins with a fine differentiation, i.e., with a strong branching and small sizes of Al + Mg eutectic inclusions or compact inclusions with rounded borders. The size of the strengthening phases in the specimens from the indicated AlMg5 alloy, produced by additive microplasma surfacing, is smaller than in the specimens grown by the CMT method, which made it possible in this case to provide higher values of mechanical properties for the microplasma technology (Table 3).

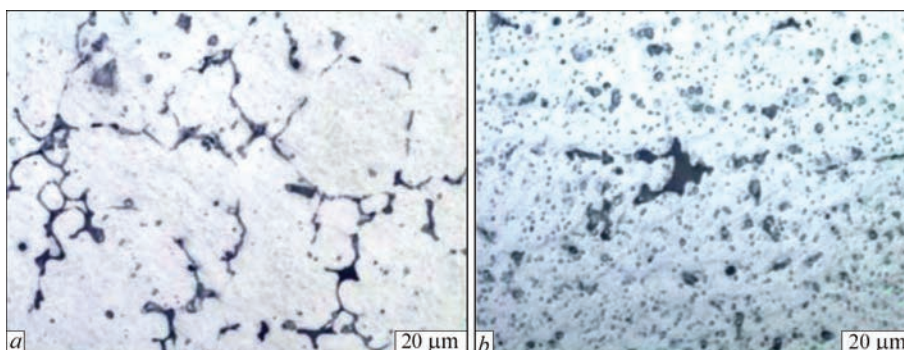


Figure 6. Microstructure of three-dimensional specimens grown by different methods of 3D printing ($\times 500$): *a* — microplasma; *b* — CMT

The results of mechanical tests confirmed that the methods of microplasma and CMT additive surfacing correspond to GOST 17232–99 and EN ISO 18273 standards for aluminium AlMg5 alloy. At the same time, for this alloy, the APAS technology showed a slightly higher level of mechanical properties than for 3D printing using the CMT method.

A comparison of the structure and mechanical characteristics of volumetric products manufactured by APAS of the wire from 5A06 alloy and arc MIG surfacing using a similar consumable electrode shows a significantly lower degree of anisotropy of the structure and mechanical characteristics for plasma-arc technology [13]. For the MIG method, the average values of the tensile and yield strength of the specimens in the direction perpendicular to the orientation of the texture are 251 and 101 MPa. The same indices in the direction parallel to the orientation of the texture are 239 and 90 MPa. The average indices of relative elongation in the direction parallel and perpendicular to the orientation of the texture are 37 and 34 %, respectively. In APAS of 5A06 alloy, the average values of the tensile and yield strength of the specimens in the direction perpendicular to the texture orientation are 295 and 150 MPa. The same indices in the direction parallel to the orientation of the texture are 290 and 145 MPa. In

Table 3. Mechanical properties of volumetric materials from AMg5 alloy produced using different technologies [15, 16]

Method of 3D printing	Mechanical properties		
	σ_t , MPa	$\sigma_{0.2}$, MPa	δ , %
Microplasma additive surfacing	274	154	25.2
CMT additive surfacing	261	124.5	13.7
Norms for AlMg5 alloy according to GOST 17232–99	>270	>120	>13.0
Norms according to EN ISO 18273	250	120	9

general, the strength indices of the specimens produced by APAS of 5A06 wire are at the level of 0.92–0.94 of the strength of the sheet metal 5A06.

The possibility of manufacturing complex-profile cylindrical parts of the “car wheel disc” type, which operate under the conditions of increased dynamic and impact loads, and the “adapter”, APAS wire from aluminium-magnesium 1580 alloy, which is deformable, with additions of scandium at direct current of reverse polarity (Figures 7, 8) [17].

Figure 9 shows the macrostructure of layers of the upper (Figure 9, a) and lower (Figure 9, b) parts of the wall made of aluminium-magnesium 1580 alloy, produced by APAS at direct current of reverse polarity (Table 4) [17]. There are regions of increased growth of



Figure 7. Disc of a car wheel of aluminium-magnesium 1580 alloy, made by APAS at direct current of reverse polarity [17]: appearance of outer surface (a) and inner cavity (b) after 3D printing; appearance after machining (c)



Figure 8. Transition piece of 1580 aluminium-magnesium alloy, made by APAS at direct current of reverse polarity [17]: outer appearance after 3D printing (a) and after machining (b)

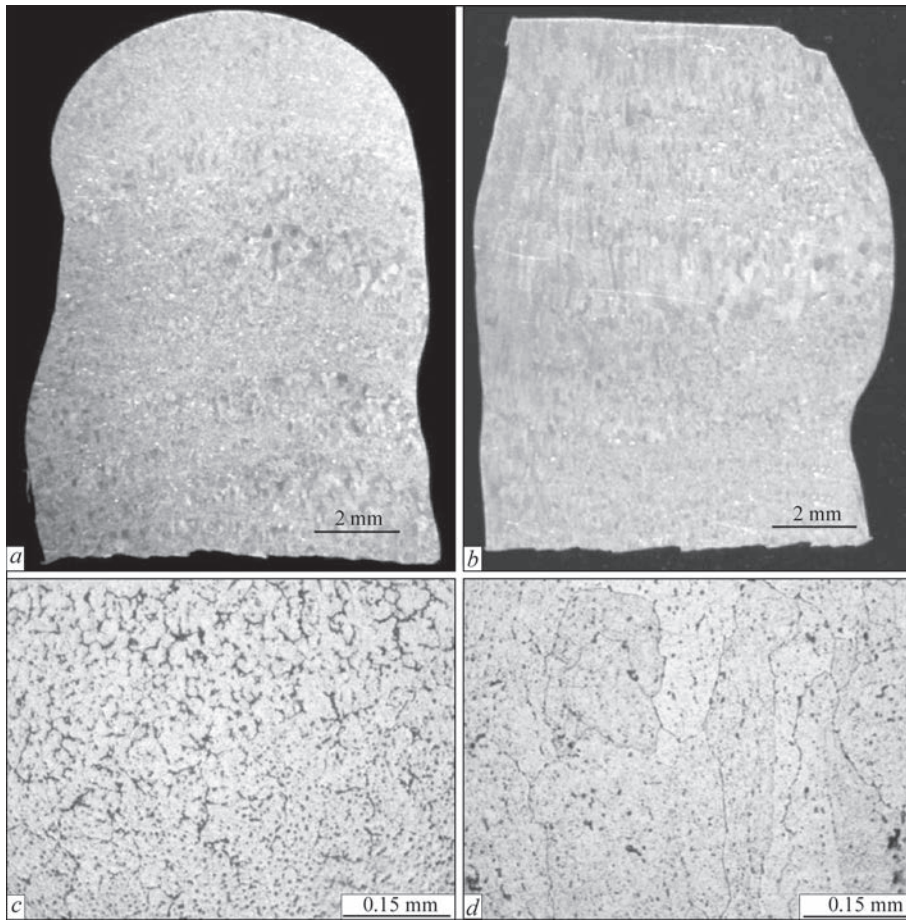


Figure 9. Macro- (*a, b*) and microstructures (*c, d*) of different zones of volumetric elements from 1580 aluminium-magnesium alloy made by APAS at direct current of reverse polarity [17]: *a, c* — upper part; *b, d* — lower part

dendrites on the macrosections, and mainly in the lower part of the surfacing. In the upper part of the surfacing, they are less pronounced, which is explained by a decrease in the effect of thermal cycling and reheating of the metal as the wall grows. There are also differences in the microstructure of the upper (Figure 9, *c*) and lower (Figure 9, *d*) parts of the wall at different magnification. The structure represents an aluminium-magnesium solid solution with individual particles of the primary β -phase (Al_3Mg_2) on the grain boundaries, where clusters of primary intermetallics are also encountered $Al_3(Sc, Ti)$, $Al_3(Sc, Cr)$, Al_3Sc . The microstructure of the upper part of the surfacing (Figure 4, *a*) is more finely dispersed with a larger volume fraction of β -phase precipitation along the grain boundaries — up to 2.5 %. The differences in the microstructure of the lower and upper parts of the surfacing (Figure 9, *c, d*) once again indicate that

the metal heating cycles of the previous layers, which are associated with repeated surfacing, lead to the effect of increased directed growth of dendrites, which is the more intensive, the more often it is repeated.

Therefore, APAS of deformable aluminium-magnesium alloys provides the relative stability of the structural and phase composition of the material of the previous layers under the influence of subsequent thermal cycles in the course of forming a billet. The values of the tensile strength of the surfacings are at the level of the properties of the cast material, inferior to the deformed one; the ductility of the deposited metal significantly exceeds both the ductility of castings — by 2–3 times, and the ductility of annealed rolled semi-finished products — by 1.5 times.

When using APAS on multipolar asymmetric current with the filler wire ER2319 made of high-strength

Table 4. Mechanical properties of aluminium 1580 alloy produced using different deposited materials [17]

Material and specimen state		σ_p , MPa	$\sigma_{0.2}$, MPa	δ , %	φ , %
1580 alloy, APAS	Surfacing 1	294	192	24.5	33.5
	Surfacing 2	296	193	25.0	27.0
P-1580 alloy, cast	Cast rod	312	183	9.1	—
P-1580 alloy, rolling	Hot formed	369	266	16	—
	Cold formed	453	429	5	—
P-1580 alloy, rolling + annealing	Annealed	390	277	14	—

hard-to-weld AlCu6MnZrTi alloy, prone to hot cracking during welding, the tensile strength of a volumetric specimen produced from the deposited metal is 258 MPa, or 63 %, which is 0.63 of the strength of a sheet material of the aluminium-copper 2219 alloy in the state of complete heat treatment [18]. Conducting the heat treatment of such printed material by quenching and artificial aging allows increasing the strength of the metal of a part to 0.8–0.85 of the strength of a massive billet treated in the process of manufacturing and heat-treated. When using the TIG process for 3D printing of this alloy, the average tensile strength is 237 MPa, which is only 57 % of this value for the sheet material from 2319 alloy.

By optimizing the APAS technological modes at alternating (multipolar) current, it is possible to form volumetric products from high-strength aluminium alloys of the Al–Cu–Li (AA2319) system, which also belong to the hard-to-weld class [19]. The structure and properties of the material produced by APAS of this alloy are influenced by the value of the constricted arc current and the wire feed speed, the ratio of direct/reverse current pulses, and the heating temperature of the previous deposited layers. At the same time, any shielding gas atmosphere, composition of the plasma-forming mixture, consumption of working gases and plasma flow rate have a rather significant effect on the reduction of porosity in the deposited layers of this alloy. Thus, during APAS of AA2319 alloy, a high-quality wall was produced at a plasma-arc current of 120 A (frequency of 50 Hz, balance 50 %), deposition rate of 140 mm/min, wire feed rate of 0.9 m/min, when using a mixture of Ar/He15/N0.015 gases, the flow rate of shielding gas is 15 l/min and plasma-forming gas is 0.3 l/min, as well as at a preliminary heating of the substrate to a temperature of 200 °C (Figure 10).

1.3. APAS OF VOLUMETRIC PRODUCTS FROM TITANIUM ALLOYS

The APAS process using both wires and powders is one of the most promising for the production of volumetric titanium parts, including in such industries as aerospace, automotive, shipbuilding and marine engineering [20]. Compared to laser and electron beam additive technologies, it becomes possible to manufacture parts from different materials. The main advantage of this group of technologies is the possibility of 3D printing of large-sized structures at significantly lower consumption of materials and investments [21]. Even without solving the problem of maximum productivity when using APAS technologies, the rate of growing the volume of titanium alloys reaches 170 cm³/h and higher. Such productivity cannot be provided by most beam methods [22].

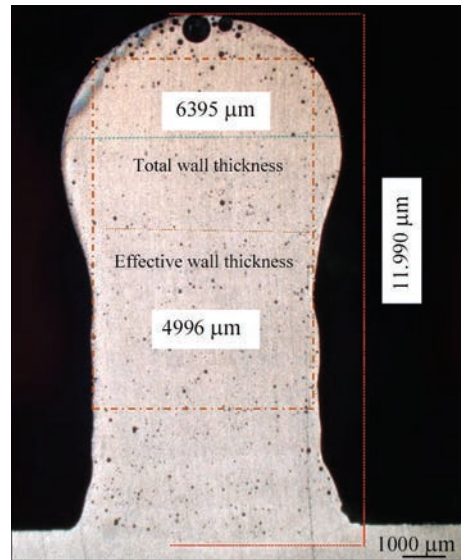


Figure 10. Result of high-quality APAS at alternating current of volumetric element in the form of a multilayered wall from AA2319 alloy of the Al–Cu–Li system [19]

The main technological difficulty of APAS of volumetric products from titanium alloys is the reliable provision of effective gas shielding of both the welding pool as well as regions of parts that can be heated to temperatures above 300 °C. Such heated regions intensively absorb gases from the surrounding atmosphere. To eliminate this, local gas shielding with the help of various devices and systems, as well as

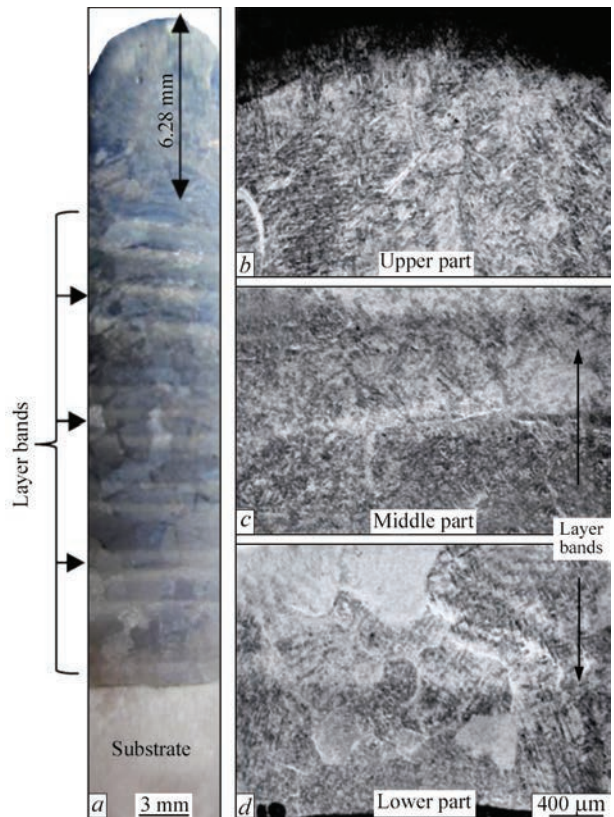


Figure 11. Macro- (a) and microstructure (b–d) of a wall of Ti–6Al–4V alloy, produced by APAS: b — upper region; c — middle region; d — lower region

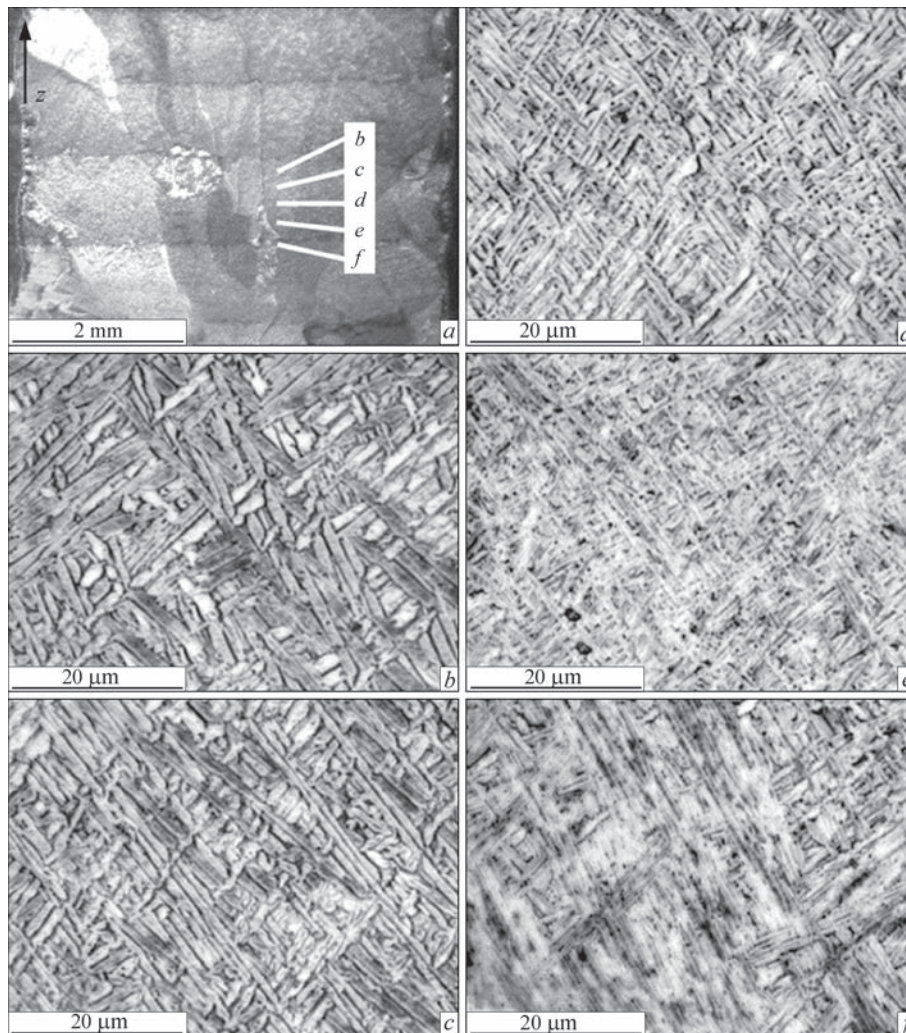


Figure 12. Structures of layer zones of a spatial element of the type “wall” of up to 17.4 mm width, made by APAS with the use of the wire from Ti–6Al–4V alloy: *a* — macrostructure of deposited wall; *b–f* — microstructure of places, mentioned in *a*

3D printing in a controlled atmosphere are used. The most effective solution to the problem of gas shielding is the creation of a special chamber with an argon atmosphere. However, creating such a chamber requires some investment. There is also a limitation of the dimensions of the grown three-dimensional parts by the dimensions of this chamber.

The application of local gas shielding in APAS also allows achieving excellent results and satisfactory mechanical characteristics of printed products from titanium alloys. Thus, when using a pulsed direct current of a plasma-arc power source and a filler wire made of Ti–6Al–4V alloy with a diameter of 1 mm in local gas shielding, spatial defect-free structures with a thickness of 4 mm or more from this alloy with excellent mechanical characteristics can be created [23].

In the process of 3D printing, a coarser-grained structure is formed in the lower layers, and in the layers located above, the size of β -phase grains, martensite and Widmanstätten elements decreases (Figure 11). The similar structures were previously found in the processes of 3D printing of this alloy using laser radiation [24],

as well as WAAM process using a consumable electrode [25]. At the same time, the average yield strength (YS) and ultimate tensile strength (UTS) reach 909 and 988 MPa, respectively, and the elongation reaches about 7.5 %. Such indices exceed the requirements of the standards for this alloy produced by cast technologies, and are also higher than in materials of a similar composition after thermal deformation treatment (forging). This provides grounds for the successful use of such material in the aerospace industry.

The work [26] describes the APAS 3D printing process of Ti–6Al–4V alloy wires, which is aimed at the production of large aerospace components. The technology made it possible to produce direct walls of up to 17.4 mm thick, which provided the maximum wall width after mechanical treatment of 15.9 mm and in this case surpassed the competing processes. The coefficient of using Ti–6Al–4V material was on average 93 %, and the maximum productivity of 3D printing was 1.8 kg/h. During deposition, in the layers facing the substrate, coarse columnar grains were formed, which, upon cooling, turned into a structure

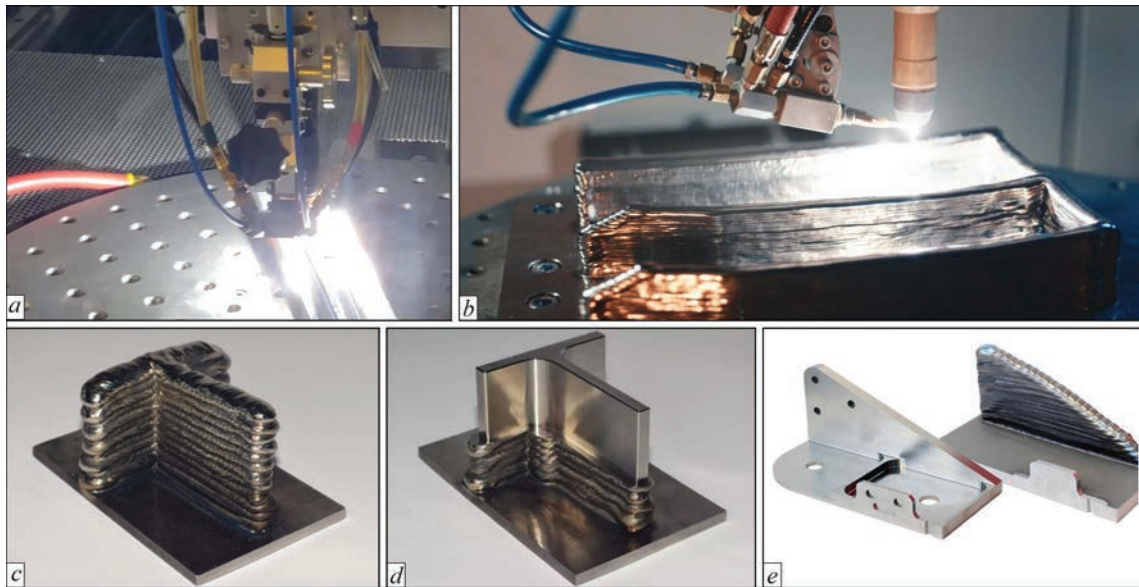


Figure 13. 3D printing process of aircraft parts of titanium alloys using APAS technology in a controlled medium (*a, b*) in Camarc Additive LLC Company, USA and examples of printed parts before and after machining (*c–e*)

of Widmanstätten lamellae (Figure 12). In the deposited layers, bands were found, which had a repeating basket weave microstructure with variable dimensions. It is possible to see an increase in the size of Widmanstätten elements. The average microhardness was 387 *HV*, which is 12 % higher than that of a substrate made of the material of a similar composition.

At present time, some practical experience has been accumulated in the production of aircraft parts from titanium alloys using APAS technology in a controlled environment. As examples of the successful application of this technology in the aerospace industry, it is possible to cite the results obtained by the Companies Camarc Additive LLC, USA (Figure 13) and Norsk Titanium, the Netherlands (Figure 14). Since 2017, the latter has been producing aircraft parts using high-tech industrial machines for 3D printing. The parts, printed by the Norsk Company using the APAS method with titanium alloy filler wires were approved at the federal level for commercial aircrafts Boeing, USA. The technologies used here are not only by 75 % more efficient than conventional forging, but also reduce costs for the manufacture of titanium products by 50–75 % and require fewer resources. Currently, Norsk is joined by a number of other companies in the issue of 3D printing aerospace products, including the British Company Renishaw and Stratasys.

One of the main problems that arise in the APAS 3D printing process, as in practically all additive technologies, is the formation of significant residual stresses in the volumetric structure, which are manifested in the distortion (deformation) of printed elements [27]. To control the influence of heat accumulation on the mass transfer of the filler metal, the wall formation and arc stability during 3D printing of spatial products

from titanium alloys under the conditions of local gas shielding, an infrared pyrometer was used to measure the temperature between passes [28]. The arc stability and metal transfer were monitored using a high-speed chamber. Such an approach makes it possible to optimize APAS modes and minimize the residual stresses.

For the manufacture of thin-walled Ti6Al4V structures, an innovative APAS wire process with forced interpass cooling using a compressed CO₂ was proposed [29]. It was shown that forced interpass cooling not only improves surfacing properties, but also contributes to geometric repeatability and improved production efficiency by reducing the time between layers application.

2. ALLOYING, SYNTHESIS OF NEW ALLOYS, MANUFACTURING VOLUMETRIC PRODUCTS FROM COMPOSITE AND GRADIENT MATERIALS IN PRODUCTION USING APAS TECHNOLOGIES

Additive arc technologies, such as CMT, use a single filler wire, while APAS technology allows feeding multiple wires. Thus, an increase in the produc-



Figure 14. Example of printed aircraft parts from titanium alloys before and after machining, produced by APAS in the controlled medium in the Norsk Titanium Company, Netherlands

Table 5. Combination of different types of steel wires in the technology of double-wire APAS [30]

Materials, produced as a result of 3D printing	Grades of steel wires which were combined in the combinations of a multiwire APAS	
	Material A	Material B
Combination 1	G3Si1	G 19 9 L Si
Combination 2	G 18 L Nb	G 19 9 L Si
Combination 3	G3Si1	G Mn4Ni2CrMo

tivity of using the energy potential of this process is achieved by increasing the number of filler wires. When implementing a multiwire APAS, in this case, an increase in the productivity of the 3D printing process is achieved, which is proportional to a number of filler wires, or a higher stability of the surfacing process and the quality of the deposited material. However, the most promising result of multiwire APAS is the alloying of a volumetric material in the process of 3D printing. Alloying can be local (change in the chemical composition of certain areas of the printed material) or full, which is the synthesis of new alloys in the process of 3D printing of a volumetric product.

German researchers have gained a positive experience in a simultaneous use of two or more filler wires of different chemical composition [30]. Thus,

by changing the rate and diameter of filler wires, it is possible to adjust the chemical composition of certain elements in the deposited metal. Double-wire APAS with a combination of different types of low-alloy ferritic steel wires, as well as wires of austenitic steels containing Ni, Cr, Mo, Nb (Table 5) confirmed the possibility of a smooth change in the chemical composition of the printed material during the 3D printing process and the control of the chemical composition by controlling the arrangement of low and high ductility phases to avoid the negative influence of intermetallic phases (Figure 15) [30].

In argon-arc surfacing using a nonconsumable electrode, also the possibility of adjusting the chemical composition of the deposited metal was confirmed by combining the feed of heterogeneous wires from aluminium 2319 (Al–Cu) and 5087 (Al–Mg) alloys (Figure 16). Thus, spatial products were manufactured from the high-strength 2024 (Al–Cu–Mg) alloy synthesized in the 3D printing process [31]. The regulation of the feed rate of each wire was obtained by the chemical composition of the printed material and its properties, which allowed achieving an optimal combination of physical and mechanical properties of manufactured spatial products (Figure 17) [31].

Namely this possibility of performing additive growing of parts from aluminium wires of different chemical composition was also confirmed when using a multipolar asymmetric current as a heating source using a constricted arc. In APAS with the use of a filler wire, a finer structure of the deposited metal is formed compared to the conventional argon-arc surfacing with a tungsten electrode, which improves the strength indices of parts deposited by APAS by 10–15 % compared to similar indices of parts produced by argon-arc surfacing.

The use of APAS technologies, in which the formation of spatial products can be carried out with simultaneous feeding of different types of powder

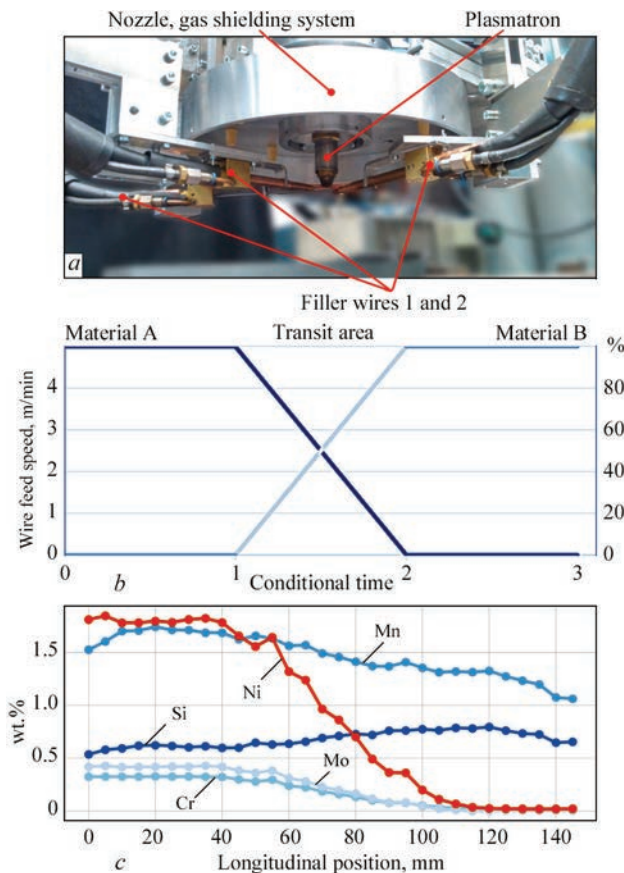


Figure 15. Use of four-wire system in APAS with the feed of heterogeneous wires (a, b) and change of chemical composition over the volume of specimen, produced on the data of combination No. 3 of heterogeneous wires feed (Table 5) (c) [30]



Figure 16. Appearance and microstructure of a product of the type “wall” from synthesized high-strength 2024 (Al–Cu–Mg) alloy produced by additive surfacing with the feed of two heterogeneous types of 2319 (Al–Cu) and 5087 (Al–Mg) aluminium alloys [31]

materials into the plasma-arc (for example, powders of structural, wear-resistant, heat-resistant alloys, carbides, borides, silicides, etc.) opens up the possibilities of creating new volumetric materials with a unique combination of functional properties. Such materials are extremely promising for the production of parts and tools of a new generation, in which, for example, a certain part of the volume provides the specified strength indices, and the other — increased wear resistance, corrosion resistance, heat resistance, special magnetic and electrophysical properties.

Such materials can include:

- metal-ceramic composites of a permanent composition;
- gradient materials (of a variable chemical composition over the volume of a product);
- multilayer materials and their combination with gradient materials.

The examples of such technological developments, produced at the PWI, are mentioned in Figures 18, 19.

Figure 18 shows the process of manufacturing a cylindrical billet of a tool for metal treatment with the use of powder APAS, in which powder of wear-resistant FeNiCrBSH alloy and tungsten carbide WC was supplied from two powder dispensers. Applying automated control of powder feed parameters, the regulation of WC content can be reached in the range of 0–50 rpm % in the surface layers and achieving the hardness of up to 68–70 HRC.

Figure 19 shows an example of APAS of the composition of a titanium alloy and a spherical tungsten carbide (Ti–6Al–4V + WC) applying the hybrid additive technology “plasma surfacing with the use of a filler wire — plasma-powder surfacing”. This technology allows surfacing a volumetric multilayer material of a gradient type (with a layer thickness of about 2 mm) and varying the hardness over the vol-

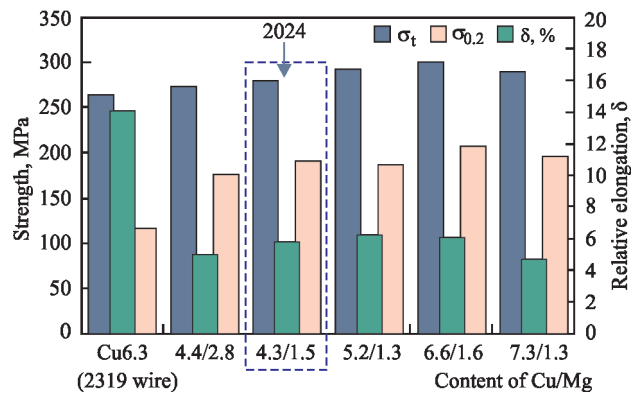


Figure 17. Optimization of physicomechanical properties of volumetric products manufactured by a double-wire APAS with the feed of heterogeneous wires of 2319 (Al–Cu) and 5087 (Al–Mg) aluminium alloys [31]

ume from HRC 32 for the lower layers of titanium alloy to HRC \geq 56 to the surface layers.

4. DIRECTIONS OF EQUIPMENT DEVELOPMENT FOR THE IMPLEMENTATION OF TECHNOLOGICAL CAPABILITIES OF APAS IN ADDITIVE MANUFACTURING

In the creation and the use of equipment for the implementation of 3D printing processes by the APAS method, both directly product manufacturing companies as well as specialized companies that traditionally deal with welding technologies are involved. Thus, the Norsk Company has created 3D printing machines like MERKE IV RPD for the Rapid Plasma Deposition (RPD) process. The specialized Company Camarc Additive’s, USA has developed APAS processes for steels, niobium, titanium and aluminium alloys, for which it has created PAAWS (Plasma-arc Additive Wire System), the equipment of which offers four axes of movement (X , Y , Z and rotation) together with a table for printing with a liquid cooling. Printing in



Figure 18. Process of manufacturing a cylindrical billet of the tool for metal treatment by APAS of powders of wear-resistant FeNiCrBSH alloy and tungsten carbide WC (a, b) and microstructure of a product in different zones (c)

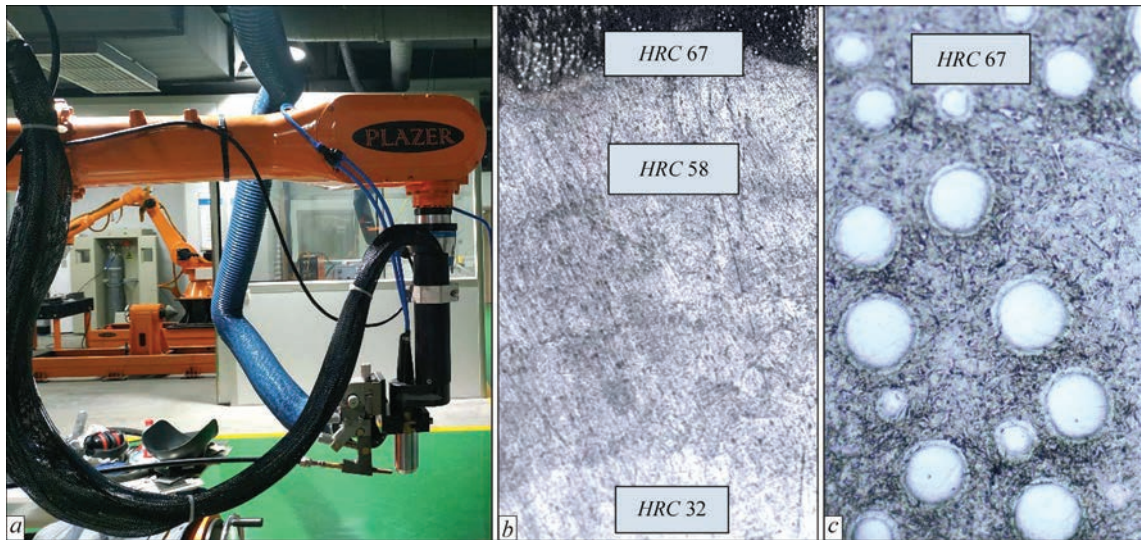


Figure 19. System for implementation of hybrid additive technology of “plasma surfacing using filler wire – plasma-powder surfacing” (a) and structure of the deposited multilayered wall Ti-6Al-4V + WC (b) Ch50, and upper deposited layer (c), Ch200

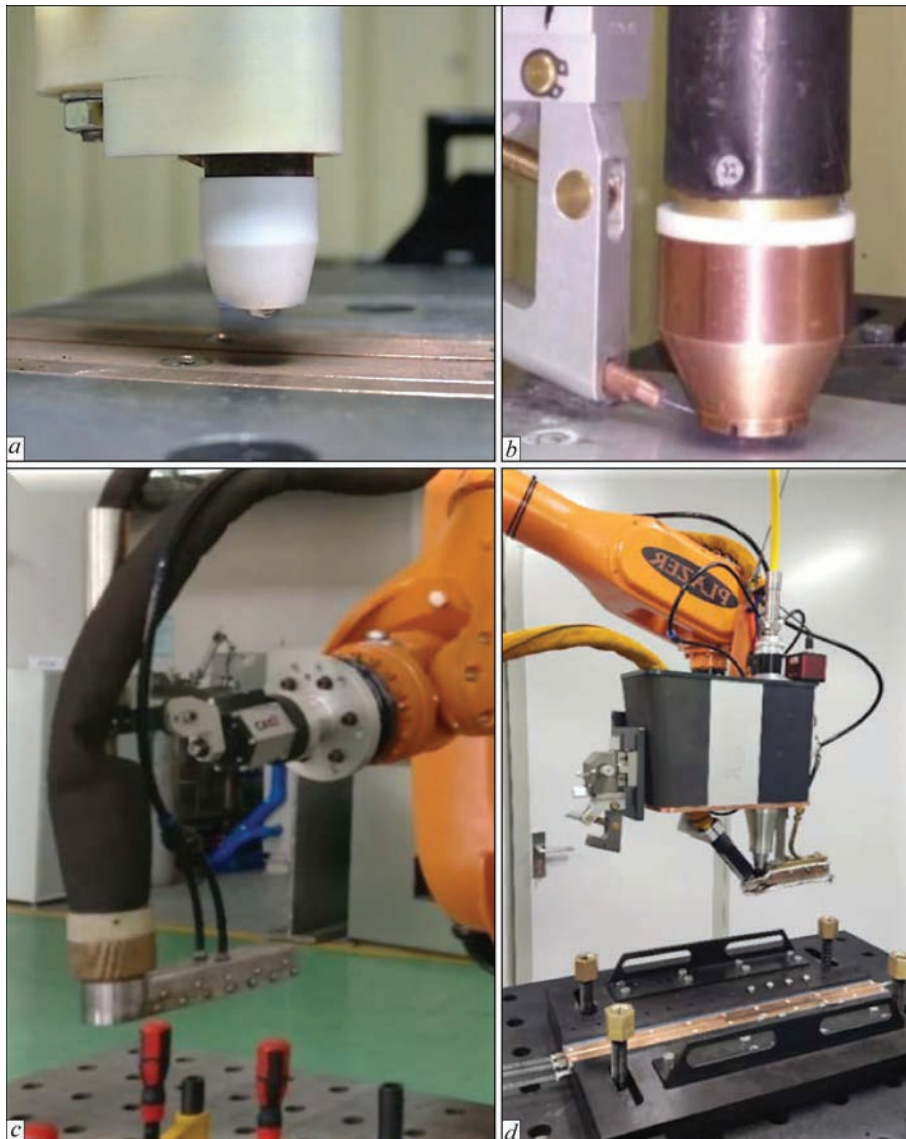


Figure 20. Appearance of plasmatrons designed at the PWI for using in additive manufacturing



Figure 21. General appearance of the robotic complex of equipment for single- and multiwire APAS, powder APAS and hybrid process of “APAS with the use of plasma-arc and arc with consumable electrode” (a), stand with the power sources of a robot, plasmatron, cabinet for adaptation of robot commands and smart automatic system of equipment monitoring (b) and robotic complex for implementation of additive laser-plasma (laser-microplasma) surfacing (c) [32]: 1 — anthropomorphic robot; 2 — plasmatron; 3 — smart control system of robotic welding process; 4 — plasma module; 5 — plasma-arc power source; 6 — table for surfacing with technological equipment; 7 — system for linear movement of robot by rails; 8 — two-axial rotator-manipulator; 9 — mechanism for feeding filler wire

a working field of $1000 \times 10000 \times 600$ mm can be carried out in a closed chamber with a controlled inert atmosphere with a real-time process control. Another well-known manufacturer of 3D printing machines is SBI Company, Austria, whose equipment is designed for the manufacture of products from titanium and aluminium alloys, austenitic and chrome-nickel steels, copper, bronze, etc.) on a direct current of direct polarity or on an alternating current.

At the PWI, in the direction of the development of APAS processes, the main attention is paid to the development of technologies and equipment that allow expanding the technological capabilities of additive manufacturing, increasing the quality of the deposited material, synthesizing new materials with a unique set of properties.

The differences between such technologies lie in the plasma-arc parameters, namely:

APAS is carried out by a plasma-arc of an alternating asymmetric current with a frequency of 150 Hz at currents from 3 A (in the mode of microplasma additive surfacing) to 320 A (in the mode of high-performance additive surfacing with wires of increased diameters or multiwire surfacing) with an accuracy of stabilizing the welding current amplitude up to ± 1 A

for joining materials with a refractory oxide film on the surface (for 3D printing of products from aluminium, magnesium and other light alloys, including such high-strength aluminium alloys that are difficult-to-weld — Al-Cu-Li, Al-Mg-Li, Al-Cu-Mg-Li, Al-Zn-Mg, Al-Zn-Mg-Cu, etc.);

APAS is carried out by a plasma-arc of direct current of direct polarity from 3 A (in the mode of microplasma additive surfacing) to 450 A (in the mode of high-performance additive surfacing with wires of increased diameters or multiwire surfacing) with the superimposition of current modulation with a frequency of up to 2000 Hz (for 3D-printing of alloy and high-strength steels, titanium and nickel alloys, copper, refractory metals, etc.).

These technologies have the following opportunities:

- independent selection of the waveform of alternating current in the half-periods of the passage of the current of direct and reverse polarity;
- the use of pulsed supply of plasma-forming gas (argon) at a set frequency and the difference in consumption of plasma-forming gas, as well as the use of pulsed supply of a filler wire;
- in welding at direct current, the application of the welding wire preheating with an alternating asym-



Figure 22. General appearance of an area with three robotic complexes for 3D printing of large-sized and cylindrical shells and lengthy complex-profile structures of aluminium and titanium alloys with the use of additive plasma-arc technologies

metric current, as well as modulation of the welding current to improve the mixing of the metal pool to be deposited.

For the realization of APAS technologies at the PWI, a variety of local gas shielding systems and a series of plasmotrons and corresponding installations have been developed, for example for:

- additive microplasma powder surfacing and surfacing with filler wires for work on asymmetric alternating and direct current in the current range of 3–35 A (Figure 20, *a*);
- powder APAS and APAS with filler wires for work on asymmetric alternating and direct current for work in the range of currents 50–320 (450 A) (Figure 20, *b*);
- for the realization of the hybrid additive process “plasma surfacing with a filler wire – plasma-powder surfacing” (Figure 18, *a*);
- to implement the hybrid additive process “plasma surfacing using a plasma-arc and an arc with a consumable electrode” (Figure 20, *c*);
- for the implementation of additive laser-plasma (laser-microplasma) surfacing (Figure 20, *d*).

The described processes are used at the Paton Research Institute of Welding Technologies in Zhejiang Province, China in two robotic complexes equipped with a smart automatic control and monitoring system (Figure 21). The mentioned complexes implement 3D printing processes of large-sized parts and bodies of rotation of up to 3000 mm long, up to 600 mm in diameter, 600 mm wide and 1000 mm high. The total weight of a volumetric part reaches up to 1000 kg [32].

At present, the works started on the creation of a technological area at the PWI, which includes three robotic complexes that use the plasma-arc 3D printing technologies described above (Figure 22) and allow manufacturing:

- large-sized (diameter from 100–200 mm to 2–3 m and height of up to several meters and higher) cylindrical shells made of aluminium alloys with elements and inner stiffeners of a complex shape;
- lengthy (up to 4–12 m) structures with a complex profile, including aluminium and titanium alloys and box structures with inner stiffeners.

CONCLUSIONS

1. The potential and advantages of APAS compared to widespread conventional arc WAAM methods, including CMT technology, were revealed and substantiated, namely:

- wide adjustment of 3D printing productivity (0.02–25 kg/h) and a degree of detailing of volumetric elements (from 2.5 to 10–20 mm width) by implementing the process both in the mode of microplasma surfacing with a low-ampere plasma-arc (at currents of 5–35 A) as well as at currents of 50–450 A and higher;
- a wide range of adjustment of input energy, heating zone and penetration depth of previous deposited layers by means of APAS with the use of direct or contacting plasma-arc;
- 3D printing at direct current of direct and reverse polarity, alternating current, including the implementation of the process of cathodic cleaning and destruction of oxide films during surfacing of light metals and alloys with refractory oxide films on their surface;
- 3D printing using powder or wire, including one to four filler wires, with a current-conducting filler wire with preheating;
- implementation of hybrid 3D printing technology — combination of a plasma-arc with an arc or laser heating source;
- implementation of 3D printing process using an additive that does not move together with plasmatron during layer surfacing (metal grit, foil, thin bands of

metal) and applied alternately after surfacing of each layer (analogue of lamination);

- the possibility of using plasma-arc without the addition of wire or powder, which allows performing a preheating of the base or deposited layers before additive surfacing.

2. The possibilities of using APAS technologies for manufacture of volumetric products from structural, alloyed and high-strength steels, heat-resistant nickel alloys, aluminium high-strength alloys, titanium alloys with physical and mechanical characteristics that contain mostly 90 % or higher of the indices of similar materials produced by conventional metallurgical methods were confirmed, which in a number of cases meet the requirements of the standards for such materials after thermomechanical treatment.

3. New possibilities of using APAS are shown, in which the formation of spatial products can be carried out with a simultaneous feeding of different types of heterogeneous wires of powder materials (for example, powders of structural, wear-resistant, heat-resistant alloys, carbides, borides, silicides, etc.) or with the simultaneous feeding of wire and powder (granules) into the plasma-arc. This allows carrying out local or volumetric alloying of the material of a volumetric product, performing 3D printing simultaneously with the synthesis of new alloys, creating new materials with a unique combination of functional properties (metal-ceramic composites of a permanent composition, gradient materials of a variable chemical composition over the volume of a product, multilayer materials and their combination with gradient materials). Such materials are promising for the production of critical parts and tools of the new generation, in which, for example, a certain part of the volume provides the specified strength indices, and the other — increased wear resistance, corrosion resistance, heat resistance, special magnetic and electrophysical properties.

4. At the PWI of the NASU, a number of innovative APAS technologies were developed and corresponding original equipment for 3D-printing of large-sized products from aluminium and titanium alloys were created, including for the implementation of:

- additive microplasma powder surfacing and surfacing using filler wires for work on asymmetric alternating and direct current in the range of currents of 3–35 A;

- powder APAS and APAS using filler wires for work on asymmetric alternating and direct current for work in the range of currents of 50–320 (450 A);

- hybrid additive process “plasma surfacing using a filler wire – plasma-powder surfacing”;

- hybrid additive process “plasma surfacing using a plasma-arc and an arc with a consumable electrode”;

- additive laser-plasma (laser-microplasma) surfacing.

REFERENCES

1. Laue, R., Colditz, P., Möckel, M., Awiszus, B. (2022) Study on the milling of additive manufactured components. *Metals*, **12**, 1167. DOI: <https://doi.org/10.3390/met12071167>
2. Antonysamy, A.A. (2012) *Microstructure, texture and mechanical property evolution during additive manufacturing of Ti6Al4V alloy for aerospace applications: Microstructure*. University of Manchester, Faculty of Engineering and Physical Sciences.
3. Peleshenko, S., Korzhyk, V., Voitenko, O. et al. (2017) Analysis of the current state of additive welding technologies for manufacturing volume metallic products (Review). *Eastern European J. of Enterprise Technologies*, 3/1(87), 42–52. DOI: <https://doi.org/10.15587/1729-4061.2017.99666>
4. Kvasnytskyi, V., Korzhyk, V., Lahodzynkyi, I. et al. (2020) Creation of volumetric products using additive arc cladding with compact and powder filler materials. In: *Proc. of the 2020 IEEE 10th Inter. Conf. on Nanomaterials: Applications and Properties, 9–13 November, NAP 2020*, 9309696. DOI: <https://doi.org/10.1109/NAP51477.2020.9309696>
5. Korzhik, V.N., Khaskin, V.Yu., Grinyuk, A.A. et al. (2016) 3D-printing of metallic volumetric parts of complex shape based on welding plasma-arc technologies (Review). *The Paton Welding J.*, **5–6**, 117–123. DOI: <https://doi.org/10.15407/tpwj2016.06.20>
6. Ge, J., Lin, J., Lei, Y., Fu, H. (2017) Location-related thermal history, microstructure, and mechanical properties of arc additively manufactured 2Cr13 steel using cold metal transfer welding. *Materials Sci. & Eng.: A*, **715**, 144–153. DOI: <https://doi.org/10.1016/j.msea.2017.12.076>
7. Alberti, E.A., Bueno, B., D’Oliveira, A.S. (2015) Additive manufacturing using plasma transferred arc. *The Inter. J. of Advanced Manufacturing Technology*, **83**, 9–12. DOI: <https://doi.org/10.1007/s00170-015-7697-7>
8. Colegrove, P., Williams, S. (2013) *High deposition rate high quality metal additive manufacture using wire + arc technology*. Cranfield University. <https://www.xyzist.com/wp-content/uploads/2013/12/Paul-Colegrove-Cranfield-Additive-manufacturing.pdf>
9. Özel, T., Shokri, H., Loizeau, R. (2023) A review on wire-fed directed energy deposition based metal additive manufacturing. *J. Manuf. Mater. Process.*, **7(1)**, 45. DOI: <https://doi.org/10.3390/jmmp7010045>
10. Korzhik, V.N., Vojtenko, A.N., Peleshenko, S.I. et al. (2017) Development of automated equipment for manufacturing 3D metal products based on additive technologies. *The Paton Welding J.*, **5–6**, 79–85. DOI: <https://doi.org/10.15407/tpwj2017.06.15>
11. Alhuzaim, A.F. (2014) *Investigation in the use of plasma-arc welding and alternative feedstock delivery method in additive manufacture*. Master of Science General Engineering. Montana Tech. of the University of Montana.
12. Alaluss, K., Mayr, P. (2019) Additive manufacturing of complex components through 3D plasma metal deposition — A simulative approach. *Metals*, **9(5)**, 574. DOI: <https://doi.org/10.3390/met9050574>
13. Geng, H., Li, J., Xiong, J. et al. (2017) Geometric limitation and tensile properties of wire and arc additive manufacturing 5A06 aluminium alloy parts. *J. of Materials Engineering and Performance*, **26**, 621–629. DOI: <https://doi.org/10.1007/s11665-016-2480-y>
14. Gnatenko, M., Chigileichik, S., Sakhno, S. (2021) Manufacture of aviation parts from heat-related nickel alloys by multilayer plasma surfacing. *Aerospace Technic and Technology*, **175(5)**, 48–52 [in Ukrainian]. DOI: <https://doi.org/10.32620/akt.2021.5.06>

15. Gnatenko, M., Zhemaniuk, P., Petrik, I. et al. (2019) Detecting the influence of heats sources on material properties when production aviation parts by a direct energy deposition method. *Eastern-European J. of Enterprise Technologies*, 1(12(97)), 49–55. DOI: <https://doi.org/10.15587/1729-4061.2019.157604>
16. Gnatenko, M., Naumyk, V., Matkovska, M. (2019) Influence of sources of heating and protective gases on the properties of the material obtained by the direct deposition. *Materials Science and Technology*, 68–74. DOI: https://doi.org/10.7449/2019/MST_2019_68_74
17. Grinyuk, A.A., Korzhik, V.N., Shevchenko, V.E. et al. (2015) Main tendencies in development of plasma-arc welding of aluminium alloys. *The Paton Welding J.*, **11**, 31–41. DOI: <https://doi.org/10.15407/tpwj2015.11.04>
18. Bai, J.Y., Yang, C.L., Lin, S.B. et al. (2016) Mechanical properties of 2219-Al components produced by additive manufacturing with TIG. *Int. J. Adv. Manuf. Technol.*, **86**, 479–485. DOI: <https://doi.org/10.1007/s00170-015-8168-x>
19. Qi, Z., Cong, B., Qi, B. et al. (2018) Microstructure and mechanical properties of double-wire + arc additively manufactured Al–Cu–Mg alloys. *J. of Materials Processing Technology*, **255**, 347–353. DOI: <https://doi.org/10.1016/j.jmatprotec.2017.12.019>
20. Lin, Z., Song, K., Yu, X. (2021) A review on wire and arc additive manufacturing of titanium alloy. *J. of Manufacturing Processes*, **70**, 24–45. DOI: <https://doi.org/10.1016/j.jmapro.2021.08.018>
21. Hoefler, K., Mayr, P. (2018) Additive manufacturing of titanium parts using 3D plasma metal deposition. *Mat. Sci. Forum*, **941**, 2137–2141. DOI: <http://dx.doi.org/10.4028/www.scientific.net/MSF.941.2137>
22. R'ios, S., Colegrove, P.A., Williams, S.W. (2019) Metal transfer modes in plasma wire + arc additive manufacture. *J. of Materials Processing Tech.*, **264**, 45–54. DOI: <https://doi.org/10.1016/j.jmatprotec.2018.08.043>
23. Lin, J.J., Lv, Y.H., Liu, Y.X. et al. (2016) Microstructural evolution and mechanical properties of Ti–6Al–4V wall deposited by pulsed plasma-arc additive manufacturing. *Materials & Design*, **102**, 30–40. DOI: <https://doi.org/10.1016/j.matdes.2016.04.018>
24. Kelly, S.M., Kampe, S.L. (2004) Microstructural evolution in laser-deposited multilayer Ti–6Al–4V builds: Pt II. Thermal Modeling. *Metall Mater. Transact.: A*, **35**(6), 1869–1879. DOI: <https://doi.org/10.1007/s11661-004-0095-7>
25. Xu, F.J., Lv, Y.H., Xu, B.S., Liu, Y.X. (2013) Effect of deposition strategy on the microstructure and mechanical properties of Inconel 625 superalloy fabricated by pulsed plasma-arc deposition. *Mater.*, **45**, 446–455. DOI: <https://doi.org/10.1016/j.matdes.2012.07.013>
26. Martinaa, F., Mehnen, J., Williams, S.W. et al. (2012) Investigation of the benefits of plasma deposition for the additive layer manufacture of Ti–6Al–4V. *J. of Materials Processing Technology*, **212**(6), 1377–1386. DOI: <https://doi.org/10.1016/j.jmatprotec.2012.02.002>
27. Colegrove, P.A., Martina, F., Roy, M.J. et al. (2014) High pressure interpass rolling of wire + arc additively manufactured titanium components. *Advanced Materials Research*, **996**, 694–700. DOI: <https://doi.org/10.4028/www.scientific.net/AMR.996.694>
28. Wu, B., Ding, D., Pan, Z. et al. (2017) Effects of heat accumulation on the arc characteristics and metal transfer behavior in wire arc additive manufacturing of Ti6Al4V. *J. of Materials Processing Technology*, **250**, 304–312. DOI: <http://dx.doi.org/10.1016/j.jmatprotec.2017.07.037>
29. Wua, B., Pana, Z., Dingb, D. et al. (2018) The effects of forced interpass cooling on the material properties of wire arc additively manufactured Ti6Al4V alloy. *J. of Materials Processing Technology*, **258**, 97–105. DOI: <https://doi.org/10.1016/j.jmatprotec.2018.03.024>
30. Reisgen, U., Sharma, R., Oster, L. (2019) Plasma multiwire technology with alternating wire feed for tailor-made material properties in wire and arc additive manufacturing. *Metals*, **9**(7), 745. DOI: <https://doi.org/10.3390/met9070745>
31. Qi, Z., Cong, B.Q., Qi, B. et al. (2018) Microstructure and mechanical properties of 1 double-wire + arc additively manufactured Al–2 Cu–Mg alloys. *J. of Material Processing Technology*, **255**, 347–353. DOI: <https://doi.org/10.1016/j.jmatprotec.2017.12.019>
32. Korzhyk, V.M., Grynyuk, A.A., Khaskin, V.Yu. et al. (2023) Influence of the speed of plasma-arc welding at a variable polarity asymmetrical current on the formation of joints of high-strength aluminium alloys. *The Paton Welding J.*, **8**, 17–28. DOI: <https://doi.org/10.37434/tpwj2023.08.02>

ORCID

V.M. Korzhyk: 0000-0001-9106-8593,
 A.A. Grynyuk: 0000-0002-6088-7980,
 V.Yu. Khaskin: 0000-0003-3072-6761,
 O.M. Voitenko: 0000-0003-4946-6517,
 O.M. Burlachenko: 0000-0003-2277-4202,
 O.O. Khuan: 0009-0001-2623-5321

CONFLICT OF INTEREST

The Authors declare no conflict of interest

CORRESPONDING AUTHOR

V.M. Korzhyk
 E.O. Paton Electric Welding Institute of the NASU
 11 Kazymyr Malevych Str., 03150, Kyiv, Ukraine.
 E-mail: vnkorzhyk@gmail.com

SUGGESTED CITATION

V.M. Korzhyk, A.A. Grynyuk, V.Yu. Khaskin, O.M. Voitenko, O.M. Burlachenko, O.O. Khuan (2023) Plasma-arc technologies of additive surfacing (3D printing) of spatial metal products: application experience and new opportunities. *The Paton Welding J.*, **11**, 3–20.

JOURNAL HOME PAGE

<https://patonpublishinghouse.com/eng/journals/tpwj>

Received: 26.10.2023

Accepted: 07.12.2023

INFLUENCE OF GMAW AND PAW METHODS OF ADDITIVE ARC SURFACING AND SHIELDING GAS COMPOSITION ON SURFACE GEOMETRY AND METAL STRUCTURE OF PRODUCTS FROM LOW-CARBON 09G2S STEEL

V.V. Kvasnytskyi, I.M. Lahodzinskyi

National Technical University of Ukraine “Igor Sikorsky Kyiv Polytechnic Institute”
37 Prospect Beresteyskiy (former Peremohy), 03056, Kyiv, Ukraine

ABSTRACT

With the development of Wire Arc Additive Manufacturing (WAAM) technologies, there is a need in ensuring stable quality characteristics of spatial products, and it is desirable to obtain a final surface with minimal geometrical nonuniformity. Arc surfacing, in particular the process with short-circuiting (Cold Metal Transfer — CMT), and pulse-arc surfacing (Pulse process) allow improving the control of weld pool melt behaviour, and reducing material losses for spatter and burn-out, which ensures higher productivity of the process. At the same time, investigations of the regularities of the influence of arc melting methods, in particular CMT, Pulse and PAW technologies, and the composition of shielding gas atmosphere on the formed layer geometry, deposited metal structure and proneness to defect formation are urgent. Analysis of specimen geometry indicates that the shielding gas mixture composition has an essential influence on the deposited layer height, irrespective of the surfacing method (CMT/Pulse). Thus, for M11 mixture, the height of individual beads increases by 0.4–11.7 %, compared to the use of M21 mixture. Application of pulsed current leads to 10–11 % increase in the bead width, compared to CMT process. Metallographic examinations reveal that the metal product structure is typical for multilayer surfacing. A clear boundary between the individual deposited metal layers was not revealed.

KEYWORDS: WAAM, GMAW, Cold Metal Transfer, plasma, additive technologies, 09G2S, layer-by-layer surfacing, shielding gas mixture

INTRODUCTION

The rapid development of industry requires optimization of the existing technological processes of manufacturing not only individual products (prototypes, models), but also serial ones. However, from the point of view of serial manufacturing, there is a problem of the ratio of the cost of raw materials spent on the fabrication of a product and the cost of a final product. I.e., the amount of wastes remaining after the final processing of a product significantly affects the cost of each unit of a finished product. In other words, it is necessary to reduce the BTF — Buy to Fly ratio, which is used in the aerospace industry, which will provide a reduction in the amount of waste after final treatment [1].

Wire Arc Additive Manufacturing (WAAM) is a kind of additive manufacturing technology based on the use of arc heat sources and a compact filler material [2]. The processes of additive arc manufacturing using an electric arc (WAAM) are based on the principle of layer-by-layer bead surfacing. In contrast to the welding process, where the main role is played by the penetration depth and filling of the edge preparation with filler metal, in additive processes, on the contrary, researchers are trying to obtain the smallest penetration of the base (substrate) and mixing of the metal of the next layer with the previous one. They

are also trying to achieve the highest possible height when building each individual bead.

The technology of Gas Metal Arc Welding (GMAW) surfacing with a consumable electrode in shielding gases has gained a significant development. This method involves continuous feeding and melting of a solid cross-section wire in a shielding gas. Thus, surfacing is carried out with the help of electric arc heating and continuous melting of the filler wire, which is deposited to the base surface. The weld pool and arc exist in the atmosphere of active or inert shielding gases. The process makes it possible to widely adjust the mechanical properties of manufactured products by using a diverse range of welding consumables for surfacing. The main advantages of using GMAW technologies in additive manufacturing are sufficiently high accuracy of bead formation during the central (axial) feeding of the electrode wire; a small number of controlled parameters of the surfacing mode, which contributes to the ease of the process control and its automation; simplicity, availability and relatively low cost of equipment.

However, the mentioned processes also have a number of disadvantages: relatively large heat input compared to highly concentrated heat sources (laser, electron beam); presence of significant metal spattering in the process of surfacing when using typical

gases or methods [3]. In order to reduce the heat input into the preliminary formed layers, the technology of Cold Metal Transfer (CMT) and pulsed arc (Pulse) processes is successfully used [4]. Regulation of the heat input allows a significant expansion of the range of materials suitable for GMAW technologies.

It is known that GMAW processes are characterized by quite significant nonuniformity of the surface produced by layer-by-layer formation [5]. The geometric accuracy and nonuniformity of the deposited layer surface are significantly influenced by surfacing modes, in particular, the value of current, arc voltage, filler wire feed rate and torch movement [6, 7]. It is also necessary to take into account the direction of the surfacing trajectory when generating subsequent layers [8]. A separate important influence parameter is the shielding gas mixture composition, since it is known that the presence of oxygen changes the value of the surface tension of the weld pool metal melt.

The main role of gas mixtures in GMAW processes consists in shielding the weld pool metal melt from interaction with environmental gases. Also, the shielding gas composition significantly affects the degree of arc gap ionization and, as a result, the arc burning stability. The authors of [9] confirmed the influence of the shielding gas composition on the process of metal transfer through the welding arc and on the geometric shape of deposited beads. The issue of the influence of shielding gas mixture components on the formation of shapes and surface nonuniformity during additive growing of products was considered in [10] regarding products of low-carbon steel of type 09G2S. The authors note that the thermal conductivity of each specific gas in the mixture also has a significant impact on the surface nonuniformity. Thus, gases with the lowest value of thermal conductivity, in particular Ar, contribute to lower heat input and, as a result, spread of the weld pool metal. When applying the CMT process, a decrease in the deviation from the straightness of the bead generatrix in the vertical direction is achieved, and the losses of filler material on spattering are reduced, which increases the material utilization ratio. The authors of [11] also confirmed that gases with higher thermal conductivity, in particular He, when added to gas mixtures of Ar–CO₂ composition, although lead to a decrease in the arc spot radius, which contributes to the formation of narrower beads, they also cause an increase in the penetration depth of the preliminary formed layers. As a result, a significant deviation of the geometric shape of the formed product walls is observed during successive surfacing of the subsequent layers. From the point of view of effective use of the material, this effect is negative, as the amount of metal waste grows during final machining. In addition to the influence on the geometric shape of the beads, different gas mixtures significant-

ly affect the formation of the deposited metal structure. Thus, in [12] the authors considered the effect of the content of carbon dioxide in the mixture with argon on the deposited metal structure formation for high-strength steels (with strength of up to 950 MPa). The authors determined the ratio of the content of acicular and Widmanstätten ferrite and found that with an increase in the concentration of CO₂ in the composition of shielding gas, the amount of Widmanstätten ferrite grows. In [13–15], based on the results of their own research, the authors confirmed the influence of the composition of gas mixtures on the formation of the deposited metal structure. In particular, in [13] a comparison of geometric characteristics and quantity of individual structural components in the deposited metal is given. An important characteristic is the amount of nonuniformity of the specimen surface, which requires the introduction of the necessary tolerance for surface treatment to obtain a finished product. However, when studying the influence of gas mixtures composition on geometric characteristics of deposited layers during additive surfacing, as a rule, only GMAW surfacing or its variant — CMT process are considered. The literature provides limited information on the influence of the gas environment composition when using the Pulse process [16].

The aim of the work is to establish the regularities of the effect of GMAW-CMT/Pulse and PAW methods of arc surfacing and the shielding gas environment composition on geometric characteristics of the surfaces of products of low-carbon 09G2S steel, the structure of the deposited metal and the proneness to defect formation.

To achieve the aim, it was necessary to complete the following tasks:

- to analyze the information available in the literature regarding the peculiarities of the formation of the geometric shape and structure of the metal, proneness to the formation of defects in the walls of products manufactured using WAAM technologies of additive manufacturing with heating of a compact filler material with arc heat sources;
- to produce specimens of a layer-by-layer deposited metal using GMAW-CMT/Pulse and PAW methods of arc surfacing in the environment of active gas M11 and M21 mixtures and a solid cross-section wire from low-carbon 09G2S steel;
- to investigate geometric characteristics of the surfaces of produced specimens;
- to investigate the features of the metal structure of specimens, produced by GMAW-CMT/Pulse and PAW methods of arc surfacing, and the proneness to defect formation.

PROCEDURE OF EXPERIMENTS

In the studies of GMAW and PAW surfacing, a test bench for surfacing rectilinear beads was used (Fig-

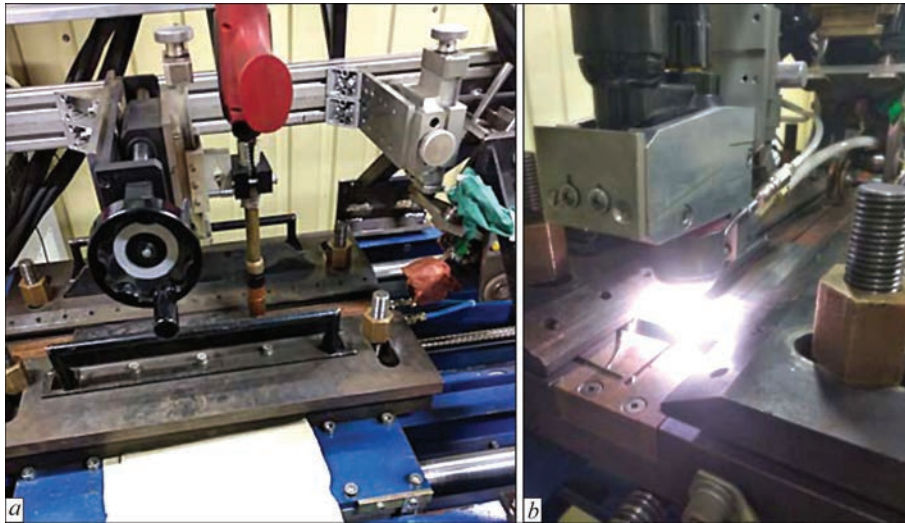


Figure 1. Test bench: *a* — suspended equipment for GMAW surfacing; *b* — plasma torch for PAW-CW surfacing

ure 1, *a*). As a power source, Fronius TransPulse Synergic 2700 unit in combination with PullMig CMT MHP 400i welding torch was used. For plasma surfacing, a specialized plasma torch was used, designed by NVTs Plazer LLC Company (Figure 1, *b*) in combination with Tetrax 421 power source and Fronius duty arc ignition module. The design of the torch provides a side feed of the filler wire and thus the process of PAW-CW (Cold Wire) surfacing is implemented. The filler wire was fed by a separate feed unit with a synchronous start. Surfacing of specimens by GMAW using Pulse and CMT methods was carried out by successive formation of individual layers in a reciprocating direction. For PAW method, the movement for each new layer formation is one-sided. The electrode wire diameter for all used grades of filler wires remained constant and amounted to $d_e = 1.2$ mm, the length of the formed walls was ~ 100 mm, the quantity of layers was 50.

Surfacing of layers by GMAW-CMT/Pulse methods was performed on 10 mm thick plates of E235-S (St3sp) steel. Layer-by-layer surfacing was performed with an electrode solid cross-section wire of type G3Si1 (Sv-09G2S). To determine the influence of the gas shielding environment composition on geometric characteristics of the deposited layers and deposited metal structure formation during additive surfacing of low-carbon steels, the gas mixtures M21 (Ar 82 % + CO₂ 18 %) and M11 (Ar 98 % + CO₂ 2 %) were used

as the most common in welding production. For each of the gas mixtures, surfacing of three specimens was performed using the CMT and Pulse methods.

Specimens were also produced by plasma-arc surfacing of a solid cross-section wire. The method of PAW-CW (Cold Wire) surfacing was used to manufacture specimens from low-carbon steel. The specimens were deposited on the substrates in the form of plates from E 235-S (St3sp-killed) steel of 10 mm thickness. As a filler material, the wire of type G3Si1 (Sv-09G2S) was used. Taking into account the features of the plasma torch, namely the possibility of a separate supply of the plasma-forming and shielding gas, argon was used as the plasma-forming gas, and as a shielding gas, M11 mixture (Ar 98 % + CO₂ %) was used. The modes of layer-by-layer surfacing of specimens are given in Table 1. The input energy of surfacing specimens was determined by calculation (Table 1).

When choosing the temperature conditions for surfacing of individual layers, the strategy of interlayer cooling to 120 °C, proposed in [17], was chosen. Cooling of each individual layer was carried out in order to avoid excessive overheating of preliminary deposited layers.

To avoid overheating and distortion of the metal structure, after surfacing specimens for micro- and macrostructure examinations were cut out from the formed walls by mechanical means with the use of a

Table 1. Modes of layer-by-layer arc surfacing of specimens

Method	Filler material	Shielding gas	Input energy, J/mm	Current, A	Voltage, V	Nozzle diameter, mm	Wire feed rate $V_{w,p}$, m/min	Surfacing rate V_s , mm/min	Gas flow rate, l/min
GMAW-CMT	G3Si1 (Sv-09G2S)	M21	157	131	12	16	3.5	600	15
		M11	146	133	11				
GMAW-Pulse		M21	240	120	20				
		M11	262	131	20				
PAW-CW	Ar	262	202	13	4	3.5	600	0.6	
	M11							15	

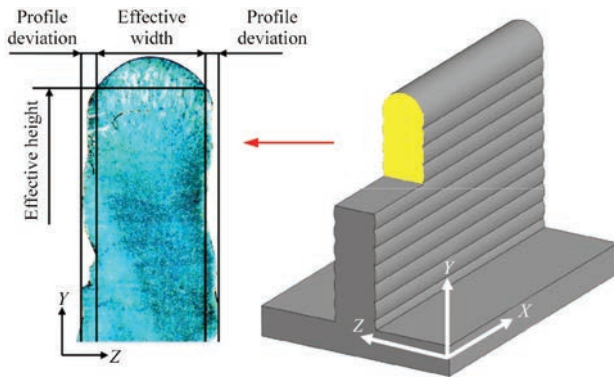


Figure 2. Determination of parameters of effective height, effective thickness and maximum profile deviation

lubricating and cooling liquid. Determination of the metal structure of the specimens was carried out by chemical etching in a 4 % alcoholic solution of nitric acid (HNO_3). The examinations were carried out in a Neophot-32 metallographic optical microscope. Metallographic examination of nonmetallic inclusions in the metal was carried out according to the scales of GOST 1778–70. The determination of grain size was carried out by comparison with the scales of GOST 5639–82. The hardness of phase components was measured by the Vickers method by means of LECO M-400 microhardness tester.

RESEARCH RESULTS AND THEIR DISCUSSION

The presented results of the analysis of changes in geometric characteristics of deposited specimens depending on the parameters of the surfacing modes, the applied method of GMAW surfacing (CMT or Pulse) in combination with different shielding environments are shown in Figures 3–6. These dependencies are quite important, because they are related to the amount of material spent on the finishing treatment of a generated billet of a product, since during additive surfacing, the shape of an almost finished part or a product with a tolerance for

finishing is created. To evaluate geometric characteristics of products, the approach proposed in [10] using the effective height and effective wall width parameters was chosen (Figure 2). By analogy with tribotechnics, to evaluate geometric characteristics of the formed surface of products, the index of the maximum value of the wall profile deviation on both sides from the central axis is used (Figure 2). The smaller the deviation index, the closer the shape of a billet approximates to the shape of a finished product and the higher the efficiency of the material use. After all, during the final treatment, the tolerance for treatment and the material, which represents a scaly surface of a deposited product, go into waste.

A feature of the coarse of GMAW-CMT process (metal transfer with short circuits) is an almost complete exclusion of the phenomenon of metal spattering in the surfacing process. However, with a change in the gas mixture composition, the thermal conductivity of the gas environment and, as a result, the level of heat input into the welding pool are changed. Replacing the shielding gas from M21 mixture where 18 % CO_2 (Figure 3, *a*) to M11 with 2 % CO_2 (Figure 3, *b*) contributes to the reduction in the effective width of each individual deposited bead from 3.92 mm (for M21) to 3.68 mm (for M11). At the same time, the effective height of the wall increases from 68.1 mm in M21 mixture to 75.2 mm while using M11 mixture (Figure 6). From the point of view of the formed surface quality (Figure 3, *a*, *b*), the replacement of M21 gas mixture with M11 leads to a significant increase in the wall profile deviation indices (Figure 6). Considering the low thermal conductivity of argon by reducing its share in the mixture with carbon dioxide, which has a higher thermal conductivity, in combination with reduced heat input when applying the GMAW-CMT process, the weld pool life time is reduced. This leads to a decrease in the amount of remelted metal of the previous layers and a non-uniform spreading of the weld pool metal with a subsequent

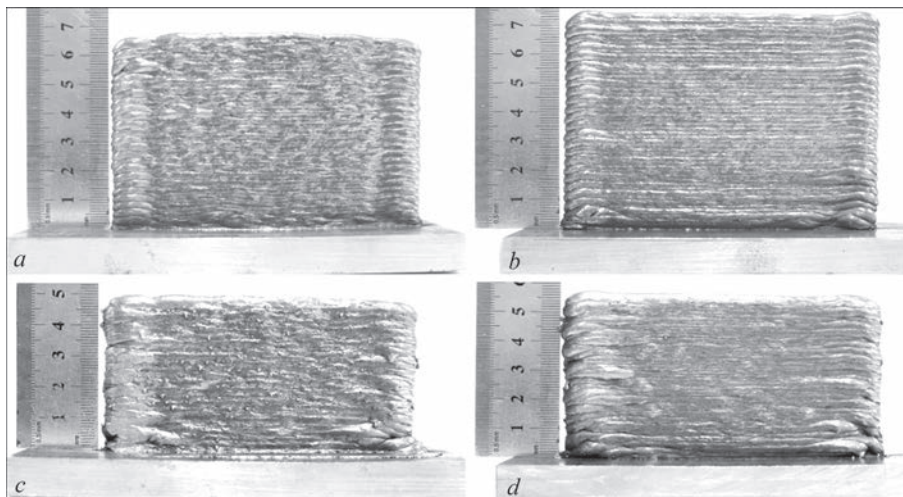


Figure 3. Specimens of low-carbon 09G2S (G3Si1) steel, produced by different surfacing methods using M21 and M11 gas mixtures: *a* — GMAW-CMT, M21 gas; *b* — GMAW-CMT, M11 gas; *c* — GMAW-CMT, M21 gas; *d* — GMAW-Pulse, M21 gas

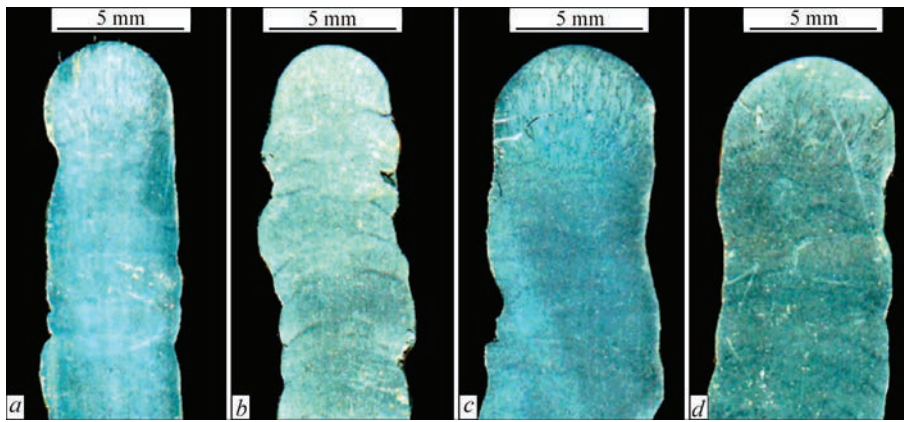


Figure 4. Macrostructure of specimens from low-carbon 09G2S (G3Si) steel, produced by different surfacing methods using M21 and M11 gas mixtures: *a* — GMAW-CMT, M21 gas; *b* — GMAW-CMT, M11 gas; *c* — GMAW-CMT, M21 gas; *d* — GMAW-Pulse, M21 gas

crystallization. This mechanism of influence of the thermal conductivity of the gas environment explains the relationship between the effective height, effective width and wall profile deviation, which is partially confirmed by the results of other studies [10].

The process of layer-by-layer formation of products with M21 gas mixture when applying the GMAW-Pulse process (Figure 3, *c*) is accompanied by active spattering of metal. Intense spattering is explained by the presence of a large amount (18 %) of carbon dioxide and a pulsed electric current supply [18]. Replacing the shielding gas environment by M11 (Figure 3, *d*) significantly reduces spraying during surfacing. As a consequence, in Figure 6, *a*, a clear dependence of the effective height of the wall on the composition of the used gas mixture can be observed. This dependence is similar to the results of surfacing obtained at the GMAW-CMT process.

Interesting is the dependence of changing the effective thickness of the wall on the composition of the gas environment. Thus, unlike the GMAW-CMT process (Figure 4, *a, b*), in the pulsed mode, the application of M11 mixture leads to an increase in the effective thickness of the manufactured wall by 10–11 %. The value of the effective width reaches 5.1 mm (Figure 4, *d*) when using M11 mixture and is decreased compared to the specimens, produced with the use of M21 mixture — 4.8 mm (Figure 4, *c*). As in the case of effective height, this is associated with a significant decrease in metal losses for spattering while reducing carbon dioxide content in the gas mixture.

Changing the content of carbon dioxide in the mixture significantly affected the value of the side wall surface deviation profile. For M1 and M21 mixtures, deviations of the wall profile amount to 0.68–0.78 and 0.57–0.62 mm, respectively (Figure 6).

For comparison with GMAW-Pulse/CMT processes, the wall was made by PAW-CW surfacing with unchanged welding speed parameters ($V_w = 600$ cm/min) and wire feed speed ($V_{wf} = 3.5$ m/min) (Figure 5).

Figure 6 presents the results of research on determination of the dependence of the effective wall thickness (Figure 6, *a*) and effective wall height (Figure 6, *b*) of the specimens. The analysis of produced results shows that, compared to GMAW processes, the wall produced by PAW-CW surfacing has the smallest side surface deviation profile.

Microstructural analysis of low-carbon steel specimens was carried out on the sections cut out from three separate zones: the last deposited layer, the transition zone between the last layer and previous layers, the zone of previous remelted layers.

Small nonmetallic inclusions of a rounded shape were found in almost all specimens (Figure 7, *a, b*). During the metallographic examination, it was established that these inclusions are oxides and silicates, which are fairly uniformly distributed over the entire cross-section of the specimens. The number and size of detected inclusions is less than the size No. 1 (based on the scale according to GOST 1778–70). In addition to single inclusions, single chains (Figure 7, *b, d*) and compact clusters of oxide and silicate inclusions are also observed (Figure 7, *b, d*). In the specimens produced by GMAW-CMT/Pulse surfacing processes in the shielding M11 gas mixture, the inclusions have an

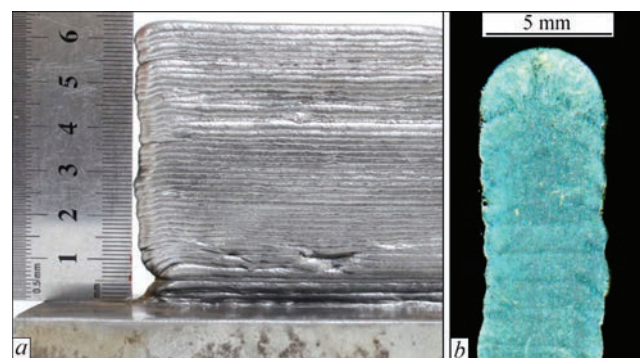


Figure 5. Specimen of 09G2S (G3Si) steel deposited by the PAW-CMT method: *a* — general view of the side surface; *b* — transverse macrosection

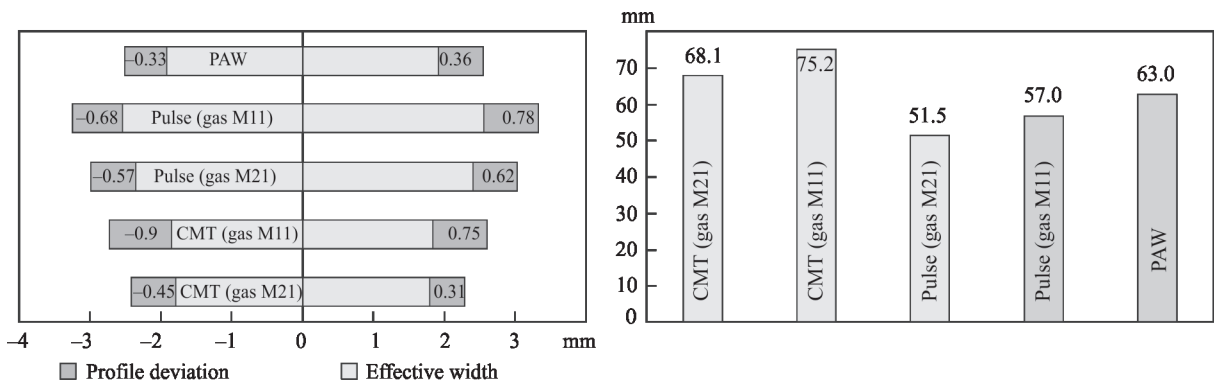


Figure 6. Dependence of the effective wall thickness (a) and their effective height (b) during additive surfacing of 09G2S steel (G3Si1) by GMAW-CMT/Pulse and PAW-CMT methods in shielding gas M21 and M11 mixtures

irregular shape, their composition differs from the composition of simple chemical compounds, in particular oxides and silicides (Figure 7, *c*). Their sizes exceed the sizes of oxides and silicates in these specimens.

The microstructure of the metal of the studied specimens of 09G2S (G3Si1) steel is characteristic of multilayer surfacings — the columnar structure of the cast metal, which indicates the orientation of crystallization from the liquid state, is observed only in the last deposited layer (Figure 8, *a, d, g, i*). The most finely dispersed structure (Figure 8, *a–c*) of the deposited metal is formed when using the GMAW-CMT method in combination with M21 gas mixture. The microstructure in the regions of the last surfacing layer is the precipitation of polygonal ferrite (sometimes with Widmanstätten orientation) and dispersed pearlite along the boundaries of the crystallites. The grain size number of the ferritic grain corresponds to Nos 9–10 according to GOST-5639–82. The share of Widmanstätten ferrite in the specimens deposited by the GMAW-Pulse method (Figure 8, *g, h*) is greater than in the specimens produced by GMAW-CMT surfacing with the same gas mixture. In the body of crystallites, several forms of ferrite are formed —

polyhedral and two modifications of lamellar — with an ordered and a disordered second phase. Among themselves, the microstructure of the specimens differs in the size of the crystallites, the width of the polygonal ferrite precipitations along the boundaries of the crystallites and a number of other ferrite forms, as well as the microhardness of the deposited metal. The crystallite size ranges from: 80–130 μm for GMAW-Pulse method, 60–80 μm for GMAW-CMT with M21 gas and 80–160 μm for GMAW-CMT method in shielding M11 gas mixture.

The transition zone consists of the metal with a changed structure (overlapping area), which arose as a result of thermal effect when applying each subsequent layer. This zone mainly consists of fragmentary remnants of a directed columnar structure (Figure 8, *b, e, h, k*). The structure is refined, granular, ferritic-pearlitic with a significant content of ferrite. Thus, in the transition zone, the columnar structure of the deposited metal structure is violated, and a disoriented fine-grained structure is formed. In all specimens, a clearly defined boundary of the layers joint is not observed. Such a structure should have an increased fracture resistance.

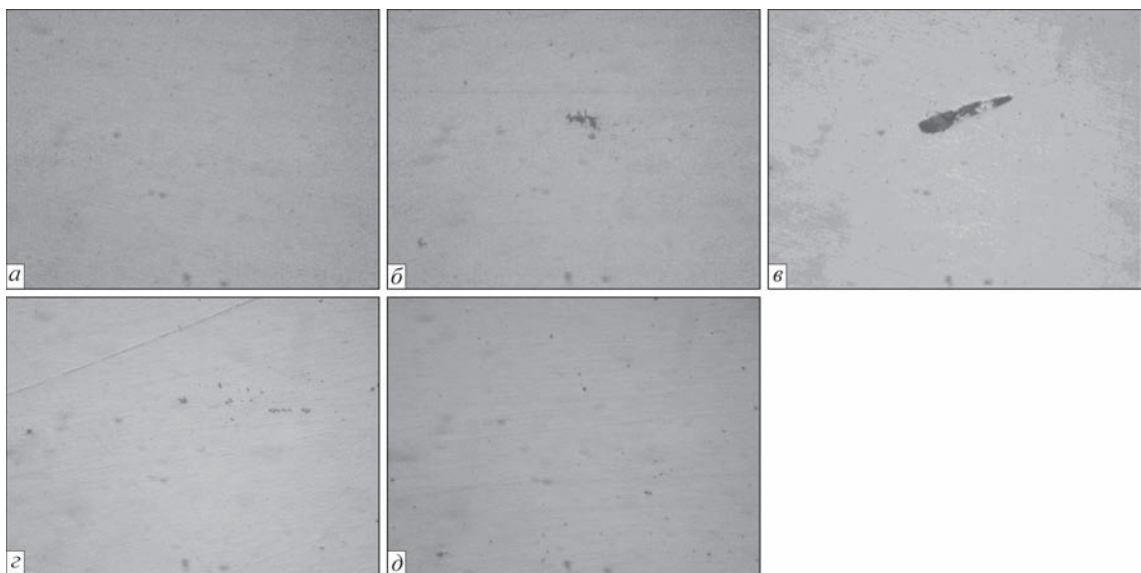


Figure 7. Microstructures ($\times 100$) of specimens from low-carbon 09G2S (G3Si1) steel, produced by different surfacing methods: *a* — GMAW-CMT, M21 gas; *b* — GMAW-CMT, M11 gas; *c* — GMAW-CMT, M21 gas; *d* — GMAW-Pulse, M21 gas; *e* — PAW-CW, M11 shielding gas, plasma-forming 100 % Ar

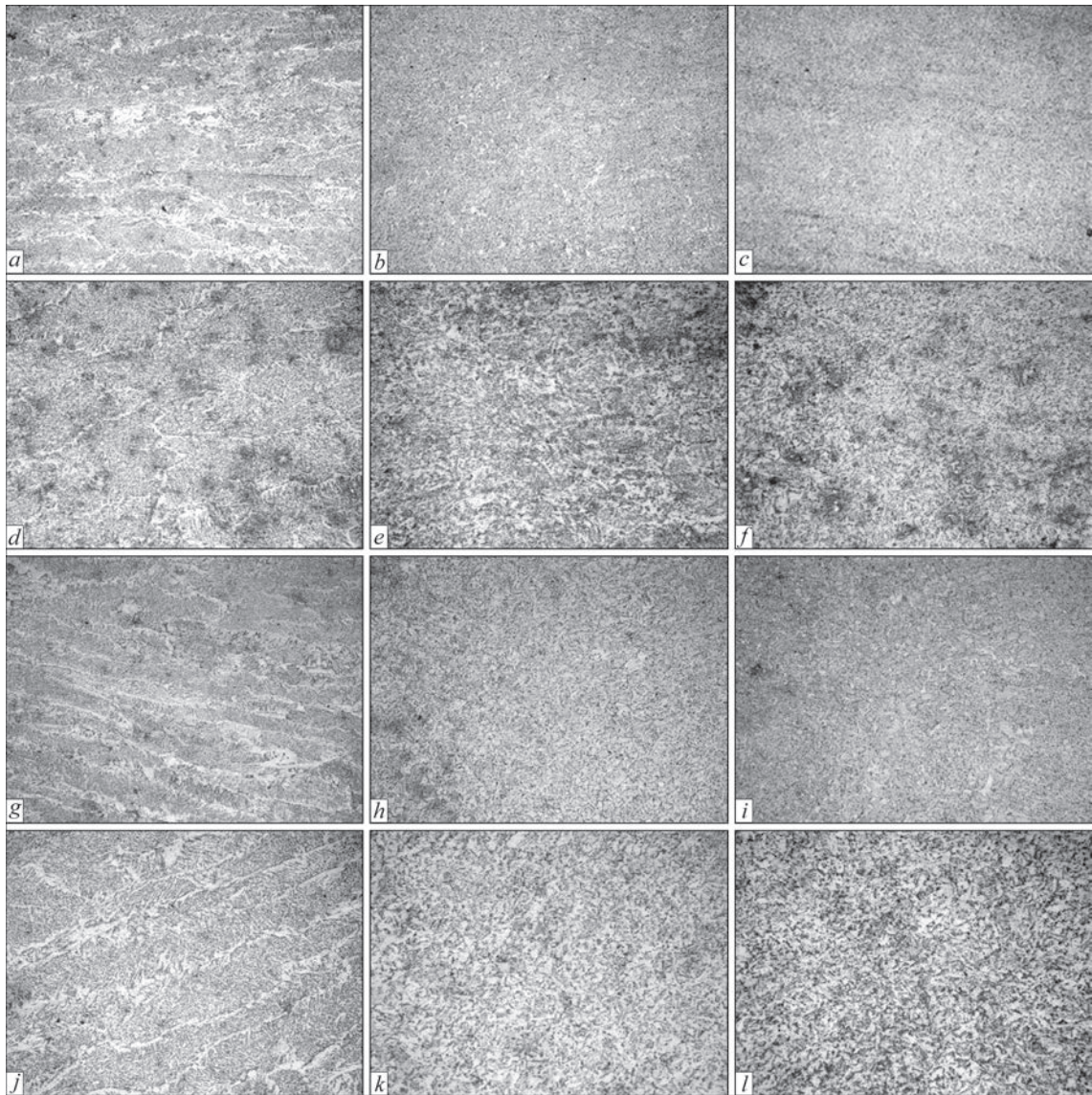


Figure 8. Microstructures ($\times 800$) of metal of specimens produced by layer-by-layer GMAW-CMT/Pulse surfacing in combination with different gas mixtures: *a* — GMAW-CMT, M21 gas; *b* — GMAW-CMT, M21 gas; *c* — GMAW-CMT, M21 gas; *d* — GMAW-CMT, M11 gas; *e* — GMAW-CMT, M11 gas; *f* — GMAW-CMT, M11 gas; *g* — GMAW-Pulse, M21 gas; *h* — GMAW-Pulse, M21 gas; *i* — GMAW-Pulse, M21 gas; *j* — GMAW-Pulse, M21 gas — the last deposited layer; *k* — GMAW-Pulse, M21 gas — transition zone; *l* — GMAW-Pulse, M21 gas — previous layers

In some places, the orientation of the structure, which is characteristic of cast metal, is preserved in the previous layers (Figure 8, *c*, *f*, *i*, *l*). The microstructure of the produced specimens differs in the size of the ferritic grain, in the transition zone and previous layers, the grain size Nos 7–8 according to GOST-5639–82 for the specimens produced by GMAW-Pulse, and No. 9 for GMAW-CMT surfacing.

The highest microhardness of the deposited metal on the HV1 scale is typical for specimens deposited by the GMAW-CMT method, when the shielding M11 gas mixture (1840–2082 MPa) is used. The microhardness of the specimens deposited with pulsed welding current supply varies within 1618–1922 MPa.

The microstructure of the metal of specimens deposited by the PAW-CW method is similar to the structure of specimens produced by GMAW-CMT/

Pulse surfacing. The lowest microhardness of the metal among all tested specimens at the level of 1766–1885 MPa is observed in PAW-CW surfacing. The microstructure of the last layer consists of massive precipitations of polygonal ferrite, a significant part of which has a Widmanstätten orientation, and a dispersed pearlite distributed along the boundaries of the crystallites (Figure 9, *a*). The last layer consists of elongated dendrites. In the transition zone and the previous layer, an almost uniform area of overlapping layers is observed. The structure is ferritic-pearlitic, the amount of ferrite in the structure significantly exceeds the amount of pearlite (Figure 9, *b*). In the lower part of the deposited specimen, at a distance of about 1 mm from the substrate, a ferritic-pearlitic structure (Figure 9, *c*) with a grain size No. 9 is observed.

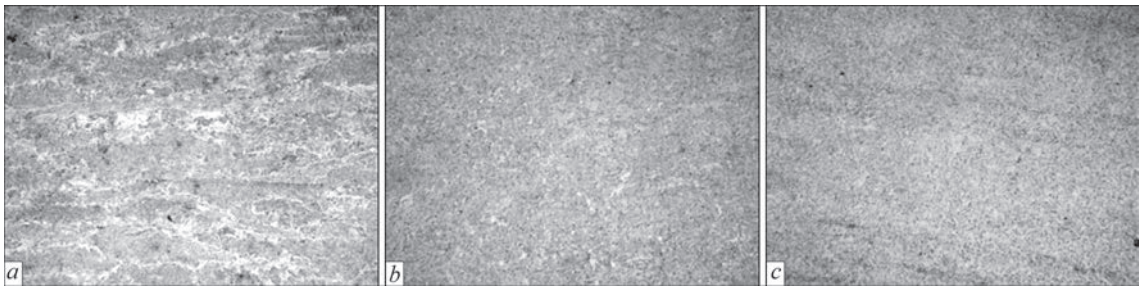


Figure 9. Microstructures ($\times 800$) of metal of specimen produced by layer-by-layer PAW-CW surfacing: *a* — last layer; *b* — transition zone; *c* — previous layers

Table 2. Average values of microhardness of deposited specimens, MPa

Method of surfacing and shielding gas mixture composition	Last layer		Transition zone	Previous layer
	Ferritic component	Body of crystals	Ferritic component	Ferritic component
GMAW-CMT (82 % Ar + 18 % CO ₂)	1760	2032	1748	1602
GMAW-CMT (98 % Ar + 2 % CO ₂)	2083	2238	1895	1840
GMAW-Pulse (82 % Ar + 18 % CO ₂)	1923	2046	1740	1618
GMAW-Pulse (98 % Ar + 2 % CO ₂)	1885	2093	1785	1766
PAW-CMT (shielding gas - 98 % Ar + 2 % CO ₂) (plasma-forming gas - 100 % Ar)	1745	1812.5	1580	1687

The metal hardness of the deposited specimens is given in Table 2.

The analysis of the microhardness data of the phase component indicates the presence of the influence of the repeated passage of the heat source on the preliminary deposited layers. Thus, the microhardness of the previous layers decreases relative to the last layer as a result of repeated heating and subsequent tempering under the effect of the heat of the subsequent layers of deposited metal. The surface layers of the metal deposited by the GMAW-CMT method in M11 mixture with the wire G3Sil (09G2S) have a maximum hardness of about 2083 MPa.

CONCLUSIONS

1. The impact of CMT and Pulse methods of GMAW surfacing on geometric characteristics of deposited layers of G3Sil (09G2S) steel was determined. The largest height of the deposited specimens (~ 75 mm) during sequential surfacing of 50 layers and the minimum wall thickness of down to 4.6 mm is provided by GMAW-CMT surfacing. Replacing the shielding M11 gas mixture with M21 leads to a decrease in the wall height to 68 mm. The effective width of the metal walls deposited in M21 mixture is ~ 4 mm, and in M11 mixture it is ~ 3.6 mm. The replacement of M21 mixture with M11 is accompanied by a significant increase in profile deviation — from 0.31–0.45 to 0.75–0.9 mm. The formation of layers with the maximum height is associated with the lower heat input methods compared to other investigation methods, which leads to a decrease in the penetration depth

of the metal of the preliminary deposited layer and a minimal spattering of the metal, especially in M11 mixture with a minimum content of CO₂.

2. In GMAW-Pulse surfacing of G3Sil (09G2S) steel, the height of the walls is minimal, and the effective width reaches the maximum values. Replacing the gas mixture from M11 to M21 leads to a decrease in the effective width of the walls with a simultaneous decrease in the deviation profile from 0.68–0.78 to 0.57–0.62 mm. The maximum values of the deviation profile are typical for GMAW surfacing when using M11 mixture. Plasma arc surfacing using cold wire (PAW-CW) provides intermediate values of the wall height of up to 63 mm and an effective width of ~ 4.4 mm. The profile deviation in PAW-CMT surfacing is minimal from the considered options and amounts to 0.33–0.36 mm.

3. In surfacing of low-carbon steel of G3Sil type (09G2S) GMAW-CMT/Pulse and PAW-CMT methods in all cases, a dense structure of the metal is formed, in which dispersed nonmetallic inclusions of oxides and silicates of a rounded shape were revealed, which are uniformly distributed over the entire cross-section of the specimens. The quantity and size of revealed inclusions is less than the size No. 1 (on the scale according to GOST 1778–70). In some regions, chains and compact clusters of inclusions are observed. The structure of the deposited metal is ferritic-pearlitic. The last deposited layer has a columnar structure that is typical of cast metal. In the transition zone, a disoriented fine-grained structure with fragmentary remnants of oriented columnar structures is observed, and in previously formed layers under the influence of subsequent

surfacing cycles, a disoriented fine-grained structure is formed. In all specimens, a clearly defined boundary of the layers joint is not observed.

4. The maximum values of microhardness are typical of the last deposited layers in all investigated methods and in GMAW-CMT surfacing in M11 gas mixture, they reach 2083–2238 MPa. The value of microhardness of the metal decreases when moving to the previously deposited layers, which is associated with the repeated action of the thermal cycle during multipass surfacing. In plasma surfacing, microhardness is minimal. For the last layer, it amounts to 1745–1813 MPa, and in the previously formed layers, the microhardness values of the metal decrease to 1580–1687 MPa.

REFERENCES

- Ding, D., Pan, Z., Cuiuri, D. et al. (2016) Adaptive path planning for wire-feed additive manufacturing using medial axis transformation. *J. of Cleaner Production*, **133**, 942–952. DOI: <https://doi.org/10.1016/j.jclepro.2016.06.036>
- Rodrigues, T.A., Duarte, V., Miranda, R.M. et al. (2019) Current status and perspectives on wire and arc additive manufacturing (WAAM). *Materials*, **12**(7), 1121. DOI: <https://doi.org/10.3390/ma12071121>
- Pan, Z., Ding, D., Wu, B. et al. (2018) Arc welding processes for additive manufacturing: A review. *Transact. on Intelligent Welding Manufacturing*, **1**, 3–24. DOI: https://doi.org/10.1007/978-981-10-5355-9_1
- DebRoy, T., Wei, H.L., Zuback, J.S. et al. (2018) Additive manufacturing of metallic components — Process, structure and properties. *Progress in Materials Science*, **92**, 112–224. DOI: <https://doi.org/10.1016/j.pmatsci.2017.10.001>
- Kvasnytskyi, V., Korzyk, V., Lahodzinkyi, I. et al. (2020) Creation of volumetric products using additive arc cladding with compact and powder filler materials. In: *Proc. of 10th Inter. Conf. on Nanomaterials: Applications & Properties*, 02SAMA16-1–02SAMA16-5. DOI: <https://doi.org/10.1109/NAP51477.2020.9309696>
- Xiong, J., Li, Y., Li, R., Yin, Z. (2018) Influences of process parameters on surface roughness of multi-layer single-pass thin-walled parts in GMAW-based additive manufacturing. *J. of Materials Processing Technology*, **252**, 128–136. DOI: <https://doi.org/10.1016/j.jmatprotec.2017.09.020>
- Graf, M., Hälsig, A., Höfer, K. et al. (2018) Thermo-mechanical modelling of wire-arc additive manufacturing (WAAM) of semi-finished products. *Metals*, **8**(12), 1009. DOI: <https://doi.org/10.3390/met8121009>
- Ogino, Y., Asai, S., Hirata, Y. (2018) Numerical simulation of WAAM process by a GMAW weld pool model. *Weld World*, **62**, 393–401. DOI: <https://doi.org/10.1007/s40194-018-0556-z>
- Rao, Z.H., Liao, S.M., Tsai, H.L. (2010) Effects of shielding gas compositions on arc plasma and metal transfer in gas metal arc welding. *J. of Applied Physics*, **107**(4), 044902. DOI: <https://doi.org/10.1063/1.3291121>
- Gurcik, T., Kovanda, K., Rohan, P. (2019) Influence of shielding gas on geometrical quality of WAAM technology. In: *Proc. of 28th Inter. Conf. on Metallurgy and Materials (METAL 2019)*, 715–721. DOI: <https://doi.org/10.37904/metal.2019.871>
- Bishal, S., Pudasaini, N., Roy, S. et al. (2022) Altering the supply of shielding gases to fabricate distinct geometry in GMA additive manufacturing. *Applied Sciences*, **12**(7), 3679. DOI: <https://doi.org/10.3390/app12073679>
- Mvola, B., Kah, P. (2016) Effects of shielding gas control: Welded joint properties in GMAW process optimization. *The International J. of Advanced Manufacturing Technology*, **88**(9–12), 2369–2387. DOI: <https://doi.org/10.1007/s00170-016-8936-2>
- Gouda, M., Takahashi, M., Ikeuchi, K. (2005) Microstructures of gas metal arc weld metal of 950 MPa class steel. *Science and Technology of Welding and Joining*, **10**(3), 369–377. DOI: <https://doi.org/10.1179/174329305X40714>
- Menzel, M. (2003) The influence of individual components of an industrial gas mixture on the welding process and the properties of welded joints. *Welding Inter.*, **17**(4), 262–264. DOI: <https://doi.org/10.1533/wint.2003.3111>
- Ebrahimnia, M., Goodarzi, M., Nouri, M., Sheikhi, M. (2009) Study of the effect of shielding gas composition on the mechanical weld properties of steel ST 37-2 in gas metal arc welding. *Materials & Design*, **30**(9), 3891–3895. DOI: <https://doi.org/10.1016/j.matdes.2009.03.031>
- Zhao, Y., Shi, X., Yan, K. et al. (2018) Effect of shielding gas on the metal transfer and weld morphology in pulsed current MAG welding of carbon steel. *J. of Materials Processing Technology*, **262**, 382–391. DOI: <https://doi.org/10.1016/j.jmatprotec.2018.07.003>
- Spencer, J.D., Dickens, P.M., Wykes, C.M. (1998) Rapid prototyping of metal parts by three-dimensional welding. Proceedings of the Institution of Mechanical Engineers, Pt B. *J. of Engineering Manufacture*, **212**(3), 175–182. DOI: <https://doi.org/10.1243/0954405981515590>
- Tokihiko, K., Rinsei, I., Koichi, Y., Yoshinori, H. (2009) Development of low spatter CO₂ arc welding process with high frequency pulse current. *Science and Technology of Welding and Joining*, **14**(8), 740–746. DOI: <https://doi.org/10.1179/136217109X449238>

ORCID

V.V. Kvasnytskyi: 0000-0002-7756-5179,
I.M. Lahodzinskyi: 0000-0002-7986-9440

CONFLICT OF INTEREST

The Authors declare no conflict of interest

CORRESPONDING AUTHOR

V.V. Kvasnytskyi
E.O. Paton Electric Welding Institute of the NASU
11 Kazymyr Malevych Str., 03150, Kyiv, Ukraine.
E-mail: kvas69@ukr.net

SUGGESTED CITATION

V.V. Kvasnytskyi, I.M. Lahodzinskyi (2023) Influence of GMAW and PAW methods of additive arc surfacing and shielding gas composition on surface geometry and metal structure of products from low-carbon 09G2S steel. *The Paton Welding J.*, **11**, 21–29.

JOURNAL HOME PAGE

<https://patonpublishinghouse.com/eng/journals/tpwj>

Received: 25.10.2023
Accepted: 07.12.2023

DOI: <https://doi.org/10.37434/tpwj2023.11.03>

3D TECHNOLOGY OF GROWING LARGE TUNGSTEN CRYSTALS

V.O. Shapovalov, Yu.O. Nikitenko, V.V. Yakusha, O.M. Gnizdylo, O.V. Karuskevych

E.O. Paton Electric Welding Institute of the NASU

11 Kazymyr Malevych Str., 03150, Kyiv, Ukraine

ABSTRACT

The evolution of liquid-phase methods for growing tungsten single crystals is analyzed. It is shown that methods of growing crystals with a single heating source cannot solve the problem of producing crystals of industrial sizes. Super large tungsten crystals of various configurations can be produced using 3D technologies and combined plasma-induction heating. This method has already been used for growing single crystal plates, billets for large-format single crystal rolling, single crystal ingots and crucibles. The next step will be the creation of a technology for growing bulk super large tungsten single crystals.

KEYWORDS: 3D additive technologies, tungsten, single crystal growth, plasma-induction zone melting, droplet transfer

INTRODUCTION

At present additive 3D technologies cover practically all the spheres of human activity: material production, medicine, science and art. A wide-scale application of 3D technologies is observed, particularly in mechanical engineering. Schweissen und Schneiden Fair held in September, 2023 in Essen, Germany can be a confirmation of this. Novel technologies are actively used in unit and small-scale production; they are introduced for manufacturing complex-shaped parts, for instance turbine blades, impellers, etc. Manufacturers note a high level of properties of the product metal, due to formation of a fine-grained structure, which can be assessed by grain size corresponding to numbers 6–10 [1].

Products are made from different metals and alloys: low- and high-alloyed and stainless steels, nickel alloys, aluminium-, copper-based alloys, etc., as well as plastics [2]. The 3D process uses initial materials in the form of wire or powder. Heating sources applied in metal product manufacturing are given in Table 1.

However, at application of 3D technologies in manufacture of parts from refractory metals and alloys ($T_m > 2000$ °C) problems arise because of the high temperature gradient, leading to internal stress formation. As regards refractory metals, known is a small number of works, reporting application of 3D technologies to manufacture products from molybdenum, tantalum, and tungsten [3, 4]. So, the publica-

tions give an example of application of additive wire surfacing technology (Figure 1).

Further heat treatment of the ingot does not solve the problem of stress relieving, as the process of grain recrystallization and growth begins.

Tungsten ingots and products are not prone to recrystallization at heating, if they have a single crystal structure. Traditionally, tungsten single crystals are grown in the form of rods of up to 25 mm diameter. Considering the high melting temperature ($W = 3690$ K), high energy density sources of electric heating are used for tungsten single crystal growing, namely the electron beam or low-temperature plasma arc. Attempts to grow sound crystals of a larger diameter failed. The cause for it is the negative influence of the scale factor, which leads to high internal stresses.

Increase of linear dimensions of single crystals leads to two problems, namely containing the melt being deposited on the pool surface (tungsten has a very high density of 19.3 g/cm³) and high thermomechanical stresses in the single crystal body (which is related to a high temperature gradient). High thermomechanical stresses promote generation of an additional number of dislocations (dislocation density may reach 10^7 – 10^8 cm⁻²) and disorientation of sub-grains, which significantly impairs the single crystal structure quality.

A PWI development became an innovative solution, namely creation of plasma-induction 3D technology of growing super large single crystals of tungsten and molybdenum of different shape: plates, ingots and crucibles. Theoretically, this method does not have any limitations as to the size of the grown crystals. It can be implemented in practice through correct organization of preheating and creation of specified thermal conditions. Figure 2 presents a diagram of the unit for additive growth of refractory metal single crystals in the form of plates using the plasma-induction method.

Table 1. Heating sources, used in 3D technology

Type of power source	Number of real processes, %
Laser	~ 60
Electric arc	~30–35
Electron beam	~5–10

Copyright © The Author(s)

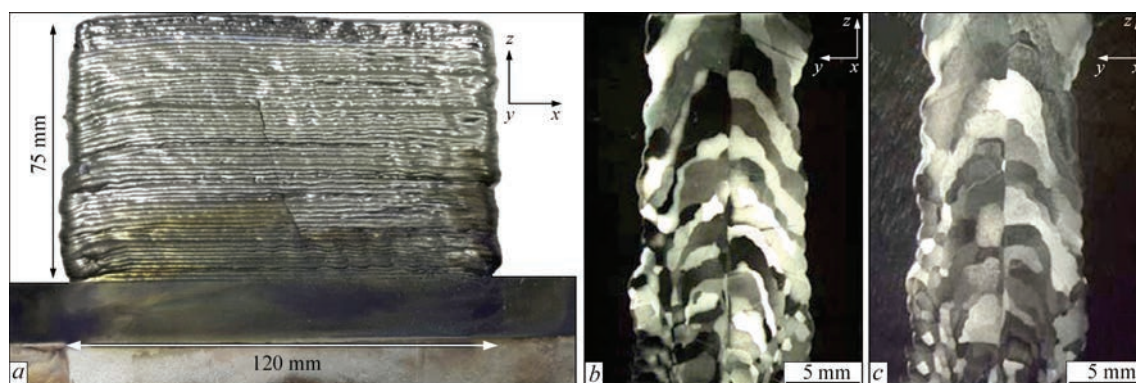


Figure 1. Formation of coarse-grained polycrystalline structure and cracks from internal thermal stresses in a tungsten ingot, produced at wire and indirect arc surfacing (a), microstructure of the cross-section (b) and after heat treatment (c)

EQUIPMENT AND MATERIALS

To solve the problem of growing large and high-quality tungsten single crystals, the objective of development of the appropriate technology was set. The idea of simultaneous application of two different sources of electric heating, namely plasma and induction sources was proposed by PWI specialists for the first time. Each of the above heating sources has its functions: plasma-arc one creates a moving local metal pool on the face of the crystal being built-up, remelts the consumable rods, fed into the melting zone, and forms the single crystal body of the specified configuration; induction source contains the local metal pool from spilling and creates the specified temperature field in the crystal body.

Additional heating of the crystal significantly reduces the radial and axial temperature gradients, which promotes lowering of the dislocation density and internal stresses and formation of a more perfect structure. In this case, despite the use of a local pool, which forms the single crystal while moving, no stresses develop in the crystal, which would promote crack initiation and increase of the number of dislocations. At such temperatures the dislocations annihilate and at evaluation of the single crystal quality

their number does not exceed $1 \cdot 10^6 \text{ mm}^{-2}$. The technology completely eliminates cracking or fracture of the crystals, either in the process of growing or during part manufacturing.

The essence of the method consists in that plasmatron, while performing a reciprocating movement, displaces the metal pool, which, while being replenished through rod remelting, forms the crystal layer by layer, being essentially similar to additive arc surfacing. After each plasmatron pass the single crystal is lowered to the height of the deposited layer, thus ensuring stable conditions for the growing process.

This method was used to develop equipment (Figure 3) and technology of growing profiled single crystals of refractory metals (tungsten and molybdenum) in the form of plates (Figure 4).

The crystal forms under the conditions of heating by an inductor high-frequency field to temperatures, characteristic for hot deformation range. It is known that at these temperatures dislocation movement takes place under a simultaneous impact of external stresses and temperature. Dislocations turn out to be not rigidly attached to “their” slip plane, and they can move from one plane into another one, choosing the easiest path. This is regarded as an additional degree of freedom of dislocations. At such an unregulated movement of dislocations the probability of their collision becomes higher, and thus, the number of their annihilation cas-

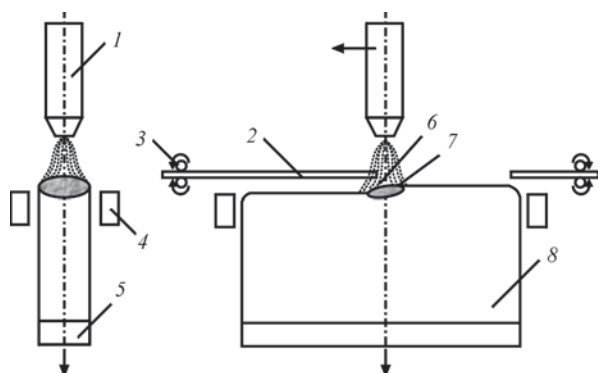


Figure 2. Schematic of the unit for additive growing of refractory metal single crystals using plasma-induction method: 1 — plasmatron; 2 — consumable rod; 3 — rod feed mechanism; 4 — inductor; 5 — seed crystal; 6 — plasma arc; 7 — local pool; 8 — single crystal



Figure 3. Unit for growing refractory metal single crystals in the form of plates

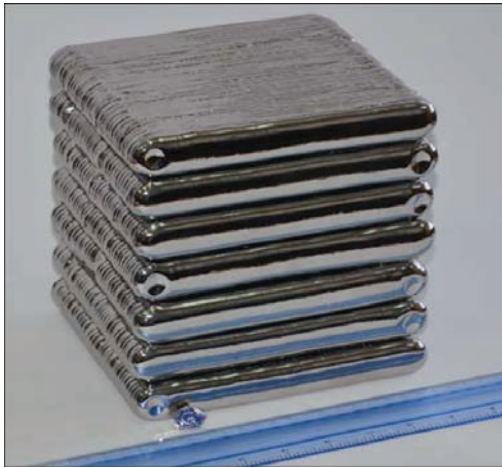


Figure 4. Appearance of flat tungsten single crystals of 170×160×20 mm dimensions



Figure 5. New unit with computer control for growing refractory metal single crystals in the form of bodies of rotation

es rises (their density is decreased) on the one hand, and on the other hand — their proneness to formation of regular dislocation structures characterized by dislocation coalescence into low-angle boundaries, is increased. Conditions, as which the single crystal forms, ensure a higher quality of the single crystal structure, than with the methods, where no additional heating is used (electron beam and plasma-arc).

Crystals grown with application of the above method have not as smooth side surface, but it does not prevent their use without any additional machining as billets for wide-format rolling.

The developed additive technology of 3D growing large commercial purity single crystals of refractory metals is based on the conducted long-term thorough investigations, which allowed establishing and studying the following:

- thermal field distribution in the single crystal using mathematical models and experimental data;
- working ranges of the change of technological parameters of crystal growth process;

- structural characteristics and regularities of structure formation in the grown single crystals.

Calibrated tungsten rods of 8 mm dia, 800 mm length and $W \geq 99.97$ wt.% purity were used as consumable materials for replenishing the pool (Table 2).

EXPERIMENTAL STUDIES AND DISCUSSION OF THE RESULTS

Further study of the process enabled development of a new unit for 3D growing of super large tungsten single crystals in the form of bodies of rotation, based on the same principles (Figure 5).

Developed equipment is a qualitatively new generation of equipment, featuring a completely computerized system of controlling the actuators, sensors of displacement and control of single crystal growth process. The design envisages the possibility of growing single crystals in the form of bodies of rotation (cylinder or hollow cylinder) of up to 100 mm outer diameter. At present a thermal unit has been developed, and optimization of the technology of growing tungsten single crystals of 85 mm diameter is going on.

The developed technology is fundamentally based on the technology of growing flat single crystals. However, in the new unit the crystal is continuously rotating around a vertical axis. A cylindrical billet made from a flat single crystal of a set orientation is used as a seed crystal. Figure 6 shows a photo of the process of single crystal growing, where arrows mark the direction of feeding the consumable rod into the plasma arc melting zone and the direction of single crystal rotation.

Building up takes place layer-by-layer due to movement of the local pool and the plasmatron from the central to the peripheral parts so that the liquid pool covers the entire surface and the previous deposited layer. After layer deposition on the entire upper surface of the crystal, it is lowered down. Equipment allows feeding the rods from both sides, both in the ingot center, and with radial displacement relative to the center. Figure 7 shows a tungsten crystal of 85 mm diameter with 90 mm of built-up layers [5].

At this stage after technology optimization preliminary evaluation of single crystallinity of the produced ingot was performed using chemical etching of the surface in a mixture of equal volume fractions of hydrofluoric and nitric acids. The ingot surface etched in such a way had alternating longitudinal (vertical) matte and shiny stripes characteristic for single crystals. The pattern of

Table 2. Chemical composition of 8 mm tungsten rods

Element	Si	Mg	Sn	Ni	Al	Mo	N	C
wt. %	<0.001	0.0001	<0.0001	0.0002	0.0002	0.017	0.002	0.001
Element	As	Sb	Pb	Fe	Bi	Ca	P	O
wt. %	<0.0001	<0.0001	<0.0001	0.0013	<0.0001	<0.001	<0.001	0.0046

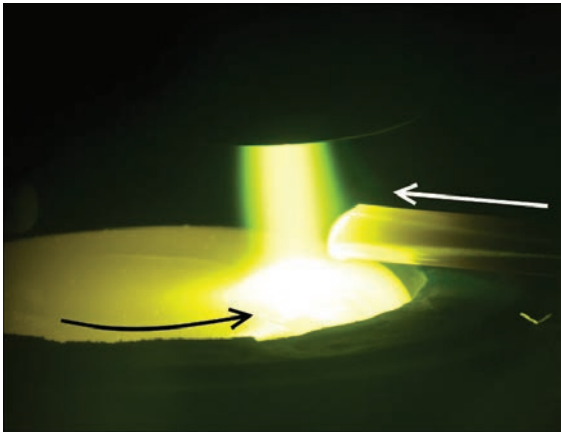


Figure 6. Process of growing a tungsten single crystal in the form of the body of rotation



Figure 7. Appearance of a tungsten crystal of 85 mm diameter

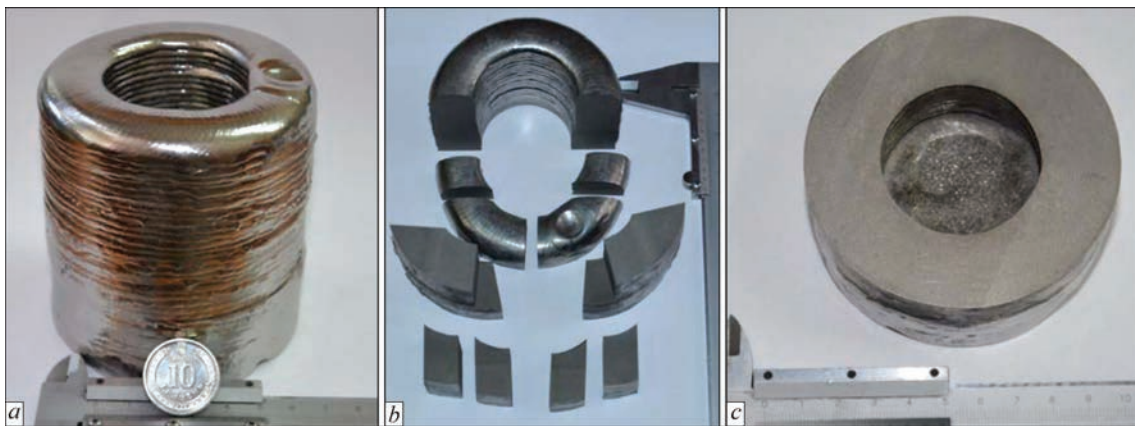


Figure 8. General view of a tungsten single crystal in the form of a hollow body of rotation of 85 mm diameter (a); view of the upper part (b) and bottom part with the seed crystal (c) after cutting up the ingot

stripe distribution was indicative of the provided by the seed crystal heredity of the single crystal structure and absence of sub-blocks of another crystallographic orientation on the ingot side surface.

The next step in development of the technologies of growing super large tungsten single crystals was an attempt to grow a crystal in the form of a hollow cylinder, as a billet for manufacturing crucibles and pipes. It resulted in growing by the novel 3D technology a tungsten crystal in the form of a hollow cylinder on a continuous seed single crystal of 85 mm diameter for the first time in the world. The grown crystal has a built-up wall of 68 mm height and 20–22 mm thickness (Figure 8). Surface examination after ingot etching by chemical reagents showed the heredity of the structure from the seed single crystal and all the signs of structure single crystallinity in the entire crystal.

Microstructural studies yielded the average value of 4150 MPa for the vertical plane, and 3840 MPa for the horizontal plane. A pronounced difference in microhardness in different planes points to anisotropy of properties, characteristic for the single crystal structure. Variations of microhardness values within 10 % in one plane is attributable to structural inhomogeneity of metal

single crystals, consisting of sub-blocks and subgrains with low misorientation angles of up to 3°.

CONCLUSIONS

A unique additive 3D technology of growing refractory metal single crystals in the form of 170–160–20 mm plates and bodies of rotation (cylinder and hollow cylinder) of 85 mm diameter was developed at PWI. The next step was optimization of the technology of growing tungsten single crystals in the form of hollow bodies of rotation. An ingot of 85 mm diameter, 20–22 mm wall thickness (for hollow ingots) and 68 mm height was grown. Such a shape will allow using tungsten as tubular billets, for manufacturing elements of a complex curvature or crucibles.

REFERENCES

1. ISO 643:2019: *Steels — Micrographic determination of the apparent grain size*. <https://www.iso.org/standard/72193.html>
2. Mukherjee, T., Elmer, J.W., Wei, H.L. et al. (2023) Control of grain structure, phases, and defects in additive manufacturing of high-performance metallic components. *Progress in Materials Sci.*, **138**, 101153. DOI: <https://doi.org/10.1016/j.pmatsci.2023.101153>
3. Marinelli, G., Martina, F., Lewtas, H. et al (2019) Microstructure and thermal properties of unalloyed tungsten deposited by Wire +

Arc additive manufacture. *J. of Nuclear Materials*, **522**, 45–53. DOI: <https://doi.org/10.1016/j.jnucmat.2019.04.049>

4. Marinelli, G., Martina, F. Ganguly, S., Williams, S. (2020) Grain refinement in an unalloyed tantalum structure by combining Wire + Arc additive manufacturing and vertical cold rolling. *Additive Manufacturing*, **32**, 101009. DOI: <https://doi.org/10.1016/j.addma.2019.101009>
5. Shapovalov, V.O., Nikitenko, Yu.O., Yakusha, V.V. et al. (2020) Manufacture of super large tungsten single crystals in the form of rotation bodies. *PAST*, **125(1)**, 60–63. DOI: <https://doi.org/10.46813/2020-125-060>

ORCID

V.O. Shapovalov: 0000-0003-1339-3089,
 Yu.O. Nikitenko: 0000-0002-3603-2333,
 V.V. Yakusha: 0000-0001-5962-9194,
 O.M. Gnizdylo: 0000-0001-7537-6481,
 O.V. Karuskevych: 0000-0002-7037-5903

CONFLICT OF INTEREST

The Authors declare no conflict of interest

CORRESPONDING AUTHOR

Yu.O. Nikitenko
 E.O. Paton Electric Welding Institute of the NASU
 11 Kazymyr Malevych Str., 03150, Kyiv, Ukraine.
 E-mail: nikyu80@gmail.com

SUGGESTED CITATION

V.O. Shapovalov, Yu.O. Nikitenko, V.V. Yakusha, O.M. Gnizdylo, O.V. Karuskevych (2023) 3D Technology of growing large tungsten crystals. *The Paton Welding J.*, **11**, 30–34.

JOURNAL HOME PAGE

<https://patonpublishinghouse.com/eng/journals/tpwj>

Received: 20.10.2023

Accepted: 07.12.2023

Wire & Tube 2024 15–19 April 2024, Messe Düsseldorf



Trend forums, expert meetings and themed pavilions for stainless steel, hydrogen, other regenerative energy carriers, separating and cutting, plastic pipes & tubes and finished products for Fastener & Spring Making Technologies will be in focus.

Ranges on display at wire 2024, wire will be staged in exhibition halls 9 to 17 in 2024. It will be

as big as ever, occupying some 66,900 square metres of exhibition space. With 1,026 exhibitors from 60 countries it will even surpass pre-pandemic levels.

On show will be machinery and equipment for the manufacture and processing of wire, finished products at Fasteners & Springs, tools and auxiliaries for process engineering, materials, glass fibre technologies, special wires and cable as well as innovations from sensor, control and testing technology

In addition to wire and cable machinery producers, wire and cable products and glass fibre technologies, impressive wire mesh welding machines will be displayed in Hall 17. These pose logistics with particular challenges because thick cables have to be laid and connected in the supply ducts to transport the electric power this heavy machinery requires for its live operations.

Fastener & Spring Making Technologies and their finished products in Hall 16. Here the complete value chain for fasteners and springs can be found: from raw materials, machinery and equipment to fasteners, connectors and industrial springs. This once again makes #wire Düsseldorf 2024 a highly topical information and order platform for the producers, dealers and buyers of screws, brackets, construction components and fittings, all types of springs and wire bending parts.

Ranges on display at Tube 2024. Tube also enjoys excellent booking levels. So far, 768 exhibitors from 49 countries have registered. They will occupy a total of 49,600 square metres' exhibition space in Halls 1 to 7.1.

Tube 2024 presents the entire process chain of the tube & pipe industry — in a focused and compact array: machinery and equipment for manufacturing pipes and tubes, finishing and processing of pipes & tubes as well as raw materials, plastic pipes, tube products and accessories, used machinery, tools for process engineering, auxiliaries, sensor technology, control, measuring and testing technology all form part of the extensive ranges. This line-up is complemented by tube & pipe, pipeline, OCTG technology and profile trading.

International satellites in booming markets of the future. Over a time span of almost 40 years wire and Tube Düsseldorf have developed into the leading trade fairs for their industries — now also “giving birth” to satellite events on the Wire, Cable and Tubes & Pipes themes. In their regions, they are the market leaders and drivers for the local industries and boast high growth potential. Satellites in Turkey, Egypt, Mexico, China, Thailand and India now already form an integral part of the growing portfolio of the Metal and Flow Technologies made by Messe Düsseldorf.

CONTROL OF FORMATION OF METAL PRODUCED BY ARC METHODS OF LAYER-BY-LAYER DEPOSITION OF MATERIAL WITH FLUX-CORED WIRES

A.A. Babinets

E.O. Paton Electric Welding Institute of the NASU
11 Kazymyr Malevych Str., 03150, Kyiv, Ukraine

ABSTRACT

Integrated comparative studies of the possibility of controlling formation and properties of metal by changing the electric parameters in single-layer arc deposition were conducted. The materials used were flux-cored electrode wires of 1.8–2.8 mm diameter, which were developed for three conditions of material deposition: in shielding gas atmosphere (GMAW), with open arc (SSAW) and submerged-arc (SAW). Metal part of the wires was designed so as to produce deposited metal of the type of heat-resistant tool 25Kh5FMS steel. Studies were conducted in a broad mode range: current of 150–450 A, and voltage of 20–32 V. The optimal ranges of current and voltage were experimentally determined for each material deposition method and flux-cored wire diameter, which ensure sound formation of the deposited beads, minimal penetration depth and dilution of deposited metal by base metal. Respective dependencies of the influence of current and voltage on the deposited bead geometry were plotted. Obtained experimental data can be used in the processes of additive manufacturing at selection of optimal modes of layer-by-layer arc deposition of metallic materials — wire arc additive manufacturing (WAAM) of part elements.

KEYWORDS: arc deposition, flux-cored wire, control, deposition modes, deposited metal formation, deposited bead dimensions

INTRODUCTION

It is known that in electric arc deposition of metallic materials deposited metal formation and its properties are largely determined by electric and technological parameters of the process [1].

Under the current conditions of technology development, the question arises of the possibility of using powder metallic materials for deposition and some deposition methods in additive production. We are talking about layer-by-layer arc methods of material deposition (Wire Additive Manufacturing — WAAM), which include, in particular, such technologies as gas-shielded deposition (Gas Metal Arc Welding — GMAW) or MIG/MAG Welding) or deposition by Cold Metal Transfer (CMT) method [2–9].

The process of flux-cored arc surfacing in part manufacturing in shielding gases (GMAW) or by an open arc (Self-Shielded Arc Welding (SSAW)) when solving some problems can be actually regarded as the above-mentioned additive manufacturing under one condition that machining of the thus deposited product should be absent or minimal [6].

Therefore, a priority task when studying the possibilities of application of arc surfacing methods and surfacing materials for deposition in additive manufacturing is determination of the regularities of the influence of deposition mode parameters on the geometrical dimensions and quality of deposited bead formation.

The objective of the work is experimental study of the possibility of controlling the formation and properties of metal produced by different methods of arc deposition with flux-cored wires of the same chemical composition, but of different diameter, due to variation of the electric parameters of deposition.

MATERIALS AND EXPERIMENTAL PROCEDURES

To conduct comparative studies, nine test batches of flux-cored wires of 1.8; 2.4 and 2.8 mm diameters were manufactured for deposition in shielding gas atmosphere (80 % Ar + 20 % CO₂), by an open arc (with self-shielded flux-cored wire) and by submerged arc (AN-26P flux). Metal part of the charge of all the flux-cored wires was calculated so as to obtain deposited metal of one type — 25Kh5FMS. St3 steel plates of 15 mm thickness were used as the base metal. During the experiments voltage and current were varied in a broad range of 20–23 V and 150–450 A, taking into account the flux-cored wire diameter. Deposition rate was constant in all the experiments and was equal to 20 m/h. Deposition was performed in an all-purpose unit U-653, which was connected to VDU-505 power source. The average values of current and voltage were determined using a computerized information-measurement system [10].

During the experiments, a comparative expert assessment of the quality of formation of beads deposited in one layer in one pass was performed, presence of pores and other defects was determined. Measure-

Table 1. Influence of the modes on formation of beads deposited by 1.8 mm self-shielded flux-cored PP-Np-25Kh5FMS wire

Bead number	Deposition mode		Formation quality/defects	Bead average dimensions, mm			$\gamma_{0\text{av}}$, %
	<i>I</i> , A	<i>U</i> , V		<i>e</i>	<i>g</i>	<i>h</i>	
1.1	178	20.3	Poor/Pores, wormholes	5.4	1.6	1.1	33.5
1.2	183	23.5	Satisfactory	7.2	1.4	1.9	42.8
1.3	185	25.8	Satisfactory/Pores, wormholes	9.8	1.2	2.1	50.5
2.1	212	26.3	Good/pores	10.4	1.0	1.3	53.0
2.2	218	23.4	Good	8.8	1.7	1.5	45.0
2.3	213	20.2	Poor/Pores, wormholes	6.3	2.1	1.2	35.0

Table 2. Influence of the modes on formation of beads deposited by 1.8 mm flux-cored PP-Np-25Kh5FMS wire in shielding gases

Bead number	Deposition mode		Formation quality/defects	Bead average dimensions, mm			$\gamma_{0\text{av}}$, %
	<i>I</i> , A	<i>U</i> , V		<i>e</i>	<i>g</i>	<i>h</i>	
23.1	204	26.6	Satisfactory	11.2	4.0	2.9	42.3
23.2	225	24.0	Satisfactory, narrow bead	7.4	4.8	3.2	35.5
23.3	258	23.4	Satisfactory	12.3	4.4	4.8	38.0
23.4	350	26.7	Good	16.4	4.1	5.0	53.0
23.5	317	26.5	Good	15.7	3.8	3.3	48.5
23.6	331	26.5	Good	16.8	4.0	4.8	50.0

Table 3. Influence of the modes on formation of beads deposited by submerged arc with 1.8 mm flux-cored PP-Np-25Kh5FMS wire

Bead number	Deposition mode		Formation quality/defects	Bead average dimensions, mm			$\gamma_{0\text{av}}$, %
	<i>I</i> , A	<i>U</i> , V		<i>e</i>	<i>g</i>	<i>h</i>	
29.2	245	27.9	Satisfactory	16.6	3.9	3.8	46.0
29.3	320	27.8	Good	18.9	4.2	5.5	48.5
29.4	325	27.7	Satisfactory	16.0	4.0	5.5	50.5
29.5	301	28.9	Good	20.1	3.9	4.8	48.0
29.6	311	26.8	Good	21.8	3.8	4.4	47.5

ment of width (*e*), height (*g*) and depth (*h*) of penetration of the deposited beads, as well as deposited metal dilution by base metal (γ_0) was conducted on 6–8 macrosections, cut out of the deposits. All the obtained information was entered into the Table. After that the derived data were used to plot the graphs of dependence of the respective parameters of the deposited beads on deposition modes. For example, in-

formation derived at deposition of 1.8 mm flux-cored wire on three samples by different methods is given in Tables 1–3, and characteristic macrosections of the deposited samples — in Figure 1.

EXPERIMENTAL RESULTS

The method of submerged-arc surfacing became the most widely applied in surfacing heavily worn parts.

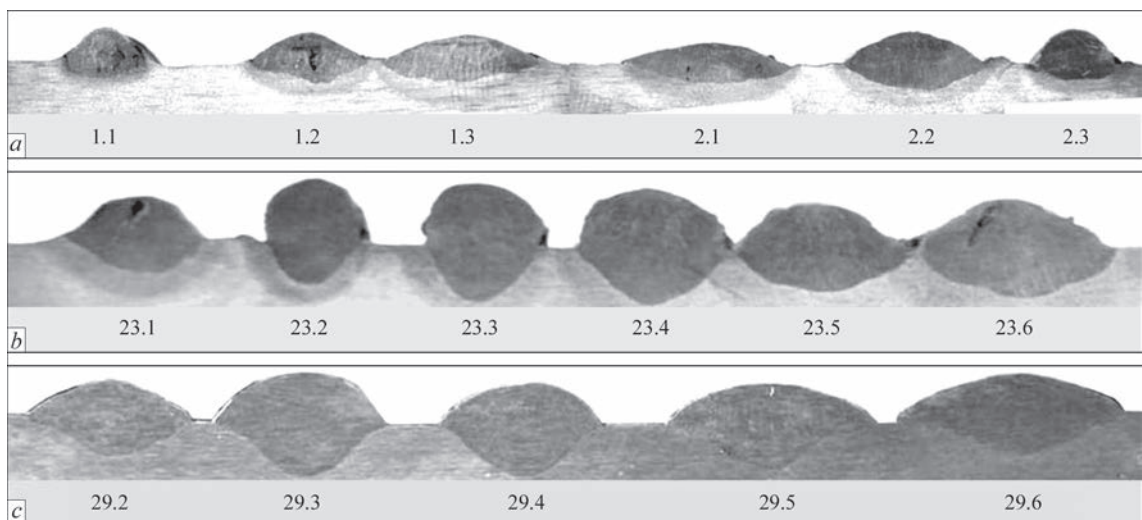


Figure 1. Macrosections of samples deposited by 1.8 mm PP-Np-25Kh5FMS flux-cored wire (for designations see Tables 1–3): *a* — by open arc; *b* — in shielding gases; *c* — by submerged-arc

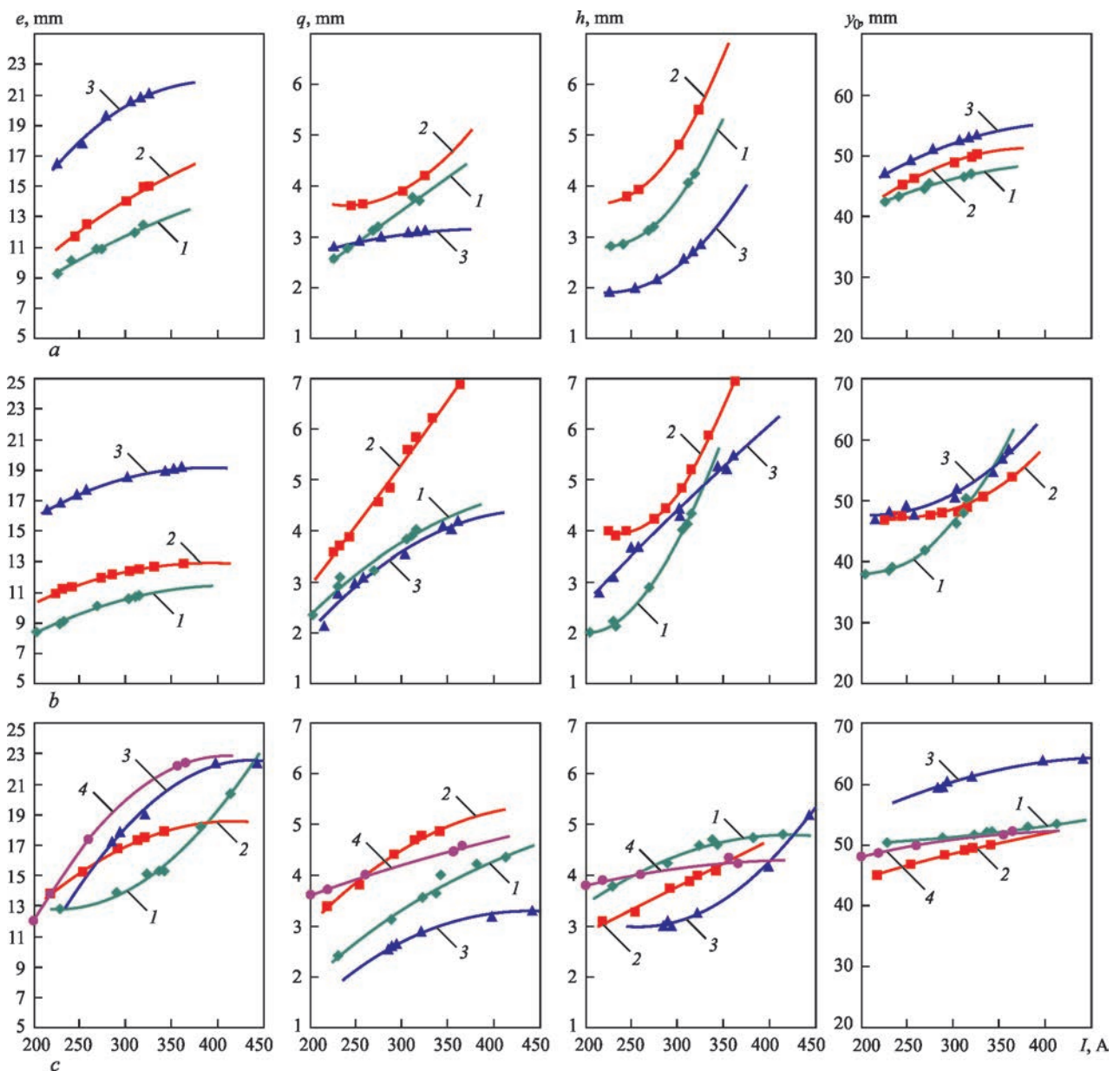


Figure 2. Current and voltage influence on dimensions of beads deposited by submerged arc with PP-Np-25Kh5FMS wire of 1.8 mm (a), 2.4 mm (b) and 2.8 mm (c) diameter: $U = 26$ V (1); 28 V (2); 30 V (3); 32 V (4)

However, application of this method to solve problems, close to additive manufacturing, for instance, restoration of flanges of wheeled vehicles, is significantly limited, because of the need for additional technological fixtures, both for containment of the liquid weld pool, and for containing the flux, which essentially complicates performance of this operation. Therefore, the information obtained under these conditions, was used as a standard, as this method allows deposition mode regulation in a broad range, while producing a well formed deposited metal. It, however, is characterized by considerable penetration depth and deposited metal dilution by base metal [11].

Graphs of dependencies of the influence of electric parameters (current and voltage) on the geometrical characteristics of beads deposited by a submerged arc,

are given in Figure 2. Absence of pores or other defects in the deposited metal was noted in the entire studied range.

As one can see from Figure 2, the depth of base metal penetration becomes greater as a result of current rise, leading to increase of the effective thermal power of the arc. Voltage increase directly proportionally affects the increase of bead width, but at the same time it leads to a certain lowering of their height. It results in the bead upper part acquiring a flatter shape, the deposited metal area becoming smaller and that of the molten metal becoming larger, leading to greater dilution of the deposited metal by base metal.

Minimal value of penetration depth and deposited metal dilution by base metal, at which sound formation of the deposited metal is ensured in the studied

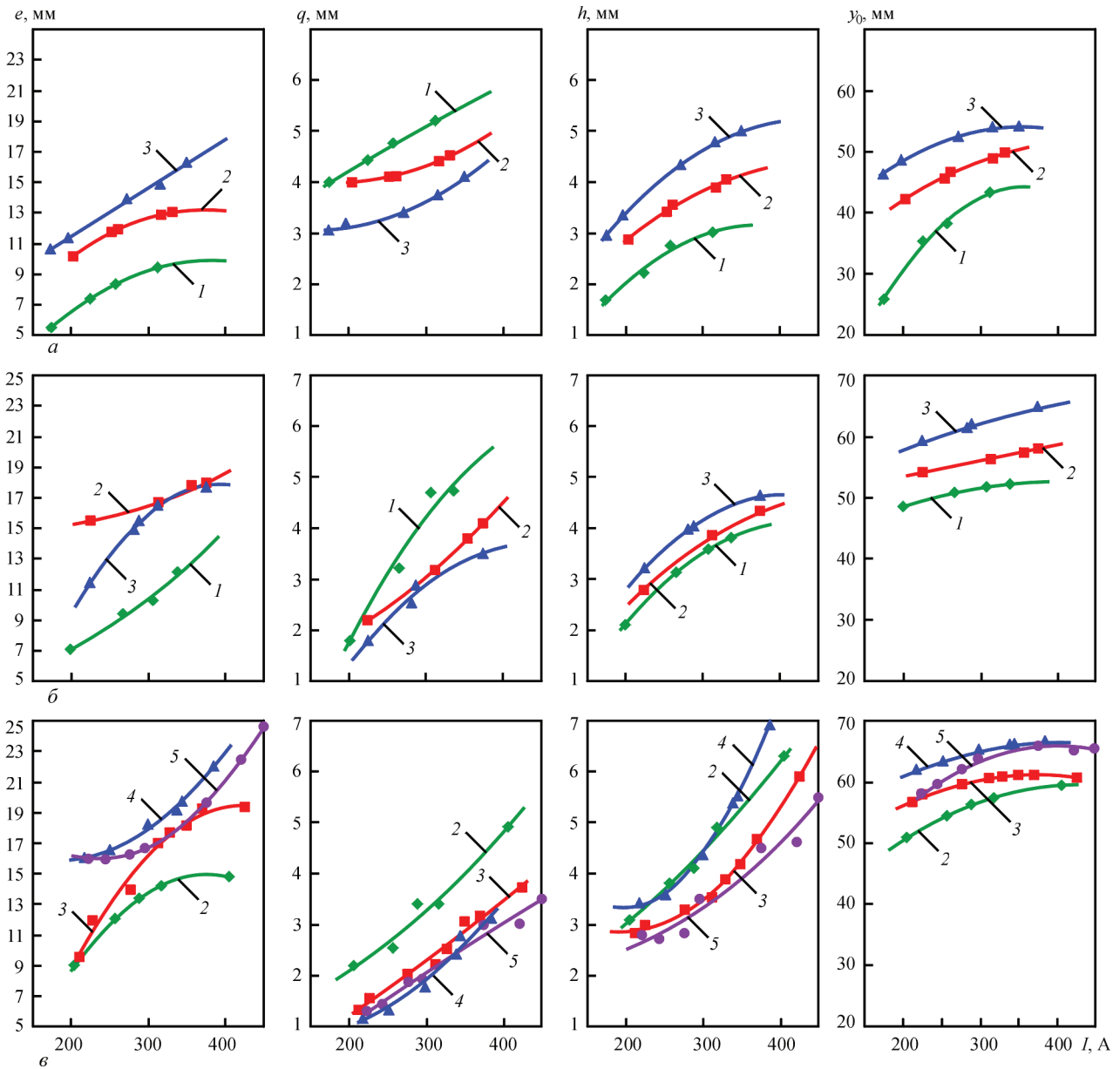


Figure 3. Current and voltage influence on dimensions of beads deposited in shielding gases with PP-Np-25Kh5FMS wire of 1.8 mm (a), 2.4 mm (b) and 2.8 mm (c) diameter: $U = 24$ V (1); 26 V (2); 28 V (3); 30 V (4); 32 V (5)

mode range at submerged-arc deposition, is equal to: 2.0 mm and 49–50 % (1.8 mm wire; $U = 30$ V; $I = 250$ A). For flux-cored wire diameter of 1.8 mm the following modes are optimal: $U = 28$ –30 V; $I = 220$ –300 A; here $h = 2.0$ –4.8 mm; $\gamma_0 = 48$ –52 %. For 2.4 mm diameter: $U = 28$ –30 V; $I = 250$ –350 A; here $h = 3.7$ –5.4 mm; $\gamma_0 = 48$ –56 %. For 2.8 mm diameter: $U = 28$ –32 V; $I = 250$ –400 A; here $h = 3.8$ –4.4 mm, $\gamma_0 = 45$ –52 %.

Application of gas shielding expands the technological capabilities, compared to submerged-arc deposition, allowing deposition on complex-shaped parts with application of different spatial positions, etc. Actually, as was said above, when minimizing machining of the deposited surfaces, this method can be used with success in additive manufacturing. Influence of current and voltage on the quality of forma-

tion and dimensions of beads deposited in shielding gas atmosphere, is shown in Figure 3.

One can see from Figure 3 that both at gas-shielded and at submerged-arc deposition, increase of current and voltage, on the whole, leads to increase of penetration depth, deposited bead width and deposited metal dilution by base metal.

Lower intensity of the influence of current and voltage on bead formation compared to submerged-arc deposition can be noted, which is attributable to lower thermal efficiency of this process through burn-out and spattering losses.

For the method of gas-shielded deposition the minimal values of penetration depth and deposited metal dilution by base metal is equal to 3.4 mm and 43–45 % (1.8 mm diameter wire; $U = 26$ V, $I = 250$ A). The optimal range of modes, in which sound forma-

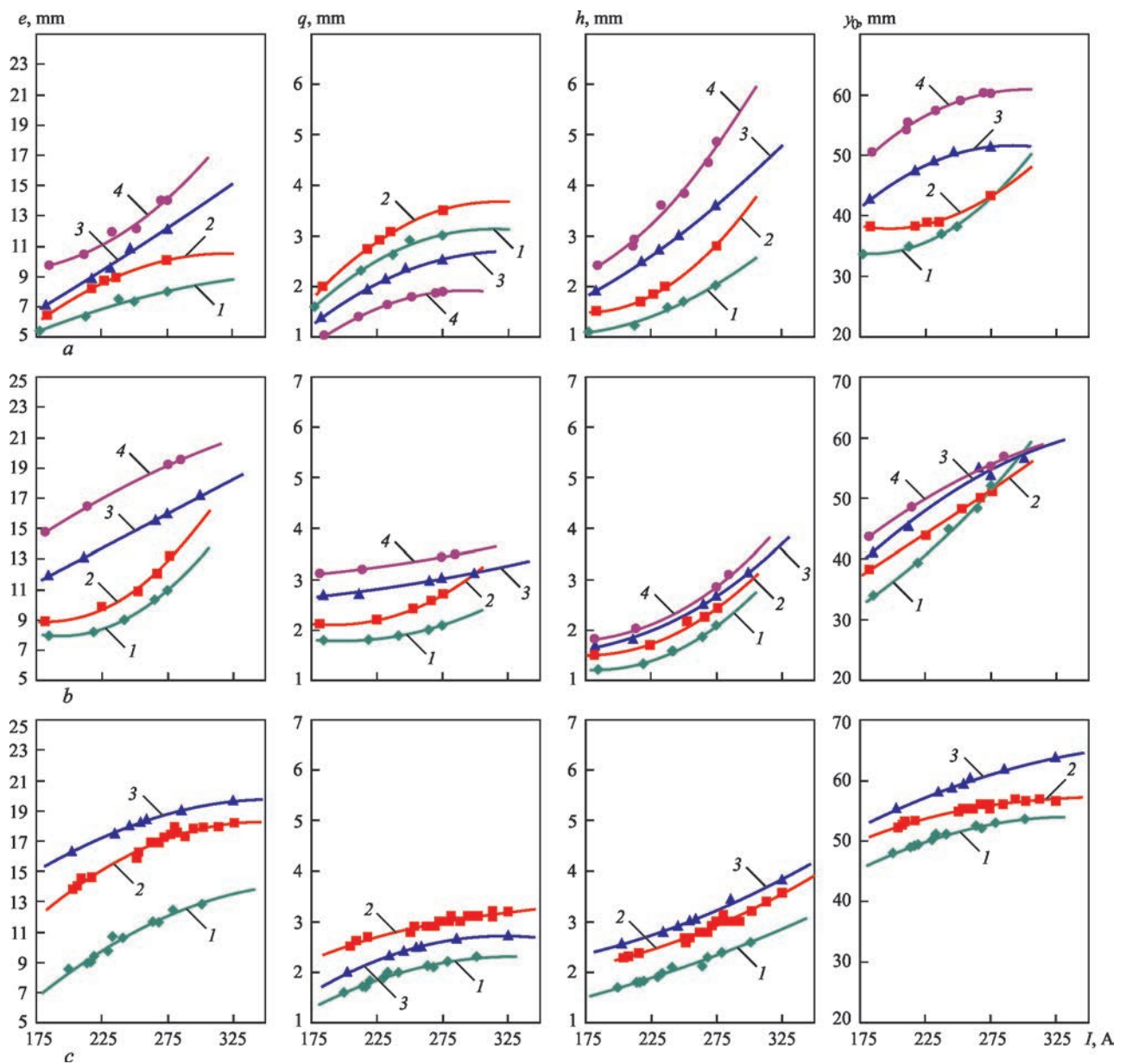


Figure 4. Current and voltage influence on dimensions of beads deposited by self-shielded PP-Np-25Kh5FMS wire of 1.8 mm (a), 2.4 mm (b) and 2.8 mm (c) diameter: $U = 20$ V (1); 22 V (2); 24 V (3); 26 V (4); 28 V (5); 30 V (6)

tion of the deposited beads is ensured for 1.8 mm wire is as follows: $U = 26\text{--}27$ V, $I = 250\text{--}320$ A; here $h = 3.4\text{--}3.8$ mm; $\gamma_0 = 45\text{--}50$ %. For 2.4 mm diameter: $U = 26\text{--}28$ V, $I = 270\text{--}350$ A; here $h = 3.6\text{--}4.0$ mm; $\gamma_0 = 56\text{--}58$ %. For 2.8 mm: $U = 27\text{--}29$ V; $I = 270\text{--}350$ A; here $h = 3.2\text{--}3.7$ mm; $\gamma_0 = 60\text{--}64$ %.

Open-arc deposition (with self-shielded flux-cored wire) has a number of advantages over the above-considered deposition processes, for instance, it does not require any additional shielding of the weld pool from the environment. It, however, has one main disadvantage, which limits a wide application of this process: this is a rather narrow range of admissible deposition modes, deviation from which leads to deterioration of the quality of deposited metal formation and appearance of pores. This factor can be a problem at development of additive manufacturing technology.

Investigations of the influence of electric parameters on metal formation at open-arc deposition showed (Figure 4) that in this case a similar influence of current and voltage on the geometrical dimensions of the beads is seen, as with the previous two methods.

Increase of current value at unchanged voltage leads to an abrupt increase of penetration depth, and to formation of high and narrow beads. This is related to the intensity of liquid metal displacement from under the electrode, as a result of higher arc pressure and energy input.

Arc voltage has little effect on penetration depth, but has a significant influence on the deposited bead width and height, quality of formation and presence of defects in the deposited metal. Here, at too low or too high voltage bead formation is poor and the beads have pores. This process is characterized by a very narrow range of “optimal” modes, primarily by voltage value.

Minimal penetration depth and deposited metal dilution by base metal, at which sound formation of the deposited metal is ensured at open-arc deposition is equal to 1.6 mm and 34–37 % (1.8 mm diameter wire; $U = 22\text{V}$; $I = 220\text{A}$).

For flux-cored wire of 1.8 mm diameter the optimal mode range is as follows: $U = 22\text{--}24\text{ V}$; $I = 200\text{--}250\text{ A}$; here $h = 1.6\text{--}2.4\text{ mm}$, $\gamma_0 = 37\text{--}40\%$. For 2.4 mm diameter: $U = 22\text{--}24\text{ V}$, $I = 210\text{--}300\text{ A}$; here $h = 1.6\text{--}2.4\text{ mm}$, $\gamma_0 = 38\text{--}52\%$. For 2.8 mm diameter: $U = 23\text{--}25\text{ V}$, $I = 220\text{--}300\text{ A}$; here $h = 2.0\text{--}2.6\text{ mm}$, $\gamma_0 = 48\text{--}54\%$.

For all the above deposition methods it is necessary to note the availability of such deposition parameter ranges, in which current and voltage increase leads to a less abrupt increase of penetration depth and deposited metal dilution by base metal, or even their certain decrease. This is attributable to the ratio of current and voltage values in each case, which determine the thermal power and pressure of the arc, and rate of increase of the areas of the deposited and molten metal, accordingly. More over, the penetration depth and deposited metal dilution are influenced by current density that is why in some ranges of current values the depth of penetration for larger diameter wires can be smaller, or it can be equal to that obtained at deposition with smaller diameter wire.

CONCLUSIONS

1. Optimal ranges of current and voltage were established for arc deposition with 1.8, 2.4 and 2.8 mm flux-cored wires in shielding gases, by open arc and by submerged-arc from the view point of achieving sound formation of the deposited beads, absence of defects and minimal penetration depths and deposited metal dilution by base metal. The established dependencies can be used in development of additive manufacturing technology, based on WAAM-methods, primarily GMAW technology.

2. For the method of gas-shielded deposition (GMAW) and 1.8 mm flux-cored wire the minimal penetration depth and deposited metal dilution by base metal is equal to 3.4 mm and 43–45 % at $U = 26\text{ V}$; $I = 250\text{ A}$; $V = 20\text{ m/h}$.

3. The smallest penetration depth and deposited metal dilution by base metal can be achieved at open-arc deposition with 1.8 mm flux-cored wire in the following mode: $U = 22\text{ V}$; $I = 220\text{ A}$; here $h = 1.6\text{ mm}$, $\gamma_0 = 37\%$. However, it is difficult to apply this method for additive manufacturing, because of the presence of a small amount of slag crust and spatter on the deposited bead surface.

REFERENCES

- Ryabtsev, I.A., Kuskov, Yu.M., Pereplyotchikov, E.F., Babinets, A.A. (2021) *Surfacing, control of base metal penetration and formation of deposited layers*: Monography. Ed. by I.A. Ryabtsev. Kyiv, Interservice [in Russian].
- The Future for WAAM*. <https://additivemanufacturing.com/2019/08/27/the-future-for-waam/>
- Wohlers, T. (2014) *Additive manufacturing and 3D-printing state of the industry*: Annual worldwide progress report. Wohlers Associates.
- Ding, D., Pan, Z., Cuiuri, D. et al. (2015) Wire-feed additive manufacturing of metal components: Technologies, developments and future interests. *The Int. J. of Adv. Manuf. Technol.*, **811**(4), 465–481. DOI: <https://doi.org/10.1007/s00170-015-7077-3>
- Bonaccorso, F., Cantelli, L., Muscato, G. (2011) Arc welding control for shaped metal deposition process. *IFAC Proceedings Volumes*, **44**(1), 11636–11641. DOI: <https://doi.org/10.3182/20110828-6-IT-1002.01575>
- Ding, D., Shen, C., Pan, Z. et al. (2016) Towards an automated robotic arc-welding-based additive manufacturing system from CAD to finished part. *Computer-Aided Design*, **73**, 66–75. DOI: <https://doi.org/10.1016/j.cad.2015.12.003>
- Prado-Cerqueira, J.L., Dieguez, J.L., Camacho, A.M. (2017) Preliminary development of a wire and arc additive manufacturing system (WAAM). *Procedia Manufacturing*, **13**, 895–902. DOI: <https://doi.org/10.1016/j.promfg.2017.09.154>
- CMT — Cold Metal Transfer: The cold welding process for premium quality*. <https://www.fronius.com/en/welding-technology/world-of-welding/fronius-welding-processes/cmt>
- Cong, B., Ding, J., Williams, S. (2015) Effect of arc mode in cold metal transfer process on porosity of additively manufactured Al–6.3 % Cu alloy. *The Int. J. of Adv. Manuf. Technol.*, **76**, 1593–1606. DOI: <https://doi.org/10.1007/s00170-014-6346-x>
- Ryabtsev, I.A., Lankin, Yu.N., Soloviov, V.G. et al. (2015) Computer information-and-measuring system for investigation of arc surfacing processes. *The Paton Welding J.*, **9**, 32–35. DOI: <https://doi.org/10.15407/tpwj2015.09.05>
- Babinets, A.A., Ryabtsev, I.A., Panfilov, A.I. et al. (2016) Influence of methods of arc surfacing with flux-cored wire on penetration of base metal and formation of deposited metal. *The Paton Welding J.*, **11**, 17–22. DOI: <https://doi.org/10.15407/tpwj2016.11.03>

ORCID

A.A. Babinets: 0000-0003-4432-8879

CORRESPONDING AUTHOR

A.A. Babinets

E.O. Paton Electric Welding Institute of the NASU
11 Kazymyr Malevych Str., 03150, Kyiv, Ukraine.

E-mail: a_babinets@ukr.net

SUGGESTED CITATION

A.A. Babinets (2023) Control of formation of metal produced by arc methods of layer-by-layer deposition of material with flux-cored wires. *The Paton Welding J.*, **11**, 35–40.

JOURNAL HOME PAGE

<https://patonpublishinghouse.com/eng/journals/tpwj>

Received: 19.10.2023

Accepted: 07.12.2023

RECONDITIONING REPAIR OF STEAM TURBINE BLADES USING ADDITIVE TECHNOLOGY

O.V. Makhnenko, G.Yu. Saprykina, O.M. Savytska, M.S. Ananchenko

E.O. Paton Electric Welding Institute of the NASU

11 Kazymyr Malevych Str., 03150, Kyiv, Ukraine

ABSTRACT

It is rational to use additive technology to perform repair of critical structural elements, which include titanium alloy blades of powerful steam turbines, that is due to high requirements to product quality, namely the need to ensure the required microstructure and mechanical properties of blade material, as well as a low level of the residual stress-strain state and oxidation of material surface. Application of mathematical modeling methods based on computer technologies allows reduction of the scope of experimental studies and ensuring the required quality of repair, which guarantees a certain reliability and serviceability of the blades after repair.

KEYWORDS: steam turbine, blade, titanium alloy, reconditioning repair, additive technology, electron beam surfacing, computational prediction

INTRODUCTION

Five powerful steam turbines of K-1000-60/3000 type are operating in Ukrainian NPS. In them the blades of the last stages of low pressure cylinders (LPC) are exposed to wet steam environment and erosion damage (Figure 1). This factor reduces the residual service life of the blades from titanium alloy, leads to possible shutdowns and accidents in turbounits. The conducted set of studies [1, 2] resulted in determination of the mechanical properties, their possible degradation and fatigue limit of blade material under the conditions of long-term operation. Extension of the service life of 5th stage blade of LPC of K-1000-60/3000 turbines under the conditions of wet steam erosion is a relevant problem now.

Analysis of currently available means of extension of the life of titanium alloy blades under the conditions of wet erosion and vibration loads [1] showed that the safe operating life of the blades of the last stage of the turbine LPC can be extended based on rejection criteria and under the conditions specified below:

- by chord size: in keeping with [3], after removal of erosion wear of the leading edges of blades from TS5 titanium alloy, control by etching method should be performed; limiting size of profile chord in eroded sections, which requires blade replacement, when it has been reached (with allowable delay of not more than 1 year in the case of absence of a replacement blade) — 130 mm;

- by shroud state: repair is required in the case of development of wear (gaps) of more than 1 mm in the contact surfaces as well as cleavages and chipping;

- by operating time: for blades from TS5 titanium alloy the permissible service life is 100 thou h.

Note that the criterion for blade rejection by operating time is too conservative. Experience shows that blades, with more than 180 thou h operating time (SE KhNPS) have been in service almost two times longer than the service life allowed by the manufacturer.

In addition, the manufacturing plant of K-1000-60/3000 type turbines provided to the operators the technological process of repairing the defects on LPC 5th stage blades by arc welding on of inserts with subsequent scraping and control of the welding areas. The recommended modes of nonconsumable electrode gas-shielded (argon) welding without filler material were as follows: tungsten electrode $d = 2$ mm; current of 50–80 A, straight polarity, argon flow rate of 8–10 l/min.

Thus, to sum up the above-said, the blade service life can be extended, if:

- limiting size of blade chord in eroded sections is not less than 130 mm;

- wear (gap) in the shroud contact surfaces of less than 1 mm, no spallation or chipping;

- repair has already been performed with removal of erosion on blade edges and wear on shroud contact surfaces, using machining in the case, when the chord size after repair is not smaller than the limiting one, or with application of inserts, made by the technology of nonconsumable electrode argon-arc welding.

However, the manufacturing plant did not provide any substantiation for ensuring a low level of total blade deformations during repair by argon-arc welding and sufficient level of blade material fatigue resistance in the melting zone and the HAZ.



Figure 1. Erosion wear of a blade of the last stage of K-1000-60/3000 steam turbine LPC: *a* — general view of 5th stage; *b* — defect of blade edge erosion wear

A promising approach is repair of titanium alloy blades of K-1000-60/3000 turbines, using modern technologies of layer-by-layer formation by electron beam deposition in vacuum chambers, which can ensure a low level of residual shape deformations, as well as the required microstructure and mechanical properties of blade material.

THE OBJECTIVE OF THE WORK

is to show the possibility of reconditioning repair of titanium alloy blades of steam turbines, using additive technology of electron beam deposition in vacuum chambers, which can provide the required mechanical properties and geometrical accuracy of the product, compared to application of argon-arc welding.

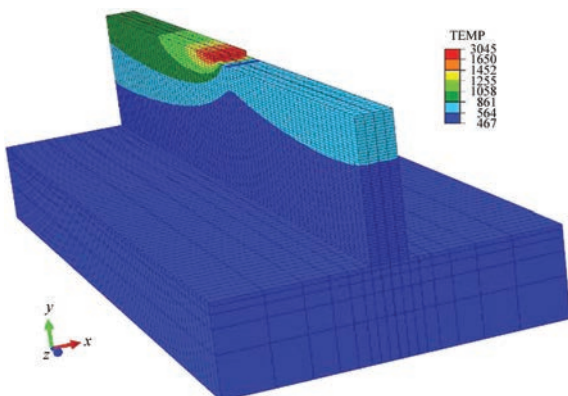


Figure 2. Results of calculation of temperature distribution in a tee sample during layer-by-layer formation of the part [5]

RECONDITIONING REPAIR TECHNOLOGY

Technology of repair surfacing of K-1000-60/3000 turbine LPC 5th stage blades with erosion damage should include the following stages:

1. Machining of erosion wear zone with damaged metal removal.
2. Multilayer electron beam surfacing of the wear zone to restore the initial dimensions.
3. Heat treatment (general) of the blade to form the required metal structure and lower the residual stress level.
4. Machining to sizes and roughness of blade surface specified in the design documentation.
5. Protective coating deposition (option) [4].

The most complicated is stage 2 of the proposed technology, namely multilayer electron beam surfacing of the wear zone to initial dimensions in vacuum chambers, as it is necessary to ensure a low level of residual shape deformations and stresses of the blade, as well as the required microstructure and mechanical properties of blade material. To analyze this issue, finite element modeling of this technological operation was performed on a model of a tee-sample of a limited size and on full-scale blade model.

INVESTIGATIONS OF THE FEATURES OF THE INFLUENCE OF TECHNOLOGICAL PARAMETERS OF LAYER-BY-LAYER SURFACING ON THE TEE SAMPLE RESIDUAL STATE

Layer-by-layer electron beam surfacing of a sample from VT6 titanium alloy by stringer beads of 3 mm width and approximately 0.5 mm thickness was considered. Surfacing speed was 14 mm/s. The results of solving the task of nonstationary heat conductivity showed that the temperature field kinetics at layer-by-layer formation of the tee sample on a substrate of 6×30×70 mm dimensions, which simulates the blade body in terms of heat conductivity and rigidity of the structure, has an essentially three-dimensional nature (Figure 2) [5].

As proved by calculation results, this process is characterized by rather high cooling rates (160–660 °C/s). In keeping with the diagram of microstructural transformations of VT6 alloy, a martensitic microstructure with α'' -phase content forms in the deposited material of the tee sample [6]. According to calculation data, grain of 180 μm size forms in the material of the first layer, where the highest cooling rate was achieved due to the presence of a massive cold substrate, and in the points at formation of the 5th and 20th layers, where the material is deposited on the already heated sample, the grain size is much larger — 300–450 μm .

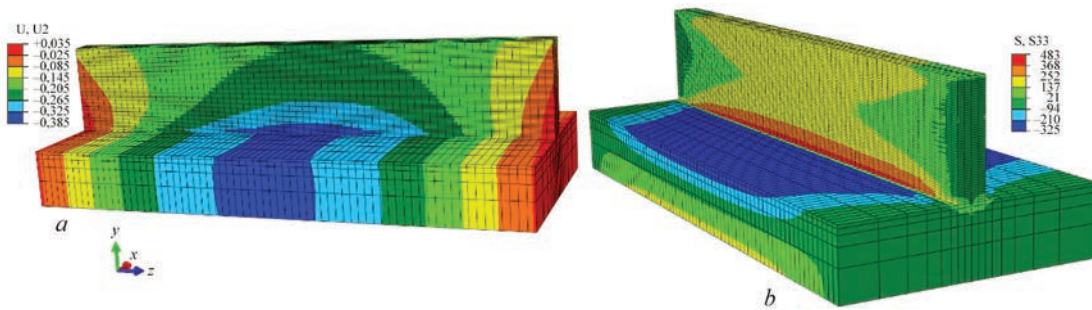


Figure 3. Results of calculation of residual stress-strain state in a tee sample [5]: *a* — longitudinal deflection; *b* — longitudinal stresses

Technological parameter of delay time Δt between bead deposition (Figure 4, *a-c*) has an essential influence on the cooling rate and grain size, and, as a result, on the part material yield limit [6]. It is seen that better mechanical characteristics and more homogeneous material structure were determined in the sample, made with greater time Δt , while insufficient time between bead deposition of $\Delta t = 10$ and 15 s results in upper layer material with a low yield limit and grain heterogeneity by height. However, a too long interpass time (65 s) leads to an excess of α' -structure, and, hence, it lowers the material ductility, compared to shorter interpass time. Thus, it is rational to consider the use of substrate preheating at $\Delta t = 29$ s. Substrate preheating makes the lower layer structure

more homogeneous and essentially improves the material ductility.

FINITE ELEMENT MODELING OF ELECTRON BEAM SURFACING OF THE BLADE

A finite element model of 5th stage blade of K-1000-60/3000 turbine LPC was developed, where repair surfacing of the material (TS5 or VT6 titanium alloy) is modeled in the characteristic erosion zone, namely in the blade upper part of 100 mm length. Surfacing mode is similar to modes for tee samples. Surfacing zone height is taken to be equal to 10 mm, which corresponds to maximal level of the depth of blade erosion damage. It is envisaged that before surfacing, machin-

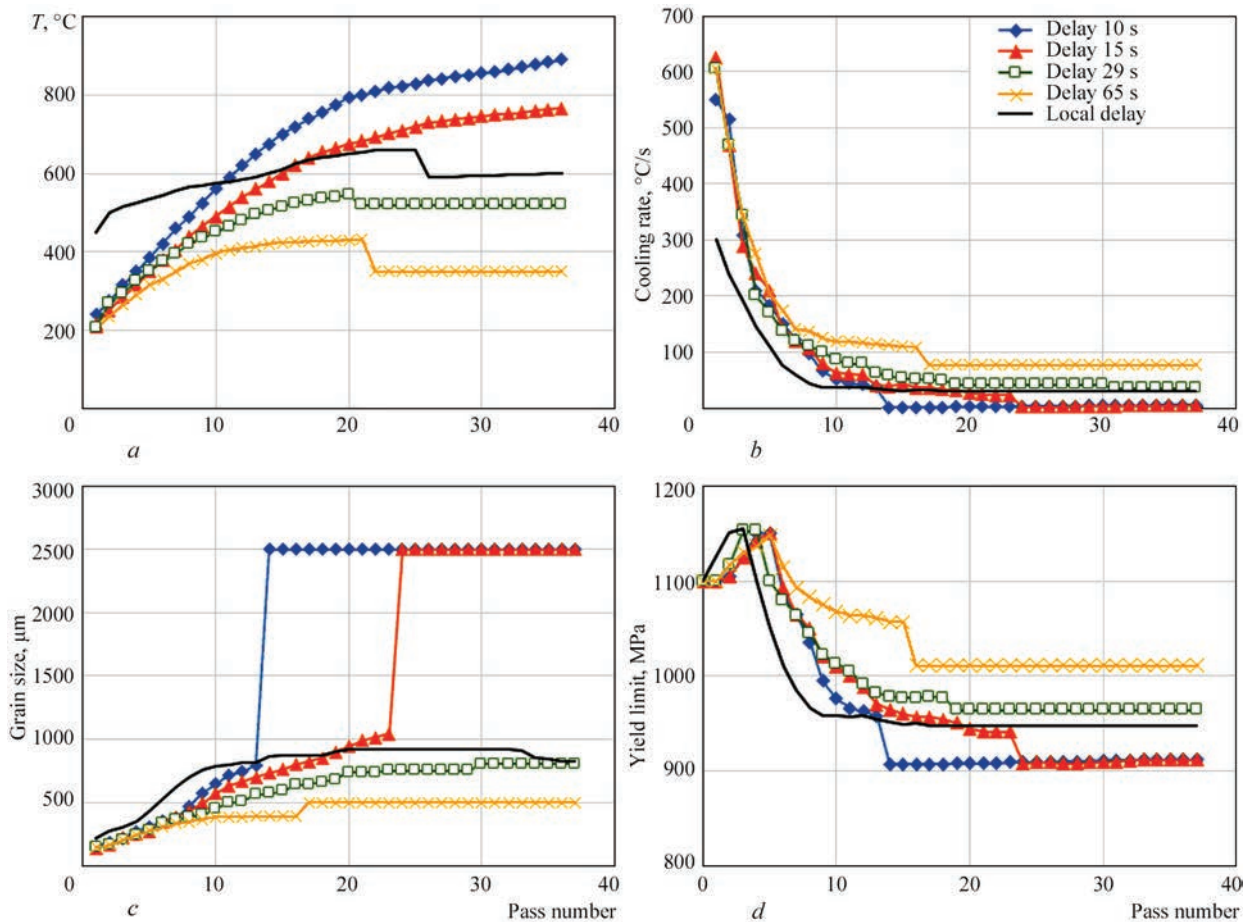


Figure 4. Dependence of temperature in a point before the next layer deposition (*a*), cooling rate (*b*), grain size (*c*) and material yield limit (*d*) on pass number for different interpass delay times [6]

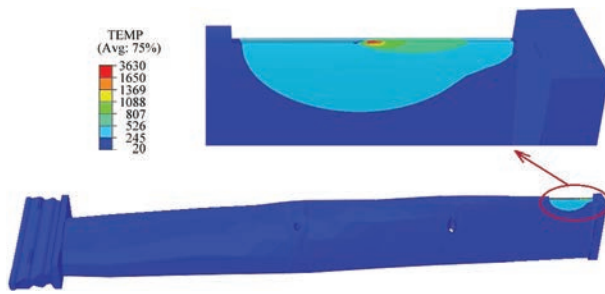


Figure 5. Temperature distribution during electron beam surfacing

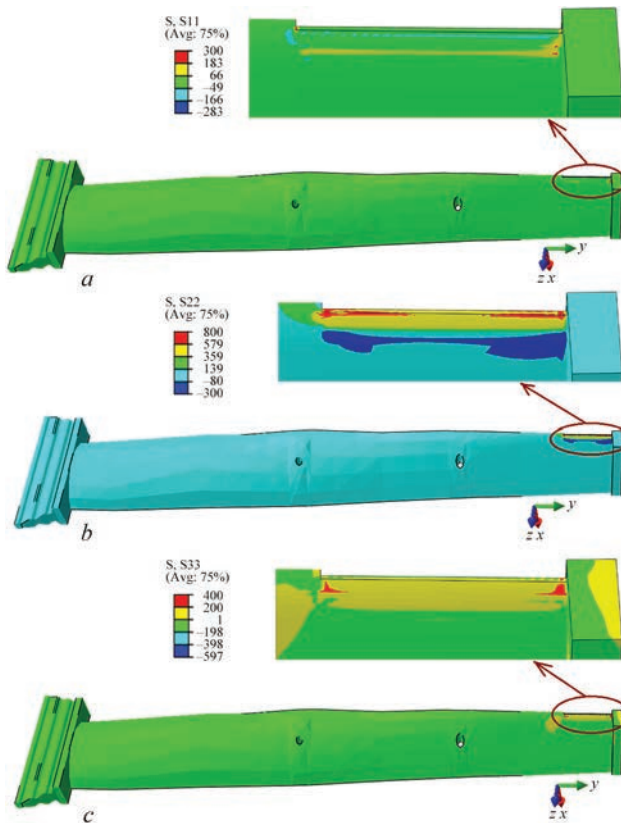


Figure 6. Residual stress distribution: *a* — σ_{xx} component by deposit height ($\sigma_{xx} = 150\text{--}300$ MPa); *b* — σ_{yy} longitudinal component ($\sigma_{yy} = -300\text{--}800$ MPa); *c* — σ_{zz} transverse component by blade thickness ($\sigma_{zz} = -200\text{--}400$ MPa)

ing of the erosion damage zone is performed with removal of blade material to the depth of 10 mm. The objective of mathematical modeling is prediction of residual level of the stressed state and total deformations of the blade shape change, as well as the material structural state in the surfacing zone, which can be used for selection of the optimal technological parameters of repair surfacing. Considering the overall dimensions of the blade (length of 1200 mm), it is possible to perform general (furnace) heat treatment after surfacing, in order to lower the residual stress level and produce a more homogeneous structure of the material.

Figure 5 shows the calculated temperature distribution during electron beam surfacing of the blade. In the surfacing mode with 29 s pauses between the layers, the material of the zone of reconditioning re-

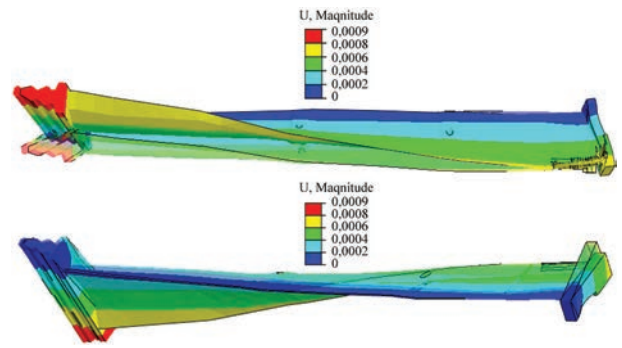


Figure 7. Blade residual deformations (torsional), up to 0.9 mm value of maximal displacements

pair of the blade is heated up to the temperature of 250–500 °C.

Total deformations of the blade shape change remain to be a critical parameter for the repair surfacing technology. Analysis of the obtained results of the numerical experiment (Figures 6, 7) on repair surfacing of the blade in the erosion damage zone showed that:

- Rather high residual stresses (longitudinal component) form in the surfacing zone (locally), on the level of the titanium alloy yield limit (up to ≈ 800 MPa).
- After surfacing undesirable total residual deformations of the blade (torsional) are predicted, the value of maximal displacements is up to 0.9 mm.
- Modeling of the general heat treatment in the furnace can show an essential lowering of the residual stresses (positive effect) and increase of the blade total deformations (negative effect).

An important issue of the technology of repair surfacing of critical structural elements is ensuring a low level of the deposited material damage during manufacture and determination of the requirements to permissible defect dimensions. As regards manufacturing using the technology of layer-by-layer formation by electron beam surfacing of T-beam structures, it was shown by numerical studies of brittle strength [7] that the required resolution of non-destructive testing is equal to approximately 0.5 mm, which ensures a strength margin of not less than $n = 2$, while maintaining the required conditions of the temperature mode of product formation, in terms of providing the required structure and mechanical properties of blade material.

CONCLUSIONS

1. An approach is proposed to repair of titanium alloy blades of a powerful steam turbine K-1000-60/3000, using additive technology of layer-by-layer formation, in order to restore the initial geometry by electron beam surfacing in vacuum chambers.

2. Results of finite element modeling showed the fundamental possibility of ensuring a low level of residual shape deformations, as well as the required

microstructure and mechanical properties of blade material after reconditioning repair, using additive technology of layer-by-layer formation. However, it is rational to perform general heat treatment, in order to lower the residual stress level and to ensure a high homogeneity of the material structure and mechanical properties in the repair zone.

REFERENCES

1. Torop, V.M., Makhnenko, O.V., Saprykina, G.Yu., Gopkalo, E.E. (2018) Results of studying the causes for cracking in titanium alloy blades of steam turbines of K-1000-60/3000 type. *Tekh. Diagnost. ta Neruiniv. Kontrol*, **2**, 3–15. DOI: <https://doi.org/10.15407/tdnk2018.02.01> [in Russian].
2. Kanel, G.I., Razorenov, S.V., Fortov, V.E. (2004) *Shock-wave phenomena and the properties of condensed matter*. New-York, Berlin, Heidelberg, Hong Kong, London, Milan, Paris, Tokyo, Springer. DOI: <https://doi.org/10.1007/978-1-4757-4282-4>
3. (2004) SO 153-34.17.462–2003: *Control by etching method blades of TS5 alloy after removal of erosion wear. Instruction*. Moscow, Minenergo RF [in Russian].
4. Bilous, V.A., Voevodin, V.M., Khoroshikh, V.M. et al. (2016) Development of experimental equipment and main technological procedures for producing cavitation-resistant coatings on working surfaces of blades of steam turbines from titanium alloy VT6 for replacement of similar imported products. *Nauka ta Innovatsii*, **12(4)**, 27–37. DOI: <https://doi.org/10.15407/scin12.04.027>
5. Makhnenko, O.V., Milenin, A.S., Velikoivanenko, E.A. et al. (2017) Modelling of temperature fields and stress-strain state of small 3D sample in its layer-by-layer forming. *The Paton Welding J.*, **3**, 7–14. DOI: <https://doi.org/10.15407/tpwj2017.03.02>
6. Makhnenko, O.V., Ananchenko, N.S., Kandala, S.M. et al. (2018) Prediction of structure and mechanical properties of

VT6 titanium alloy at layer-by-layer formation of 3D products using additive technology of electron beam surfacing. *Mechanics and Advanced Technologies*, **84(3)**, 5–14. DOI: <https://doi.org/10.20535/2521-1943.2018.84.144127>

7. Makhnenko, O.V., Milenin, A.S., Velikoivanenko, E.A. et al. (2018) Prediction of kinetics peculiarities of thermodeformational state of compacts specimens of different geometry at their layer-by-layer formation in equipment xBeam 3D Metal Printer. In: *Proc. of 9th Int. Conf. on Mathematical Modeling and Information Technologies in Welding and Related Processes*, 68–76.

ORCID

O.V. Makhnenko: 0000-0002-8583-0163,
G.Yu. Saprykina: 0000-0003-1534-7253,
O.M. Savytska: 0000-0002-9363-6184,
M.S. Ananchenko: 0000-0003-2723-6673

CONFLICT OF INTEREST

The Authors declare no conflict of interest

CORRESPONDING AUTHOR

O.V. Makhnenko
E.O. Paton Electric Welding Institute of the NASU
11 Kazymyr Malevych Str., 03150, Kyiv, Ukraine.
E-mail: oleh.makhnenko@gmail.com

SUGGESTED CITATION

O.V. Makhnenko, G.Yu. Saprykina, O.M. Savytska, M.S. Ananchenko (2023) Reconditioning repair of steam turbine blades using additive technology. *The Paton Welding J.*, **11**, 41–45.

JOURNAL HOME PAGE

<https://patonpublishinghouse.com/eng/journals/tpwj>

Received: 20.10.2023

Accepted: 07.12.2023



**VII INTERNATIONAL
CONFERENCE ON WELDING
AND RELATED TECHNOLOGIES**

7-10 October 2024 Kyiv, Ukraine

www.wrt2024.com.ua

DOI: <https://doi.org/10.37434/tpwj2023.11.06>

ADDITIVE MANUFACTURING OF STRUCTURAL ELEMENTS ON A THIN-WALLED BASE: CHALLENGES AND DIFFICULTIES (REVIEW)

M.V. Sokolovskiy¹, A.V. Bernatskiy¹, N.O. Shamsutdinova¹, Yu.V. Yurchenko¹, O.O. Danyleiko^{1,2}

¹E.O. Paton Electric Welding Institute of the NASU
11 Kazymyr Malevych Str., 03150, Kyiv, Ukraine

²E.O. Paton Education&Research Institute of Materials Science and Welding
of the National Technical University of Ukraine “Igor Sikorsky Kyiv Polytechnic Institute”
37 Prospect Beresteiskyi (former Peremohy), 03056, Kyiv, Ukraine

ABSTRACT

In the work a literature review of materials was conducted, devoted to different areas of studying selective laser melting (SLM) and selective laser sintering (SLS) technologies in order to analyze the processes associated with selective laser deposition occurring during SLM and SLS, as well as the impact of technological measures on the final structure, mechanical and service characteristics of a manufactured part in the additive manufacturing of structural elements on a thin-walled base. The main tasks of research works analyzed in the review were studies focused on the features of structural element formation on a thin-walled base by means of SLM and SLS technologies: modeling of additive manufacturing processes; aspects of planning experiments and manufacturing processes; studying the course of SLM and SLS processes in the given conditions; need in pre- or post-treatment of material; as well as analysis of the final microstructure and characteristics of samples manufactured using these technologies. Based on the results of literature review, problems were identified and the prospects of using SLM and SLS processes were considered during formation of structural elements on a thin-walled base. A number of aspects were defined, to which it is necessary to pay attention during these studies of SLM and SLS processes when working with a thin-walled base.

KEYWORDS: selective laser melting (SLM), additive manufacturing, selective laser sintering (SLS), thin-walled products

INTRODUCTION

Thin-walled parts are a category of parts, where thickness is much smaller than their dimensions (and does not exceed 3–5 mm). Thin-walled parts can include different types of products, the main characteristic of

which is absence of rigidity and high final thinness factor, which is determined as their height, divided by their thickness. As regards the product varieties by their characteristics, these parts can be classified into two groups: monolithic blocks and skin panels. Such parts are widely applied in aviation industry (Figure 1), engine building, as well as in other industries [1, 2].

These and other parts often require fabrication of structural elements, which can be manufactured using many technologies, including laser cladding [1, 3].

Laser cladding is a procedure for manufacture of structural elements by creating material layers on the product surface as a result of melting of this material powder by the laser beam [4, 5]. This process allows deposition of layers of up to 100–500 μm thickness, using 2–4 mm laser beam (of up to 5 kW power) [6, 7] and feeding metal powder or wire by different methods (Figure 2) [5].

Over the last decades, however, such additive manufacturing technologies as selective laser sintering and selective laser melting have been more and more often used for manufacturing structural elements on thin-walled parts for reasons, related to the characteristics of materials produced by these methods [8–10].

Selective laser sintering (SLS) is an additive manufacturing technology, which is used for making products of a complex shape and structure from powder materials and optional polymer additives (Figure 3). This process consists in a sequential layer-by-layer sintering (or par-

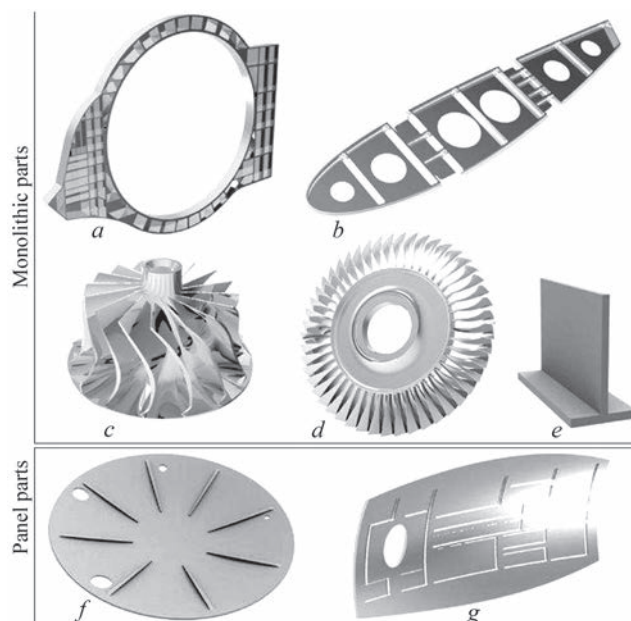


Figure 1. Examples of thin-walled parts in aviation industry: *a* — frame; *b* — stiffener; *c, d* — components of jet engine turbines; *e* — ribs; *f* — partitions; *g* — fuselage skin components [1]

Copyright © The Author(s)

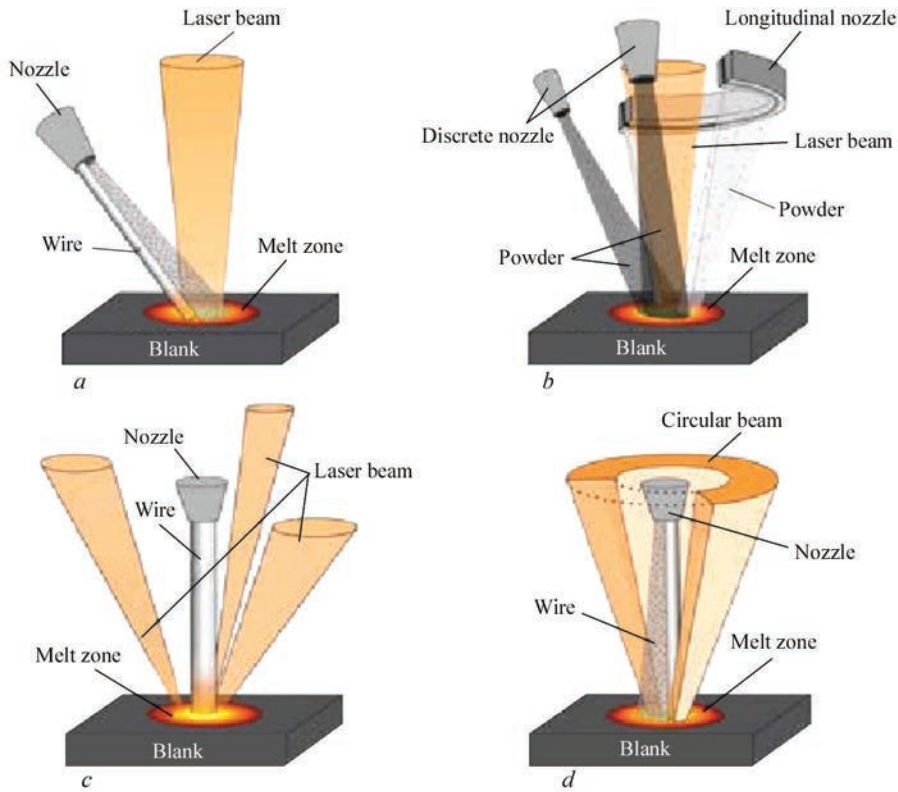


Figure 2. Schemes of material feed for laser deposition: *a* — lateral; *b* — coaxial with feeding from two angles; *c* — axial, with laser beams coming from the sides; *d* — axial with circular laser beam [5]

tial melting) of material in a pre-laid powder material, using laser radiation or the electron beam [11]. This technology allows deposition of layers of metallic, plastic or ceramic material 20–150 μm thick by a laser or electron beam of up to 300 μm diameter [12, 13].

Advantages of SLS technology application are as follows:

- wide range of possible materials;
- sufficient accuracy of the finished part;
- possibility of making parts of a more complex geometry.

The disadvantages of SLS technology are high porosity of the manufactured part surfaces and nonuniform value of internal density of the part material [5, 11, 13].

Selective Laser Melting (SLM) is one of the modern additive manufacturing technologies, which is used for making products of a complex shape and structure from powder materials. This process consists in a sequential layer-by-layer melting of pre-laid powder material in a special protective chamber using powerful laser radiation (Figure 4) [13, 14]. This technology allows deposition of up to 20–200 μm layers by a laser beam of 100 W to 2–3 kW.

The advantages of SLM technology application are the basis for serious prospects — increase of production efficiency in many industries, as:

- the process ensures high accuracy (up to 0.4 mm) and repeatability;

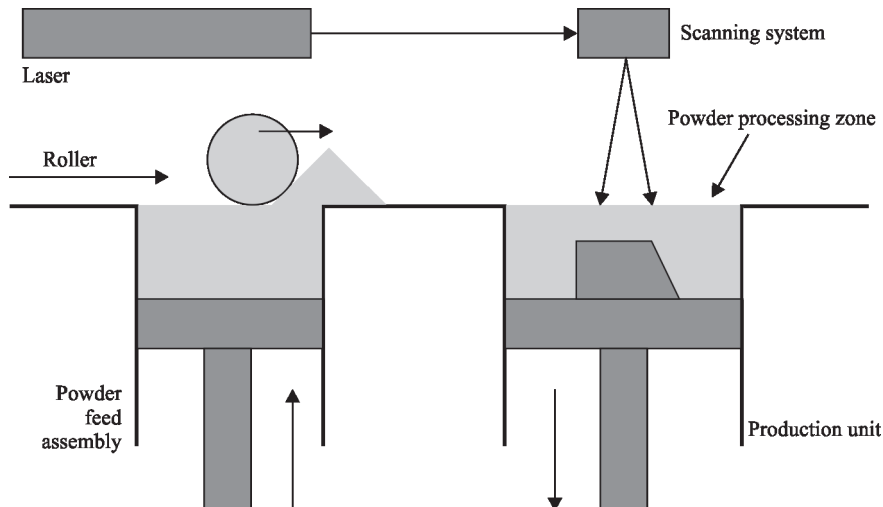


Figure 3. Schematic of the unit for SLS process [12]

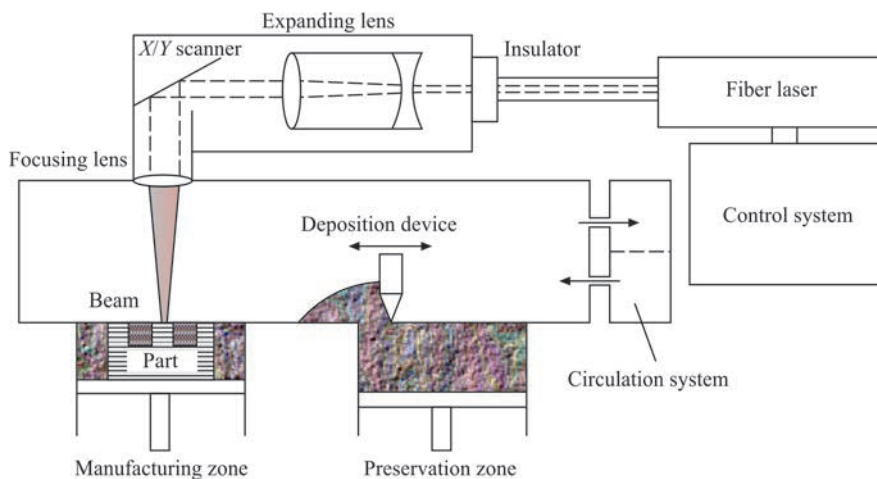


Figure 4. Schematic of the unit used for SLM [5]

- mechanical characteristics of products printed in this type of 3D-printer are comparable with castings [15];
- it solves complex technological tasks, associated with manufacturing products of a complex geometry;
- it allows reducing the weight due to construction of objects with inner cavities; and
- it allows material saving in production.

Despite the numerous advantages, the main disadvantages of SLM process, compared to deposition-based methods of part manufacturing, is a comparatively low productivity and impossibility to produce large-sized parts [5, 13, 14].

The main difference between the SLS and SLM processes consists in that SLS sinters the powder material at a temperature equal to approximately 85 % of deposited material T_m , while SLM joins the powder material by classical laser melting.

When working with thin-walled products, the problem arose of deposition of structural components on a thin-walled blank. Under these conditions laser cladding application involves a very high risk of deformations and blank melting-through [4, 7]. Manufacturing of thin-walled elements, as well as elements on a thin-walled base, remains to be one of the rapidly advancing directions of development of additive manufacturing technologies. Here, application of additive manufacturing technologies opens up new possibilities for deposition process control [9, 11, 14], as well as achieving better properties of the deposited material [14, 15].

For this reason, it was determined to be necessary to conduct analysis of the works devoted to studying the technologies of laser additive manufacturing, in order to take into account the experience of process improvement, which is used during fulfillment of this task. Special attention is given to analysis of the studies, related to products on thin-walled base, as parts of such a configuration are some of the most complex items for application of additive manufacturing

processes. In view of this issue, as well as other features inherent to SLM and SLS processes [16–18], the problem arises of studying the components of these processes. For this purpose, a number of studies were reviewed in this paper, which are devoted to SLM and SLS manufacturing of parts on a thin-walled base. The objective of this work is establishing the relevant directions of studying different scientific components of SLM and SLS process, as well as analysis of the influence of technological measures on the final structure of the finished part, and its mechanical and service characteristics, in order to determine important aspects of SLM and SLS processes in manufacture of parts with a thin-walled base.

ANALYSIS OF THE INFLUENCE OF EXPERIMENT PLANNING ON ADDITIVE TECHNOLOGY PROCESSES

When studying the additive manufacturing processes sufficient attention is given to the components of experiment planning and preliminary mathematical preparation: studying the additive manufacturing processes in the mathematical dimension, as well as preliminary modeling of the process.

Mathematical modeling is an integral part of the experiment, as it allows quickly establishing the most promising variants of processing modes, and other factors, which markedly enhances the process productivity. There exist several variants of mathematical modeling; the most widely used is the finite element method. In practical studies of the finite element method two approaches are distinguished: a procedure focused on studying the influence of a separate quantity on the process, and is aimed at obtaining an optimal result for an individual task, which was described in works [19, 20]; as well as a procedure based on application of rows of planeless numbers, which was described in the work by Mukherjee, et al. [21]. This procedure is based on Marangoni, Peclet and Fourier numbers and values of planeless energy input, and it assumes that use of groups of values simplifies the

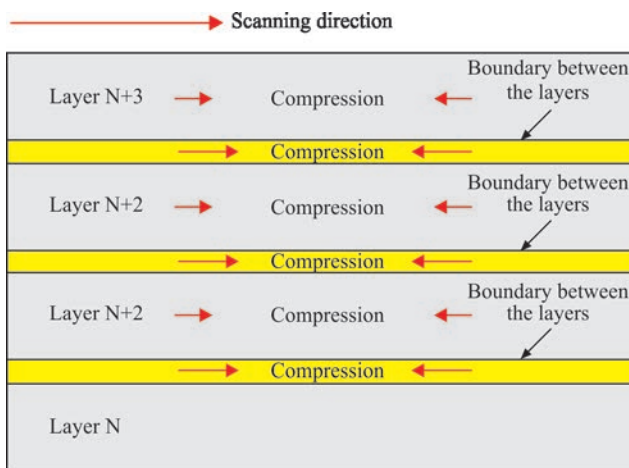


Figure 5. Abstract scheme of loads inducing deformations in additive manufacturing of thin-walled parts or elements on their surface [22]

general process of modeling the complex processes of additive manufacturing, may lead to a more profound analysis of the dynamics of behaviour of such processes, and it also allows establishing more profound principles of interdependence between the values of variables in these processes [21].

The next relevant problem of studying the processes of additive manufacturing on a thin-walled base is modeling the stresses generated when working with thin-walled elements. The process of thin-walled element manufacturing using SLM is considered in the paper by Yang et al. [22]. The results of this work point to considerable internal stresses, arising in the first deposited layers of powder material, the magnitude of which is believed to be sufficient for deformation of this surface during operation (Figure 5).

It should be noted that there is such a risk also for the pre-specified existing thin-walled part, onto which a layer will be deposited during selective laser deposition. Reduction of internal stresses can be achieved by many methods: from controlling the laser radiation energy characteristics, reported in the works by Li et al. [23] and Abele et al. [24], controlling the powder feed rate (paper by Liu et al. [25]), up to subsequent complex heat treatment of the part, which was described in the paper by Niu et al. [26].

Here, however, we should not forget about the discrepancies between the mathematical model values and the actual experimental data. Complex manifestations of the discrepancies between the results of modeling the additive manufacturing processes and the experimental results are given a lot of attention in works [19–21]. This discrepancy often is dynamic. Figure 6 gives an example in which it was reported [21] that even at confirmation of the majority of mathematical calculations by experimental data, there exist problems of accurate calculation of the melt zone during computation of the first deposited layers of the powder material.

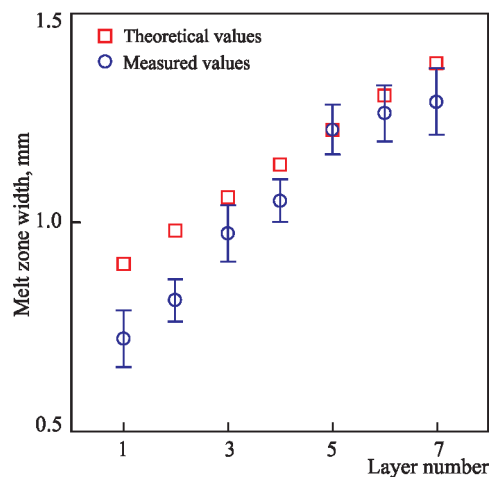


Figure 6. Comparison of calculated and experimentally measured width of the melt zone for 7 deposited layers of powder material [21]

The next important element of experiment planning is selection of the scan pattern, as it was determined that this component has a strong influence on additive manufacturing processes [5, 13]. So, in the work by AlMangour et al. [27] analysis of a number of patterns was performed, which gives argumentation as to the advantages of scan patterns where each layer differs from the previous one. In this study [27], as well as in the works by Zhao et al. [28] and Bambach et al. [29] the scanning strategy was found to influence the continuity of grain growth through the adjacent layers and grain growing inside the melt path. As a result, several schemes were considered (Figure 7):

- linear, where the process of material deposition is conducted by identical monotonic movements;
- parallel, where the deposited material paths run parallel to each other as to orientation, but not the deposition direction (see Figure 7, *a*);
- radial where material is deposited from the center to the edges or vice versa (see Figure 7, *c*);
- mixed, which combines several schemes simultaneously (see Figure 7, *b*).

The mechanism of interaction of the deposited material layers is worth mentioning separately. In works [28, 29] it was proved that the change of the angle of powder material deposition path between the layers has a positive influence on the material mechanical properties. However, in the paper by AlMangour et al. [27] it was found that the change of the angle of the path (“path rotation”) of powder material deposi-

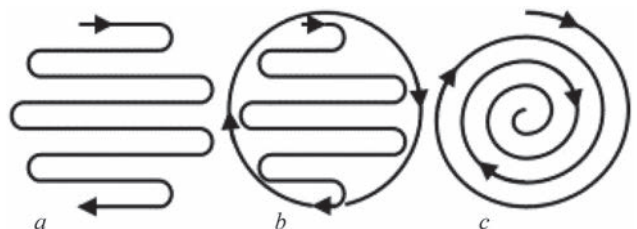


Figure 7. Scan patterns considered in the work by Bambach et al. [29]: *a* — parallel scheme; *b* — mixed scheme; *c* — radial scheme

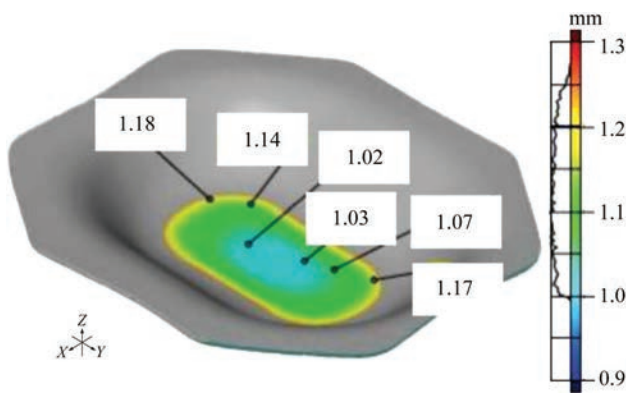


Figure 8. 3D scheme of thin-walled base deformation after selective laser melting of an element. Accuracy of ± 0.15 mm [30]

tion may lead to changes of various parameters of the deposited material. Therefore, the change of the path angle during transition to a new layer of the material is not a universally positive principle [27, 29].

ANALYSIS OF THE COURSE OF ADDITIVE MANUFACTURING PROCESSES WHEN WORKING WITH THIN-WALLED BASES

When deepening the knowledge of additive manufacturing processes while working on a thin-walled base, a lot of attention is given to studying the influence of variables on progress of SLM and SLS processes, as well as deeper understanding of the course of these processes proper under the specified conditions. The paper by Ahuja et al. [30] describes powder material deposition on a thin-walled base in the form of a stamped part 1.5 mm thick. A structural assembly from Ti-6Al-4V alloy in the form of 10×5 mm cylinder was manufactured using SLM-280HL printer with laser radiation power of 400, 700 and 1000 W and up to 10 m/s scanning speed. In paper [30] special attention is also paid to size (25–45 μm particle size), and phase composition of powder material and its compatibility with thin-walled base material. The need for correct fastening and cooling of the part is also described here, as in the presence of air behind the thin-walled base it undergoes deformations under the impact of laser radiation. The magnitude of possible deformations detected in paper [30], was visualized (Figure 8).

The need for cooling the thin-walled part during processing is also mentioned in the paper by Heile-

mann et al. [31]. To avoid deformation, the authors used a 4 mm copper substrate. Also emphasized is the need to control the energy component with separation of the processes of deposition of the first layers of powder material and next layers, highlighting the great difference between the nature of different stages of this process [32–34].

ANALYSIS OF THE PROPERTIES OF PARTS WITH MATERIALS DEPOSITED ON THEM BY SLM OR SLS PROCESSES

It is important to pay attention to the transition zone, as well as mechanical properties of the assemblies produced by additive manufacturing on a thin-walled base. In earlier mentioned works [18, 29–31], this question was seen from different angles, as the mechanical properties of the parts can be influenced by many components of additive manufacturing process: both energy and thermophysical ones. The microstructure of this zone of such elements should be considered separately, as the transition zone between the base and the deposited powder material is one of the critical areas. So, for instance, in the work by Ahuja et al. [30] formation of microcracks in the transition zone was studied. To prevent their formation, it was proposed to perform deposition with a fillet radius of 0.5 mm (Figure 9).

It should be noted, however, that correct fastening of the part affects not only the base, but also the deposited materials. So, in works [30, 35] it was noted that the evenness of material distribution directly influences the deposited material dilution and the microstructure, forming weakened zones. In the paper by Schaub et al. [55] it was determined that the strength of the bond between the sheet metal and the deposited element can be improved, preventing oxidation and reducing the temperature gradient between the upper surface of the sheet metal and the first layers of the portion molten by the laser beam. Also mentioned here was pre- and postheat treatment, which agrees with the experiments conducted by Niu et al. [26]. In this study [26], as well as in the works by Lesyk et al. [9, 36] the presence of partially melted metal powder on the side surfaces of the deposited material layers was reported. Minimizing

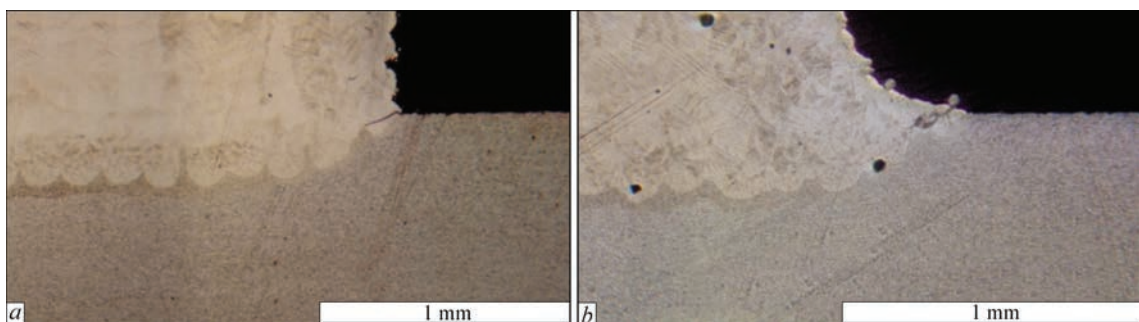


Figure 9. Transition zone structure [30]: *a* — without a fillet radius one can see cracking on the transition zone edges; *b* — with a fillet radius of 1.0 mm in the first layers of deposited material cracking is absent

of the amount of such formations is another reason for conducting the heat treatment.

ANALYSIS OF THE RESULTS OF THE CONSIDERED STUDIES. SPECIFICS OF APPLICATION OF ADDITIVE TECHNOLOGIES AT DEPOSITION OF ELEMENTS ON A THIN-WALLED BASE

Based on the results of the conducted analysis, we can note that the considered studies use a more comprehensive view of additive manufacturing processes, associated with element deposition on a thin-walled base. A difference in the approaches to modeling and consideration of the technologies is noticeable. For instance, most of the works, considering the questions of modeling of additive manufacturing processes use the finite element method, but the difference in the approaches to the variables slowly changes towards complex consideration of rows of parameters [5, 20, 21]. One can also see an additional focus on differentiation of the process of deposition of the first layers of powder material on the thin-walled base and deposition of additional layers, because of the importance of the influence of laser radiation on the thin-walled base and the transition layers. In this respect, the importance of correct fastening and cooling of the part should be noted, as there is a general understanding that this is important not only for a uniform formation of the deposited material [18, 29, 30], but also for prevention of thermal deformations of the thin-walled base [30]. There is, however, a reverse side: reduction of temperature gradient due to postheat treatment of the thin-walled base provides an increase of the strength of “base-deposited element” transition zone [35]. It is also important to single out the problem of deformations, which may develop through internal stresses, generated in the molten powder material [18], and which require additional heat treatment of the parts. It should be further noted that the “base-deposited element” transition should proceed with minimal temperature gradient — it minimizes the risk of lowering of the product strength characteristics [25, 26]. Together with the questions to phase composition, these problems add up to a complex issue of the priority of the characteristics, desirable for fulfillment of particular tasks.

CONCLUSIONS

Analysis of investigations of additive manufacturing of elements on a thin-walled base allowed establishing certain regularities, which are worth using for development of the process of selective laser deposition, namely:

- need for correct planning of the experiment, as well as the technological process, that is selection of scan pattern; processing modes, as well as modeling of “thin-walled base-deposited material” transition zone to form the smoothest and strongest transition zone;
- need to control the technology during the entire process, ensuring even distribution of the metal powder and cooling of the thin-walled base;

- need to ensure cooling of the thin-walled base to prevent thermal deformations, as well as use of heat treatment for leveling the internal stresses, developing in the upper layers of the molten material.

REFERENCES

1. Del Sol, I., Rivero, A., Lacalle, L., Gámez, A. (2012) Thin-wall machining of light alloys: A review of models and industrial approaches. *Materials*, **12**. DOI: <https://doi.org/10.3390/ma12122012>.
2. Singh R., Gupta A., Tripathi O. et al. (2020) *Powder bed fusion process in additive manufacturing: An overview*. Materials today: Proceedings. DOI: <https://doi.org/10.1016/j.matpr.2020.02.635>
3. Mazumder, J. (2017) *1 — Laser-aided direct metal deposition of metals and alloys*. Ed. by M. Brandt. Woodhead Publishing, 21–53. DOI: <https://doi.org/10.1016/B978-0-08-100433-3.00001-4>
4. Yushchenko, K.A., Borysov, Yu.S., Kuznetsov, V.D., Korzh, V.M. (2007) *Surface Engineering: Manual*. Kyiv, Naukova Dumka [in Ukrainian]. ISBN 978-966-00-0655-3
5. Li Yuan, Songlin Ding, Cuie Wen. (2019) Additive manufacturing technology for porous metal implant applications and triple minimal surface structures: A review. *Bioactive Materials*, **4**, 56–70. DOI: <https://doi.org/10.1016/j.bioactmat.2018.12.003>
6. Kritskiy, D., Pohudina, O., Kovalevskiy, M. et al. (2022) Powder mixtures analysis for laser cladding using OpenCV Library. In: *Integrated Computer Technologies in Mechanical Engineering — 2021*. Eds by, M. Nechyporuk, V. Pavlikov, D. Kritskiy. *Lecture Notes in Networks and Systems*, **367**. Springer, Cham. DOI: https://doi.org/10.1007/978-3-030-94259-5_72
7. Duriagina, Z., Kulyk, V., Kovbasiuk, T. et al. (2021) Synthesis of functional surface layers on stainless steels by laser alloying. *Metals*, **11**, 434. DOI: <https://doi.org/10.3390/met11030434>
8. Korzhyk, V., Khaskin, V., Voitenko, O. et al. (2017). Welding technology in additive manufacturing processes of 3D objects. *Mat. Sci. Forum*, **906**, 121–130. DOI: <https://doi.org/10.4028/www.scientific.net/msf.906.121>
9. Lesyk, D.A., Martinez, S., Pedash, O.O. et al. (2022) Nickel superalloy turbine blade parts printed by laser powder bed fusion: Thermo-mechanical post-processing for enhanced surface integrity and precipitation strengthening. *J. of Mat. Eng. and Perform.*, **31**, 6283–6299. DOI: <https://doi.org/10.1007/s11665-022-06710-x>
10. Peleshenko, S., Korzhyk, V., Voitenko, O. et al. (2017) Analysis of the current state of additive welding technologies for manufacturing volume metallic products (Review). *Eastern-European J. of Enterprise Technologies*, **3/1**, 42–52. DOI <https://doi.org/10.15587/1729-4061.2017.99666>.
11. Kumar, S. (2014) 10.05 – Selective laser sintering/melting. Eds by Saleem Hashmi, Gilmar Ferreira Batalha, Chester J. Van Tyne, Bekir Yilbas. *Comprehensive Materials Processing*, Elsevier, 93–134. DOI: <https://doi.org/10.1016/B978-0-08-096532-1.01003-7>
12. Serin, G., Kahya, M, Unver, H. et al. (2018) A review of additive manufacturing technologies. In: *The 17th Inter. Conf. on Machine Design and Production (Bursa, Turkey, January 2018)*.
13. Najmon, J.C., Sajjad Raesi, Tovar, A. (2019) 2 — Review of additive manufacturing technologies and applications in the aerospace industry. Eds by F. Froes, R. Boyer. *Additive Manufacturing for the Aerospace Industry*, Elsevier, 7–31. DOI: <https://doi.org/10.1016/B978-0-12-814062-8.00002-9>.
14. Del Sol, I., Rivero, A., Lacalle, L., Gámez, A. (2019) Thin-wall machining of light alloys: A review of models and in-

- dustrial approaches. *Materials*, **12**, 2012. DOI: <https://doi.org/10.3390/ma12122012>.
15. Adjamsky, S.V., Sazanishvili, Z.V., Tkachov, Y.V. et al. (2021) Influence of the time interval between the deposition of layers by the SLM technology on the structure and properties of Inconel 718 alloy. *Mater. Sci.*, **57**, 9–16. DOI: <https://doi.org/10.1007/s11003-021-00508-3>
 16. Sun, Z., Tan, X., Tor, S. Chua, C. (2018) Simultaneously enhanced strength and ductility for 3D-printed stainless steel 316L by selective laser melting. *NPG Asia Materials*, **10**(4), 127–136.
 17. Wang, Y., Voisin, T., McKeown, J. et al. (2017) Additively manufactured hierarchical stainless steels with high strength and ductility. *Nature Materials*, **17**(1), 63–71.
 18. Yang, W., Tang, Y. (1998) Design optimization of cutting parameters for turning operations based on the Taguchi method. *J. Materials Proc. Technology*, **84**(1–3), 122–129.
 19. Gibson, D. Rosen, B. Stucker (2015) *Additive manufacturing technologies: 3D printing, rapid prototyping and direct digital manufacturing Ch.10*. Springer, New York.
 20. Pulin, Nie, Ojo, O.A., Zhuguo, Li (2014) Numerical modeling of microstructure evolution during laser additive manufacturing of a nickel-based superalloy. *Acta Materialia*, **77**, 85–95. DOI: <https://doi.org/10.1016/j.actamat.2014.05.039>
 21. Mukherjee, T., Manvatkar, V., De, A., DebRoy, T. (2017) Dimensionless numbers in additive manufacturing. *J. Appl. Phys.*, **121**, 064904. DOI: <https://doi.org/10.1063/1.4976006>
 22. Yang, T., Xie, D., Yue, W. et al. (2019) Distortion of thin-walled structure fabricated by selective laser melting based on assumption of constraining force-induced distortion. *Metals.*, **9**(12), 1281. DOI: <https://doi.org/10.3390/met9121281>
 23. Zhonghua, Li, Renjun, Xu, Zhengwen, Zhang, Ibrahim, Kucukkoc (2018) The influence of scan length on fabricating thin-walled components in selective laser melting. *Inter. J. of Machine Tools and Manufacture*, **126**(1–12). DOI: <https://doi.org/10.1016/j.ijmactools.2017.11.012>
 24. Eberhard Abele, Hanns A. Stoffregen, Kniepkamp, M. et al. (2015) Selective laser melting for manufacturing of thin-walled porous elements. *J. Materials Proc. Technology*, **215**, 114–122. DOI: <https://doi.org/10.1016/j.jmatproc.2014.07.017>
 25. Jichang, Liu, Lijun, Li (2005) Effects of powder concentration distribution on fabrication of thin-wall parts in coaxial laser cladding. *Optics & Laser Technology*, **37**(4), 287–292. DOI: <https://doi.org/10.1016/j.optlastec.2004.04.009>
 26. Xu Niu, Ruixian Qin, Yunzhuo Lu, Bingzhi Chen (2021) Energy absorption behaviors of laser additive manufactured aluminium alloy thin-walled tube tailored by heat treatment. *Materials Transact.*, **62**(2), 278–283.
 27. AlMangour, B., Grzesiak, D., Yang, J. (2017) Scanning strategies for texture and anisotropy tailoring during selective laser melting of TiC/316L stainless steel nanocomposites. *J. of Alloys and Compounds*, **728**, 424–435.
 28. Zhao, C., Bai, Y., Zhang, Y. et al. (2021) Influence of scanning strategy and building direction on microstructure and corrosion behaviour of selective laser melted 316L stainless steel. *Materials & Design*, **209**, 109999.
 29. Bambach, M, Sviridov, A, Weisheit, A, Schleifenbaum, JH. (2017) Case studies on local reinforcement of sheet metal components by laser additive manufacturing. *Metals.*, **7**(4), 113. DOI: <https://doi.org/10.3390/met7040113>
 30. Bhriгу Ahuja, Adam Schaub, Michael Karg et al. (2015) High power laser beam melting of Ti–6Al–4V on formed sheet metal to achieve hybrid structures. In: *Proc. Of SPIE 9353, Laser 3D Manufacturing II, 93530X (16 March 2015)*. DOI: <https://doi.org/10.1117/12.2082919>
 31. Heilemann, M., Beckmann, J., Konigorski, D., Emmelmann, C. (2018) Laser metal deposition of bionic aluminum supports: reduction of the energy input for additive manufacturing of a fuselage. *Procedia CIRP*, **74**, 136–139. DOI: <https://doi.org/10.1016/j.procir.2018.08.063>.
 32. Vekilov, S.Sh., Lipovskyi, V.I., Marchan, R.A., Bondarenko, O.Ie. (2021) Specifics of using of technology in SLM manufacture for LRE components. *J. of Rocket-Space Technology*, **29**, 112–123. DOI: <https://doi.org/10.15421/452112>
 33. Kelly, S.M., Kampe, S.L. Microstructural evolution in laser-deposited multilayer Ti–6Al–4V builds, Pt I. (2004) Microstructural Characterization. *Metallurgical and Materials Transact.*, **35A**, June 1861.
 34. Heilemann, M., Möller, M., Emmelmann, C. et al. (2017) Laser metal deposition of Ti–6Al–4V structures: Analysis of the build height dependent microstructure and mechanical properties. In: *MS&T 2017*.
 35. Schaub, A., Ahuja, B., Karg, M. et al. (2014) Fabrication and characterization of laser beam melted Ti–6Al–4V geometries on sheet metal. In: *DDMC 2014 Fraunhofer Direct Digital Manufacturing Conf., Berlin, Germany*.
 36. Lesyk, D., Martinez, S., Dzhemelinkyi, V., Lamikiz, A. (2020) Additive manufacturing of the superalloy turbine blades by selective laser melting: Surface quality. Microstructure and porosity. New Technologies, Development and Application III. NT 2020. Eds by I. Karabegović. *Lecture Notes in Networks and Systems*, **128**. Springer, Cham. DOI: https://doi.org/10.1007/978-3-030-46817-0_30

ORCID

M.V. Sokolovskyi: 0000-0003-3243-5060,
 A.V. Bernatskyi: 0000-0002-8050-5580,
 N.O. Shamsutdinova: 0000-0002-3525-0080,
 Yu.V. Yurchenko: 0000-0001-9253-009X,
 O.O. Danyleiko: 0000-0002-8501-0421

CONFLICT OF INTEREST

The Authors declare no conflict of interest

CORRESPONDING AUTHOR

M.V. Sokolovskyi
 E.O. Paton Electric Welding Institute of the NASU
 11 Kazymyr Malevych Str., 03150, Kyiv, Ukraine.
 E-mail: m_sokolovskyi@paton.kiev.ua

SUGGESTED CITATION

M.V. Sokolovskyi, A.V. Bernatskyi,
 N.O. Shamsutdinova, Yu.V. Yurchenko,
 O.O. Danyleiko (2023) Additive manufacturing of
 structural elements on a thin-walled base: Challenges
 and difficulties (Review). *The Paton Welding J.*, **11**,
 46–52.

JOURNAL HOME PAGE

<https://patonpublishinghouse.com/eng/journals/tpwj>

Received: 10.07.2023

Accepted: 07.12.2023

DOI: <https://doi.org/10.37434/tpwj2023.11.07>

APPLICATION OF ACOUSTIC EMISSION METHOD TO EVALUATE THE CHANGES IN THE PROPERTIES OF 17G1S STEEL AFTER LONG-TERM SERVICE

S.A. Nedoseka, A.Ya. Nedoseka, M.A. Yaremenko, M.A. Ovsienko, O.M. Gurianov

E.O. Paton Electric Welding Institute of the NASU
11 Kazymyr Malevych Str., 03150, Kyiv, Ukraine

ABSTRACT

17G1S steel is widely used in pipelines. Change in the physical properties of this material with time depends on the conditions of gas pipeline operation and pipe environment. Material damage due to operating time by far not always leads to a change of such standard characteristics of the material as σ_p , σ_y , K_{IC} and a number of others. At the same time, such material can be significantly damaged, but the traditional methods do not allow determining it. The objective of this work is to demonstrate the sensitivity of acoustic emission method to changes in 17G1S steel properties after 15 years of the main gas pipeline operation. Testing results show that the analyzed acoustic emission parameters change essentially under the impact of operating time, and they can be the characteristics for evaluation of the current state of the damaged material.

KEYWORDS: acoustic emission (AE), physical properties, AE monitoring, mechanical testing

INTRODUCTION

17G1S steel is widely used in pipelines, and, in particular, in gas pipelines. Change of some properties of this material with time is quite significant, and it depends on the gas pipeline service conditions and the pipe environment [1].

It is characteristic that material damage as a result of operating for a certain time does not at all always lead to a change of the material standard characteristics, such as σ_p , σ_y , K_{IC} and a number of others. As a result of that, such a material can be essentially damaged, but the traditional methods do not allow it to be determined.

In this work, the change of the steel properties was assessed by stretching the standard, undamaged samples and samples cut out of a pipe after long-term service, in a tensile testing machine with recording of the loads and elongation, as well as acoustic emission parameters (AE).

Unlike world practice [1–3], the technology of material state evaluation, developed at PWI of the NAS of Ukraine [4, 5], is based only on obtaining data on AE activity in the material and loading parameters, while the majority of the known studies require a multistep assessment procedure, in which AE method is assigned the role of the initial stage, at which AE activity in individual areas and coordinates of these areas are determined. Further on these investigations require additional studies of the material in the areas identified as hazardous by AE method. These investigations include cutting out reference-samples and studying their mechanical properties with further calculation of stress intensity factors, or, alternatively, application of additional NDT techniques,

first of all ultrasonic testing (UT). These methods are used to determine the shape and dimensions of the defects, and then again calculations of mechanical properties are performed, taking into account the detected defect shape and with calculation of usually the same stress intensity factors, and the material state analysis is based on this characteristic. Such a multistep evaluation, first of all, is quite difficult to perform, and, secondly, it does not allow real-time evaluation of the material state.

EMA-type systems of several generations, developed at PWI, have a built-in technology of material state evaluation in real time with prediction of breaking load, which is based on image recognition [4–6]. It allows considerable acceleration of the qualitative and quantitative evaluation of the state without application of any additional methods with normalized accuracy (error within $\pm 15\%$) and probability of 95%. This work presents, in particular, the results of prediction of the breaking load during static tensile testing of the samples.

We will obtain the results of stretching 17G1S samples in R20 machine. Figure 1 shows the loading scheme and position of the sample in the tensile testing machine.

The scheme given in Figure 1 is universal for the majority of AE tests of the samples, including temperature tests. Shown below are the diagrams of the readings of AE instrument during stretching of typical samples from as-delivered material and samples of damaged material, cut out of the pipe after 15 years of gas transportation. EMA-type AE systems can provide a rather large number of parameters in real time and during subsequent repetitions of the conducted measurements in the computer, in particular:

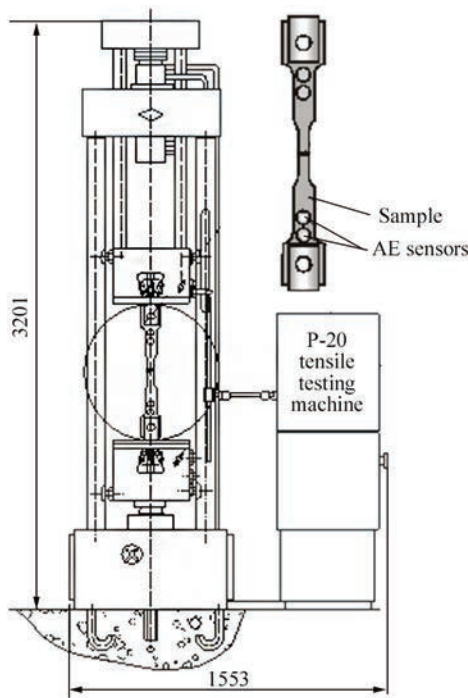


Figure 1. Sample and schematic of its mounting in R-20 machine

1. External force fields: in this experiment P is the current load, kg; e is the elongation, mm.

2. A — the maximal amplitude of the largest event being considered at this moment, mV, conditionally characterizes the volume created by the defect during its dynamic development.

3. $Rt(W)$ — the time of increment of the greatest event in the sum of events at this time or its duration, μs , characterizes material hardening as a result of deformation.

4. O — the number of oscillations in an AE event, characterizes the amount of damage generated at this moment of time.

5. A_s — the summary amplitude of AE events during testing time, dB, characterizes the overall scope of the generated damage.

6. O_s is the summary amount of damage in the material during the analyzed time period, which is determined by the sum of AE event oscillations.

7. N_s — the AE events accumulated during the destruction process characterize the total amount of damage, developing during the considered time; and may not coincide with O_s .

8. A^2 is the energy consumed in defect formation, J.

9. A_s^2 characterizes the summary AE energy consumed in sample destruction, J.

10. n is AE activity at a selected moment of time, 1/s.

11. N — the sum of events during the analyzed time, characterizes the number of defects developing over time, it can coincide with O_s .

12. X, Y are mediated with a given probability coordinates of the sum of events initiating at the moment of time being considered, in a certain area of the sample or structure, mm. The size of this area is determined automatically, depending on the tested object dimensions and AE sensor layout.

Considering that not necessarily all of the abovementioned parameters may be sufficiently indicative, such parameters as P, e, A, Rt, n, N, X will be considered in the window of the location array and plotted graphs. They provide a complete picture of the process of damage accumulation during testing, and visual demonstration of changes of the properties in the damaged material, compared to the metal in the initial state.

In addition to the abovesaid, EMA type systems have a functional which allows prediction of the breaking load in real time and after repeated viewing of the conducted measurements on the computer, the results of which are also given in this investigation.

Figure 2 shows the location screen of EMA program with instantaneous values of AE parameters, which appeared when testing a sample of as-delivered 17G1S steel. At this moment the window shows the following data:

1. Cluster coordinates are given at the top on the left, which indicate the predicted destruction site. These coordinates are determined more precisely as the sample is loaded.

2. Predicted breaking load (Destruction forecast) in the range of 9573–12087 kg is given at the top on the right, which corresponds to the actual data re-

corded by the instrumentation. It should be noted that the predicted value of breaking load appeared in the window at loading, which is equal to approximately 30 % of the actual breaking value which is equal to 11758 kg (Figure 3). Predicted values fall within the range of requirements to EMA type systems as to the destruction forecast of $\pm 15\%$.

3. Shown lower in the window is the bar of AE events combined into a cluster, which represent accumulation of damage in the sample with indication of X coordinate of the probable destruction site. A sample carrying AE sensors (their numbers and location coordinates) is schematically shown below.

4. Actual values of AE signals, accumulated in the tested area are shown still lower. Note than in Figure 2, which is a screenshot of EMA program at the moment of destruction forecast, AE events with large amplitudes are yet absent; they appear later during the sample destruction.

5. The diagram begins functioning with the testing start and follows the entire kinetics of destruction in its dynamics.

Detailed kinetics of sample destruction is presented in Figure 3. For ease of understanding the test data are divided into two graphs.

The graph in Figure 3, *a* shows:

1. Bars are the amplitudes A of AE events in the linear measurement modes. Shown on the axis on the

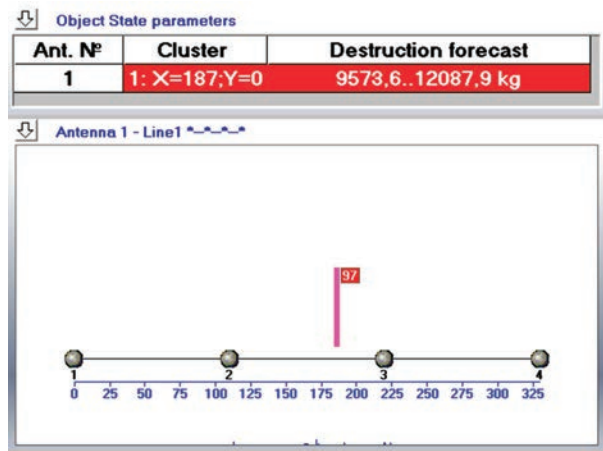


Figure 2. Location window of EMA program with AE data accumulated during testing of a sample in the initial condition left is the amplitude scale, where the maximum cannot exceed 500 mV.

2. The line is the working load P . The value of actual breaking load of 11758 kg is shown on the axis on the right.

3. Points are the activity of n AE events in time. Value n , the maximum of which is equal to 18, is shown on the axis to the right.

The graph in Figure 3, *b* shows:

1. Bars show the time of increase of AE event amplitude up to maximum Rt . Shown on the axis on the left is Rt scale, where the maximum cannot exceed 65535.

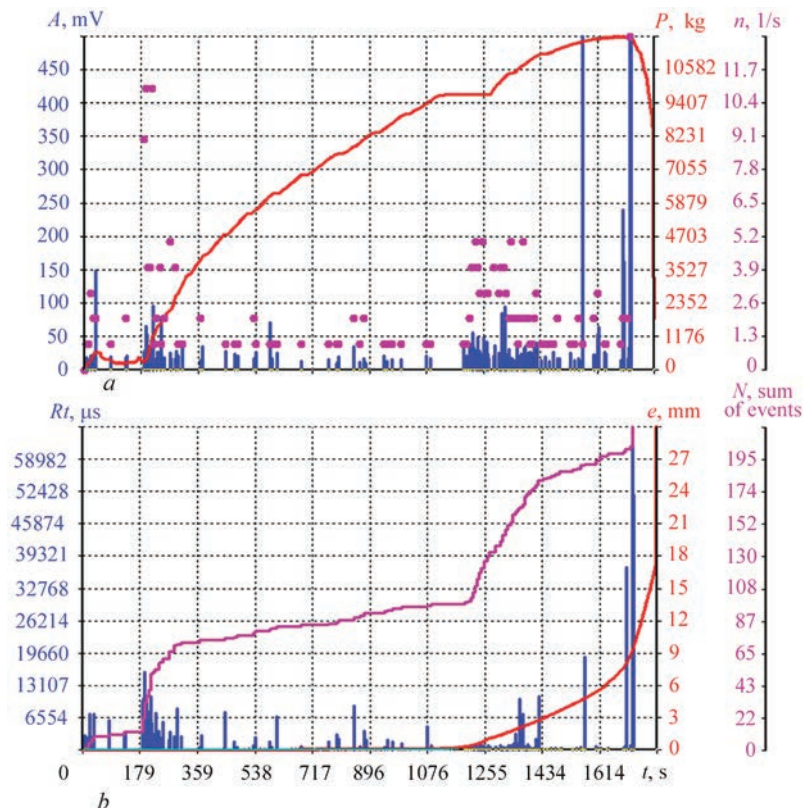


Figure 3. Graphs of development of destruction of 17G1S steel sample in the initial state

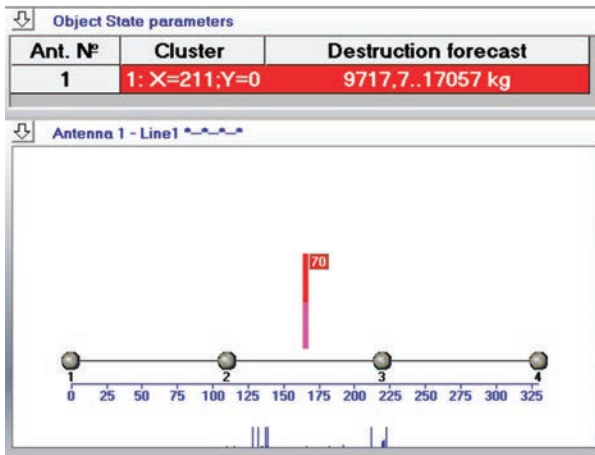


Figure 4. Location window of EMA program with AE data accumulated during testing of a damaged sample after 15 years of operation

2. Smooth exponential curve, which begins growing approximately after loading for 1000 s, shows elongation e . Marked on the axis on the right is value e , the maximum of which is equal to 30 mm – at the moment of sample destruction.

3. Steplike curve shows gradual damage accumulation in the sample, which is represented by event sum N . On the whole their quantity was equal to 217.

As we can see, the Keiser effect is absent in the initial material: AE events begin forming immediately after the start of loading, and their accumulation curve

has a typical shape for undamaged material. Note the evident presence of a yield plateau, at which deformation is increased in the section of the horizontal loading curve.

Sample rupture is characterized by AE amplitude surges up to the maximum even before the ultimate strength has been reached and directly when reaching it.

The pattern is totally different for a sample cut out of a pipe after 15 years of operation (Figures 4, 5). Parameters given in Figures 2, 4 are the same, those on the graphs in Figures 3, 5 are also the same, but their nature has changed essentially.

The sample has hardened after 15 years of operation during gas transportation which is indicated by reduction of elongation from 30 to 15.9 mm at breaking load, which increased only slightly from 11758 to 11886 kg. Kaiser effect is clearly traceable: there are no AE events at the initial loading stage.

During operation the gas gradually penetrates into the pipe material, causing its gradual embrittlement, increase of the level of destruction rigidity, and aging of pipe material [4, 5]. This is confirmed by an abrupt reduction of the parameter of the duration of the event increasing part Rt , total sum of AE events $N = 70$ (there were 217 of them in the initial material), i.e. the amount of damage in the material after long-term operation decreases abruptly. Increase of

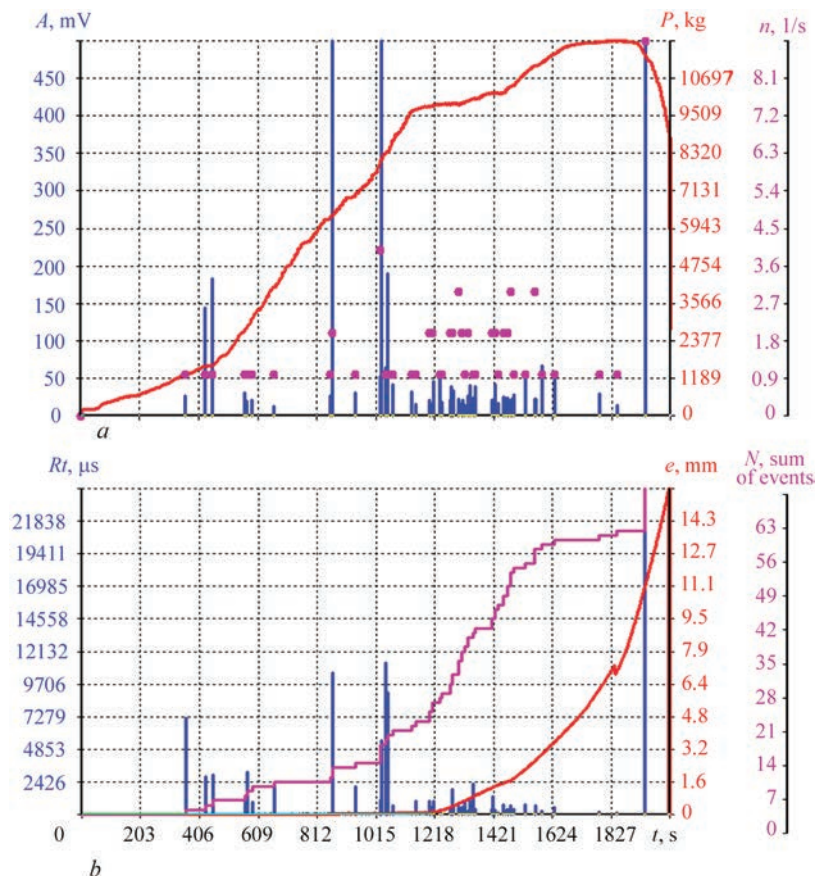


Figure 5. Graphs of development of destruction of a damaged sample from 17G1S steel after 15 years of operation

the percentage of AE events with maximal amplitudes relative to the number of the events proper is the result of embrittlement.

AE activity n became two times lower, which is also indicative of material hardening after operation.

Considering further the change of AE parameters during testing, one can see that in the damaged material AE events do not massively increase at once, but after a certain time. In this case it occurs approximately at $t = 400$ s and more intensively further on at $t = 1010$ s (active increase of sample deformation begins exactly from this moment), which, according to Kaiser effect, indicates that the pipe material was exposed to loading of approximately 27 atm in operation, and that the stress for the analyzed pipe (1020 mm diameter, 8 mm wall thickness) is equal to approximately 173.4 MPa). At the same time, it should be noted that the progressing embrittlement of pipe material can lead to destruction at emergency movements of the soil, through which the pipe is laid, as a result of washing out or shifting.

Thus, a sufficient sensitivity of AE method to changes in properties of 17G1S steel after long-term operation is shown, with preservation of the quality of state assessment and timely warning about the destruction and breaking load prediction.

CONCLUSIONS

1. AE method demonstrated sufficient sensitivity to changes of 17G1S steel properties after long-term operation. Practically all the analyzed AE parameters react qualitatively and quantitatively to the above-mentioned changes. It was possible to derive the respective qualitative and quantitative indices by comparing the results of static tensile testing of samples from the emergency stock with recording of AE parameters with the results of testing samples of a similar configuration, cut out in the main gas pipeline after 15 years of operation.

2. Continuous influence of the transported gas on the pipe material leads to an essential change of a range of material properties (see, in particular [4, 5]). Plasticity changes most strongly, which in the experiment is manifested by shorter time of AE event increase up to a maximum, reduction of the total number of AE events at considerable increase of the percentage of high-amplitude events. In practice ductility decrease leads to pipe material brittleness and to the risk of its destruction at emergency displacement of the pipe in the ground.

3. Conducted testing yielded data on the impact of previous 15 years of loading during the operation of 17G1S steel pipe on the change of this material properties which was manifested in a significant quantitative and qualitative change of a range of AE parameters.

REFERENCES

1. Junyu, Chen, Yunwen, Feng, Cheng, Lu, Chengwei, Fei (2021) Fusion fault diagnosis approach to rolling bearing with vibrational and acoustic emission signals. *CMES-Computer Modeling in Engineering & Sciences*, 129(2), 1013–1027. DOI: <https://doi.org/10.32604/cmescs.2021.016980>
2. Amirabbas, Haidarpour, Kong, Fah Tee (2020) Finite element model updating for structural health monitoring. *Structural Durability & Health Monitoring*, 14(1), 1–17. DOI: <https://doi.org/10.32604/sdhm.2020.08792>
3. Nazarchuk, Z.T., Skalskyi, V.R. (2009) *Acoustic emission diagnostics of structural elements*. Sci.-Tekhn. Manual. In: 3 Vol., Kyiv, Naukova Dumka [in Ukrainian].
4. Nedoseka, A.Ya., Nedoseka, S.A. (2020) *Fundamentals of calculation and diagnostics of welded structures*: Manual. 5th Ed. Ed. by B.E. Paton. Kyiv, Indprom [in Russian].
5. Nedoseka, A.Ya., Nedoseka, S.A. (2020) *Fundamentals of calculation and diagnostics of welded structures*: Manual, Chapt. 7. 5th Ed. Ed. by B.E. Paton. Kyiv, Indprom [in Russian].
6. Nedoseka, S.A. (2007) Forecasting the fracture by the data of acoustic emission. *Tekh. Diagnost. i Nerazrush. Kontrol*, 2, 3–9 [in Russian].

ORCID

S.A. Nedoseka: 0000-0001-9036-1413,
A.Ya. Nedoseka: 0000-0002-3239-381X,
M.A. Yaremenko: 0000-0001-9973-4482,
M.A. Ovsienko: 0000-0002-2202-827X,
O.M. Gurianov: 0000-0001-9566-1706

CONFLICT OF INTEREST

The Authors declare no conflict of interest

CORRESPONDING AUTHOR

S.A. Nedoseka
E.O. Paton Electric Welding Institute of the NASU
11 Kazymyr Malevych Str., 03150, Kyiv, Ukraine.
E-mail: inpat59@ukr.net

SUGGESTED CITATION

S.A. Nedoseka, A.Ya. Nedoseka, M.A. Yaremenko, M.A. Ovsienko, O.M. Gurianov (2023) Application of acoustic emission method to evaluate the changes in the properties of 17G1S steel after long-term service. *The Paton Welding J.*, **11**, 53–57.

JOURNAL HOME PAGE

<https://patonpublishinghouse.com/eng/journals/tpwj>

Received: 07.05.2023

Accepted: 07.12.2023

SUBSCRIPTION-2024



«The Paton Welding Journal» is Published Monthly Since 2000 in English, ISSN 0957-798X, doi.org/10.37434/tpwj.

«The Paton Welding Journal» can be also subscribed worldwide from catalogues subscription agency EBSCO.

If You are interested in making subscription directly via Editorial Board, fill, please, the coupon and send application by Fax or E-mail.

12 issues per year, back issues available.

\$384, subscriptions for the printed (hard copy) version, air postage and packaging included.

\$312, subscriptions for the electronic version (sending issues of Journal in pdf format or providing access to IP addresses).

Institutions with current subscriptions on printed version can purchase online access to the electronic versions of any back issues that they have not subscribed to. Issues of the Journal (more than two years old) are available at a substantially reduced price.

Subscription Coupon			
Address for Journal Delivery			
Term of Subscription Since	20	Till	20
Name, Initials			
Affiliation			
Position			
Tel., Fax, E-mail			

The archives for 2009–2022 are free of charge on www://patonpublishinghouse.com/eng/journals/tpwj



ADVERTISING

in «The Paton Welding Journal»

External cover, fully-colored:

- First page of cover (200×200 mm) – \$700
- Second page of cover (200×290 mm) – \$550
- Third page of cover (200×290 mm) – \$500
- Fourth page of cover (200×290 mm) – \$600

Internal cover, fully-colored:

- First/second/third/fourth page (200×290 mm) – \$400
- Internal insert: (200×290 mm) – \$340 (400×290 mm) – \$500

- Article in the form of advertising is 50 % of the cost of advertising area
- When the sum of advertising contracts exceeds \$1001, a flexible system of discounts is envisaged
- Size of Journal after cutting is 200×290 mm

Address

11 Kazymyr Malevych Str., 03150, Kyiv, Ukraine
 Tel./Fax: (38044) 205 23 90
 E-mail: journal@paton.kiev.ua
www://patonpublishinghouse.com/eng/journals/tpwj